REPORT

Form Approved
OMB No. 0704-0188

1. AGENCY USE ONLY (Leave blank)	2. REPORT DATE	3. REPORT TYPE AND DATES COVERED
	Apr 94	Final 1 Feb 93-30 Sep 93

4. TITLE AND SUBTITLE

Dynamic Response of Composite Structures

5. FUNDING NUMBERS

DAAH04-93-G-0052

6. AUTHOR(S)

David Hui (Principal investigator)

7. PERFORMING ORGANIZATION NAME(S) AND ADDRESS(ES)

Univ. of New Orleans
New Orleans, LA 70148

8. PERFORMING ORGANIZATION REPORT NUMBER

9. SPONSORING/MONITORING AGENCY NAME(S) AND ADDRESS(ES)

U. S. Army Research Office
P. O. Box 12211
Research Triangle Park, NC 27709-2211

10. SPONSORING/MONITORING AGENCY REPORT NUMBER

ARO 30904.1-EG-CF

11. SUPPLEMENTARY NOTES

The view, opinions and/or findings contained in this report are those of the author(s) and should not be construed as an official Department of the Army position, policy, or decision, unless so designated by other documentation.

12a. DISTRIBUTION/AVAILABILITY STATEMENT

Approved for public release; distribution unlimited.

12b. DISTRIBUTION CODE

13. ABSTRACT *(Maximum 200 words)*

The purpose of the workshop was to:

(i) assess the state of the art in the modeling and analysis of modern composite structures that are relevant to the Army's need to improve the design and operation of land vehicles, helicopters, weapon systems, etc.

(ii) identify new opportunities for relevant research.

The special areas or interest were crash worthiness of composite structures, composite helicopter rotor blade dynamics, stability and control, smart composite structures, etc.

The workshop contained six keynote and distinguished lectures and 34 lectures for a total of 40 paper presentations. The regular sessions include (i) Vibration of Composite Structures (ii) Smart Structures (iii) Impact of Composite Structures (iv) Damage and Failure (v) Design of Composite Structures (vi) Structural Mechanics.

14. SUBJECT TERMS

Dynamic Responses, Composite Structures, Land Vehicles, Helicopters, Weapons Systems, Workshop, Structural Mechanics

15. NUMBER OF PAGES

16. PRICE CODE

17. SECURITY CLASSIFICATION OF REPORT	18. SECURITY CLASSIFICATION OF THIS PAGE	19. SECURITY CLASSIFICATION OF ABSTRACT	20. LIMITATION OF ABSTRACT
UNCLASSIFIED	UNCLASSIFIED	UNCLASSIFIED	UL

Army Research Office Workshop on:

Dynamic Response of Composite Structures

Westin Hotel, New Orleans, LA
August 30, 31, Sept 1, 1993.

David Hui
ARO workshop chairman
University of New Orleans
Dept of Mechanical Engineering
New Orleans, LA 70148

Gary Anderson
ARO workshop monitor
US Army Research Office
Engineering Sciences Div.
Research Triangle Park
NC 27709-2221

FOREWORD

The Army Research Office is pleased to sponsor the workshop, "Dynamic Response of Composite Structures" to be held in New Orleans, August 30- September 1, 1993. The purpose of the workshop is to:

(i) assess the state of the art in the modeling and analysis of modern composite structures that are relevant to the Army's need to improve the design and operation of land vehicles, helicopters, weapon systems, etc.

(ii) identify new opportunities for relevant research.

The special areas of interest are crash worthiness of composite structures, composite helicopter rotor blade dynamics, stability and control, smart composite structures, etc. Other area of composite structural research are welcomed and the authors are encouraged to show the relevance of their work to the U.S. Army.

The workshop contains six keynote and distinguished lectures and 34 lectures for a total of 40 paper presentations. The regular sessions include (i) Vibration of Composite Structures (ii) Smart Structures (iii) Impact of Composite Structures (iv) Damage and Failure (v) Design of Composite Structures (vi) Structural Mechanics. We are pleased with the many outstanding presentations at this ARO workshop and would like to acknowledge the financial and moral support of the Army Research Office. Thanks are due to the contributions from the authors, the reviewers and the support and encouragement of Dr. John Crisp, Dean of Engineering, University of New Orleans.

David Hui
ARO workshop chairman
University of New Orleans

"Dynamic Response Of Composite Structures: Aro Workshop"
Westin Hotel, New Orleans, August 30, 31, Sept 1, 1993.

Hui, David workshop chairman
Anderson, Gary workshop monitor

Keynote and Distinguished Lecturers

1. Batra, Romesh (U. of Missouri-Rolla), distinguished lecturer
2. Chang, Fu-kuo (Stanford U.), keynote
3. Dutta, Piyush (CRREL), distinguished lecturer
4. Horgan, Cornelius (U. of Virginia), keynote
5. Measures, Ray (U. of Toronto), distinguished lecturer
6. Tessler, Alexander (NASA Langley), keynote

Lecturers:

7. Averill, Ronald C. (Michigan State U.)
8. Barrett, Ron (Lawrence, Kansas)
9. Baz, Amr M. (Catholic U. of America)
10. Berdichevsky, Victor L. (Georgia Tech)
11. Bogdanovich, Alexander (North Carolina State U.)
12. Cantwell, Wesley (Switzerland)
13. Carman, Greg (UCLA)
14. Chattopadhyay, Aditi (Arizona State U.)
15. Chaudhuri, Reaz A. (U. of Utah)
16. Coulter, John (Lehigh U.)
17. Czarnecki, Greg (Wright Patterson AFB)
18. Dong, Stephen (UCLA)
19. Fahrenthold, Eric (U. of Texas-Austin)
20. Gibson, Ron (Wayne State U.)
21. Gramoll, Kurt (Georgia Tech)
22. Hanagud, Satya (Georgia Tech)
23. Hoa, Suong V. (Concordia U.)
24. Hui, D. (New Orleans)
25. Jaeger, Zeev (Israel)
26. Joshi, Shiv (U. of Texas at Arlington)
27. Kapania, Rakesh (VPI)
28. Khorrami, Farshad (Polytechnic U., NY)
29. Lee, James (George Washington U.)
30. Mayer, Arnold (Wright Patterson AFB)
31. Nayfeh, Adnan (U. of Cincinnati)
32. Pang, Su-Seng (Louisiana State U.)
33. Rao, Vittal (U. of Missouri-Rolla)
34. Shahinpoor, Mohsen (U. of New Mexico)
35. Simitses, George (U. of Cincinnati)
36. Tzeng, Jerome (Army Research Lab, MD)
37. Vandiver, Terry (Army Missile Command)
38. Voyiadjis, George (Louisiana State U.)
39. Whitney, James (U. of Dayton)
40. Xiao, X.R. (Concordia U.)

Special Guests:

Burns, Bruce (Army Research Lab.)
Crisp, John (Dean of Engineering, Univ. of New Orleans)
Hakala, Bill (NSF)
Rajapakse, Yapa (ONR)
Kelly, James (ARPA)
Sigur, Wanda (Martin Marietta)
Spicola, Frank (Naval Undersea Warfare Center, RI)
Weiss, Marc (Naval Biodynamics Laboratory, New Orleans)

Army Research Office Workshop on
"DYNAMIC RESPONSE OF COMPOSITE STRUCTURES: ARO WORKSHOP"

KEYNOTE LECTURES

Monday, August 30, 9:00-9:45 AM
"Saint-Venant End Effects in Composite Structures"
Horgan, Cornelius O. (U. of Virginia)

Tuesday, August 31, 9:00-9:45 AM
"Computational Methods for Practical Engineering Design of Thick Composite Plates and Shells"
Tessler, Alex (NASA Langley)

Wednesday, Sept. 1, 9:00-9:45 AM
"Detection Delamination in Composite Structures with Built-in Piezoelectrics"
Chang, Fu-Kuo (Stanford U.)

DISTINGUISHED LECTURES

Monday, August 30, 2:00-2:45 PM
"Fiber Optic Structural Sensing System for a Road Bridge"
Measures*, Ray, Alavic, T., Maaskant, R., Ohn, M., Karr, S., Huang, S., Glennie, D., Wade, C., Tadros, G. and Rizkalla, S. (U. of Toronto, Canada)

Tuesday, August 31, 2:00-2:45 PM
"On the Interface Stability of a Neck Propagating in a Sheet Reinforced with Shape-Memory Fibers"
Ru, C.Q. and Batra*, Romesh C. (U. of Missouri-Rolla)

Wednesday, Sept. 1, 1:15-2:00 PM
"Dynamic Stresses in Polymer Composites at Low Temperature"
Dutta, Piyush (US Army CRREL, Hanover, NH)

	Monday	Tuesday	Wednesday
8:25-8:55	**Vibration**	**Impact**	**Design**
8:55-9:00		Opening Remarks	
9:00-9:45	**Horgan, C.**	**Tessler, A.**	**Chang, F.K.**
9:45-10:00	Coffee break	Coffee break	Coffee break
10:00-12:30	**Vibration**	**Impact**	**Design**
12:30-1:15	Lunch	Lunch	Lunch
1:15-2:00	Lunch	Lunch	**Dutta, P. K.**
2:00-2:45	**Measures, R.**	**Batra, R.**	**Structural Mechanics**
2:45-3:00	Coffee break	Coffee break	**Structural Mechanics**
3:00-6:00	**Smart Structures**	**Damage and Failure**	**Structural Mechanics**

Monday morning, August 30, 8:25-8:55 AM
and 10:00 AM-12:30 PM
(last name marked with * indicates presenter)

VIBRATION OF COMPOSITE STRUCTURES

Chair: Rakesh Kapania (VPI)
co-chair: Shiv Joshi (U. Texas-Arlington)

"Vibration Analysis of Finite Thin Laminated Doubly-Curved Panels"
Chaudhuri, Reaz A. (U. of Utah)

"The Effect of Width on the Free Vibration of Anisotropic Laminated Beams"
Whitney, James M. (U. of Dayton)

"High-Frequency Composite Beam Dynamics"
Atilgan, A.R., Berdichevsky*, Victor L., Cesnik,C.E.S., Hodges, D.H. and Sutyrin, V.G. (Georgia Tech)

"Natural Vibrations and Waves in Pretwisted Rods"
Onipede, O., Dong*, Stanley B. and Kosmatka, J.B. (UCLA)

"Vibration Damping Characteristics of Thick Composite Structures"
Hwang, S.J. and Gibson*, Ron F. (Wayne State U.)

"Analytical Modeling of Electro-Rheological Material Based Adaptive Beams"
Yalcintas, M. and Coulter*, John (Lehigh U.)

==========

Monday afternoon, August 30, 3:00PM-6:00 PM

SMART STRUCTURES

Chair: Greg Carman (UCLA)
co-chair: Ray Measures (U. of Toronto)

"Optimal Vibration Control of Nitinol-Reinforced Composites"
Baz*, Amr and Ro, J. (Catholic U. of America)

"An Innovative Technique for Monitoring Damage Evolution in Composite Materials with Fiber Optic Sensors"
Carman, Greg (UCLA)

"Delamination Dynamics and Active Control of Delaminations"
Hanagud*, S., Nagesh Babu, G.L. and Luo, H. (Georgia Tech.)

"Control Designs for Smart Structures and Their Experimental Validation"
Khorrami, F. (Polytechnic U., NY)

"Optimal Control of Infinite Order Composite Structural Systems Using Distributed PVDF Sensors"
Rao*, V. and Butler, R. (U. of Missouri-Rolla)

"Active Composite Torque-Plate Fins for Subsonic Missiles"
Barrett, Ron (Kansas)

Tuesday morning, August 31, 8:25-8:55 AM
and 10:00 AM-12:30 PM

IMPACT OF COMPOSITE STRUCTURES

Chair: George Simitses (U. of Cincinnati)
co-chair: Wesley Cantwell (Switzerland)

"High Strain-Rate Behavior of Gr/Ep Laminate Under Transverse Impact"
Dutta, P. and Hui*, David (U. of New Orleans)

"The Significance of Laminate Spallation Generated by High-Velocity Spherical Metallic Impactors"
Czarnecki, Greg J. (Wright Laboratory, OH)

"Impact Dynamics and Damage Initiation in Laminated Composites"
Joshi*, S.P., Friedrich, K., Karger-Kocsis and Bogdanovich, A. (U. Texas-Arlington)

"Damage and Energy Exchange from Impact at Super-Perforation Velocities on Carbon Fiber Epoxy Composite Plates by Rigid Sphere Projectiles"
Mayer, Arnold (Wright Laboratory, OH)

"Geometrically Nonlinear Impact Response of Thin Laminated Imperfect Curved Panels"
Kapania*, Rakesh K. and Stoumbos, T.J.G. (VPI)

"A Test Method for Dynamic Properties of Composites under Interior Ballistic Cycles"
Tzeng*, Jerome T. and Abrahamian, A.S. (Army Research Lab, MD)

==========

Tuesday afternoon, August 31, 1993 3:00PM-6:00PM

DAMAGE AND FAILURE

chair: Wanda Sigur (Martin Marietta)
co-chair: Terry Vandiver (US Army Redstone Arsenal, AL)

"Bolted Joint Strength of Graphite/Epoxy Laminates subjected to Biaxial Loading Conditions"
Hoa, S.V. (Concordia U., Canada)

"Static/Dynamic Response of Moderately Thick Composite Structures With Damage"
Averill, Ronald C. (Michigan State U.)

"Generalized Stress and Failure Analysis of Inhomogeneous Anisotropic Structures"
Bogdanovich*, Alex E. and Pastore, C. M. (North Carolina State U.)

"Progressive Failure Analysis of Composite Structures Made of Thermo-Elastic Solids"
Pachajoa, M.E., Lee, K.Y. and Lee*, James (George Washington U.)

"Damage Mechanisms in Metal Matrix Composite Plates"
Voyiadjis*, George Z., Venson, A.R. and Kattan, P.I. (Louisiana State U.)

"Anisotropic Elastic-Damage Models of Coupled Solid Dynamics and Heat Diffusion"
Fahrenthold, Eric P. (U.Texas-Austin)

Wednesday morning, Sept 1, 8:25-8:55 AM
and 10:00 AM-12:30 PM

DESIGN OF COMPOSITE STRUCTURES

chair: Paul Herrington (U. of New Orleans)
co-chair: George Voyiadjis (Louisiana State U.)

"Strength Evaluation of Composite Laminates with Various Holes under Bending"
Zhao, Y., Pang*, Su-Seng and Yang, C. (Louisiana State U.)

"Nonlinear Structural Design Sensitivity Analysis for Composites Undergoing Elastoplastic Deformation"
Chattopadhyay*, Aditi and Guo, R. (Arizona State U.)

"The Dynamic Response of Thick Anisotropic Composite Plates"
Nayfeh*, Adnan H. and Taylor, T.W. (U. of Cincinnati)

"Buckling and Collapse of Suddenly Loaded Structures"
Simitses, George J. (U. of Cincinnati)

"Study of Composite Over-wrap Cylindrical Pressure Vessels"
Kokan, D., Gramoll*, Kurt and Mensah, T. (Georgia Tech)

"Impact of Fiber CompositeLaminated Plates: A Percolation View of Perforation and Spallation"
Jaeger*, Z., Anholt, M., and Mayer, A. H. (Soreq Nuclear Research Center, Israel)

==========

Wednesday afternoon, Sept. 1, 1993 2:00PM-5:00 PM

STRUCTURAL MECHANICS

Chair: Alex Bogdanovich (North Carolina State U.)
co-chair: Adnan Nayfeh (U. of Cincinnati)

"Characterization and Modeling of Viscoelastic Response of Peek Resin and Peek Composite"
Xiao, X.R. (Concordia U.)

"Rate Effects in Composite Materials"
Cantwell, Wesley (Switzerland)

"Technology Programs in Composite Structures at U.S. Army Missile Command"
Vandiver, Terry (US Army Redstone Arsenal, AL)

"Electro-Thermal Mechanics of Spring Loaded Contractile Fiber Bundles with Application to Ionic Polymeric Gel and SMA Actuators"
Shahinpoor, Mohsen (U. of New Mexico)

==========

On the Interface Stability of a Neck Propagating in a Sheet Reinforced with Shape-Memory Fibers

C. Q. Ru and R. C. Batra
Department of Mechanical and Aerospace Engineering and Engineering Mechanics
University of Missouri-Rolla, Rolla, MO 65401-0249

One-dimensional phase transition problems in shape-memory alloys and certain polymers modeled as nonlinear elastic solids have been extensively studied, e.g. see Ericksen (1975), and the solution corresponding to a phase transition between two stable states has been referred to as necking, Hutchinson and Neale (1983). Physicists (e.g. Jacobs (1985)) working in the area of ferroelasticity have examined phase transformations in two-dimensional problems. In two-dimensional solidification problems, it has been found (Davis, 1990) that the straight interface between the solid and liquid phases will become unstable and deform into a cellular one under certain conditions, and may even develop into a more complicated dendritic pattern.

Here we consider a fiber-reinforced flat sheet of unit thickness with fibers aligned along the x-direction, and the end surfaces of the sheet subjected to uniform surface tractions in the x-direction. We assume that the sheet undergoes infinitesimal deformations so that linear kinematic relations apply, and the fibers are densely packed so that lateral deformations of the sheet are negligible. Thus every point of the sheet undergoes a time-dependent displacement u in the x-direction, and u is in general also a function of x and y. Whereas both the fibers and the matrix material are taken to be elastic, the stress-strain curve for the former is taken to be nonlinear with two stable branches, *cf.* Fig. 1, and that for the latter linear. The material of the fibers is presumed to exhibit phase transformations. Also, fibers are assumed to carry all of the tensile load and the matrix material supports the shear stress. Thus

$$\sigma_{xx} = f(\epsilon_{xx}) = \frac{\partial W}{\partial \epsilon_{xx}}, \quad \epsilon_{xx} = u_{,x}; \qquad \sigma_{xy} = 2G\epsilon_{xy} = G\frac{\partial u}{\partial y} = Gu_{,y}. \tag{1}$$

Here σ_{xx} and σ_{xy} are the nonzero components of the Cauchy stress tensor, ϵ_{xx} and ϵ_{xy} are nonvanishing components of the infinitesimal strain tensor, W is the strain-energy density for the fiber material normalized to vanish for null value of ϵ_{xx}, and G is the shear modulus of the matrix material. The axial displacement u is governed by

$$\rho u_{,tt} = f'(\epsilon_{xx})u_{,xx} + Gu_{,yy}. \tag{2}$$

We assume that $\rho > 0$ and $f'(\epsilon_{xx}) > 0$. Here f' denotes the derivative of f with respect to its argument. We note that eqn. (2) differs from that in a solidification problem wherein the governing equation is parabolic. The second term on the right-hand side of eqn. (2) describes the coupling effect between adjacent fibers.

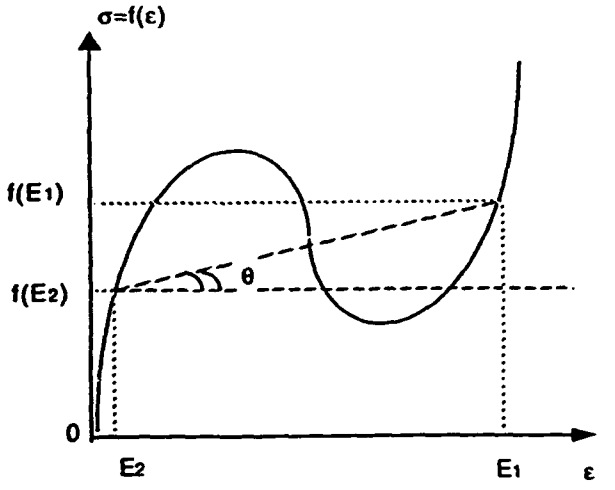

Fig. 1. The stress-strain curve for the shape-memory fibers.

Since fiber material is presumed to exhibit phase transformations, it is conceivable that there is a surface of discontinuity, or a singular surface, in the sheet in the sense that fibers are in different phases on the two sides of this surface. Across this surface, the displacements must be continuous, i.e.,

$$[\![u]\!] = 0 \tag{3}$$

where $[\![u]\!] = u^+ - u^-$ equals the difference in the values of u on the positive and negative sides of the surface; the positive side of the surface being the one on which the outward normal points in the direction of propagation of the surface. If this surface propagates with speed V in the x-direction then the Rankine-Hugoniot condition (see Hutchinson and Neale, 1983) and the balance of total energy require that

$$-\rho V [\![u_x]\!] = [\![f(u_x)]\!], \tag{4}$$

$$-V [\![W + \frac{1}{2}\rho(u_x)^2]\!] = [\![f(u_x)u_x]\!]. \tag{5}$$

We consider a necking solution that is independent of y, and with

$$z = x - Vt \tag{6}$$

can be expressed as

$$u(x,t) = U(z). \tag{7}$$

According to Mullins and Sekerka's method (e.g. see Davis, 1990), we consider a perturbation of the interface geometry in the reference frame $\{z = x - Vt, y, t\}$ moving with the speed V (*cf.* Fig. 2). Thus, let the interface geometry be perturbed to that given by

$$z = z^*(y,t) = \delta \cos ky\, e^{\omega t}, \tag{8}$$

where δ is an infinitesimal number.

We consider a few simple cases for which $V \neq 0$ and examine the interface stability of a propagating neck. For the following three cases, the interface $z = 0$ is found to be stable in the sense of Mullins and Sekerka.

(i) $k = 0$. This corresponds to a one-dimensional problem.

(ii) There is no surface tension, and the two modulii corresponding to the stretches on either side of the neck are equal to each other.

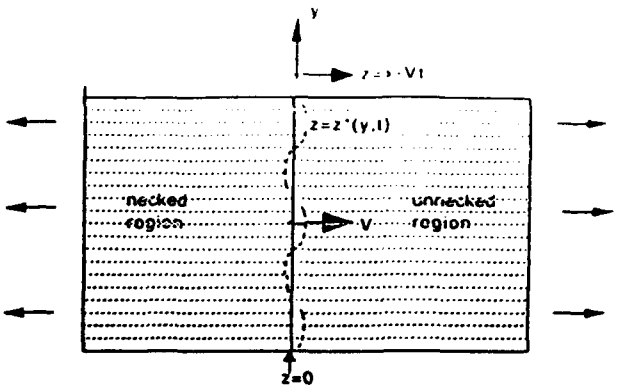

Fig. 2. A schematic sketch of a propagating neck in a uniaxially reinforced sheet.

(iii) The matrix material is very weak so that the shear modulus G can be approximated as zero.

(iv) The fibers are extremely light but are quite strong. However, the stationary interface is always unstable.

REFERENCES

Ericksen, J.L., J. Elast., 5, 191-201, 1975.

Hutchinson, J. W. and Neale, K. W., J. Mech. Phys. Solids, 405-426, 1983.

Jacobs, A.E., Phys. Rev. B, 31, 5984-9,1985; and 46, 8080, 1992.

Davis, S. H., et al., Directional Solidification, in Mechanics USA 1990 (C. F. Chen, ed.), Proc. 11th U.S. National Congress of Appl. Mechs., ASME Press.

Impact Damage Detection in Composite Structures Using Distributed Piezoelectrics

Fu-Kuo Chang

Department of Aeronautics and Astronautics, Stanford University, Stanford, CA 94305

Delamination failure is a major consideration in the design of laminated composite structures. The impact of foreign objects is one of the common causes of delamination in composite structures. However, because impact-induced delamination appears inside the laminates, it can hardly be detected by visual inspection. Therefore, locating the embedded damage is critically important for maintaining and repairing the structures to prevent a catastrophic failure in service.

In this presentation, a damage diagnostic method is proposed to detect the location and size of the embedded damage in composite structures, using measured dynamic responses from distributed piezoelectrics built into the structures. The method consists of three major parts: a dynamic structural analyzer, a response comparator, and a signal generator as shown in Figure 1. The system would function as follows:

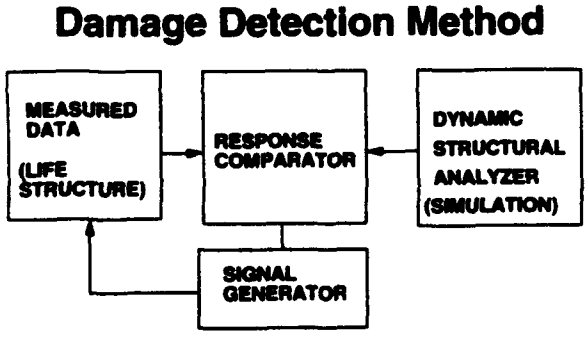

Figure 1 A schematic of the proposed damage detection method.

first, upon impact, the comparator compares the measured responses from the piezoelectrics with the calculated responses from the analyzer to estimate the impact energy and the impact location. Second, appropriate diagnostic signals will be selected by the generator and then dispatched from designated piezoelectric actuators to selected piezoelectric sensors. The measured diagnostic signals from the sensors will then be compared in the comparator with the calculations from the analyzer to determine the damage location and size.

Composite plates with and without an implanted delamination were fabricated with four pairs of piezoceramics patched on the surfaces. One pair of piezoceramics was used as actuators, and the other pairs were treated as sensors. The measured dynamic responses between the damaged and undamaged plates were compared. Figure 2 presents the comparison of the dynamic responses measured from the designated sensors. Considerable differences in dynamic responses between the damaged and undamaged plates were detected, suggesting the presence of damage in the plates.

At present, a method has been developed for detecting the location and size of a delamination in composite beams. The predictions compared with experimental results are presented in Figure 3. The technique successfully detected

the presence of delaminations and predicted with reasonable accuracy the locations and sizes of the damage in the beams.

A method has also been proposed to estimate impact location and the impact force history for a beam subjected to a transient dynamic load. Figure 4 shows that the predicted impact locations based on two sensor measurements agreed with the data very well.

It is anticipated that a health monitoring system such as the one proposed could be developed. However, considerable work both on the development of the methods and on the implementation of the technique is still required.

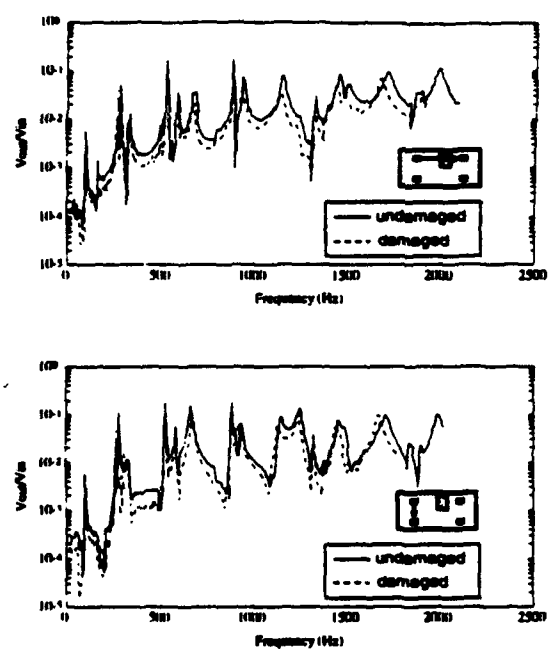

Figure 2 Comparison of sensor measurements of composite plates with and without a delamination. (Upper) Piezoceramic measurements from the sensor at upper right corner. (Below) Piezoceramic measurements from the sensor at lower left corner.

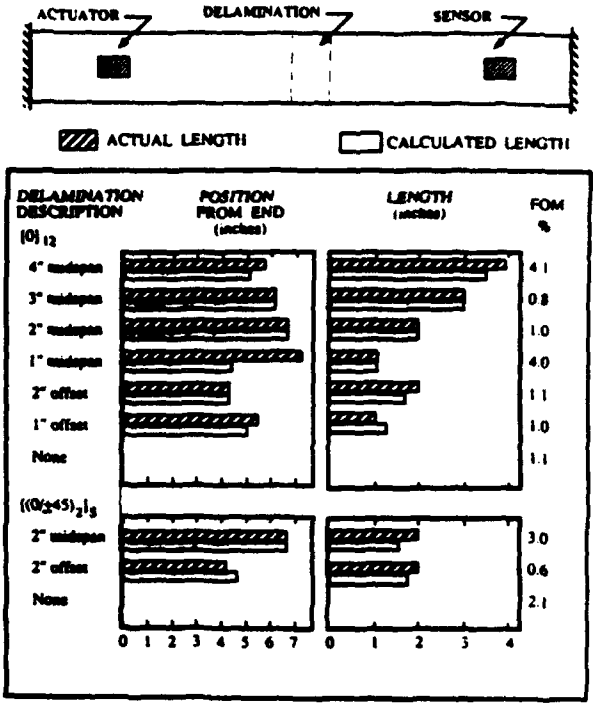

Figure 3 Comparison of predicted delamination locations and sizes in composite beams with actual measurements.

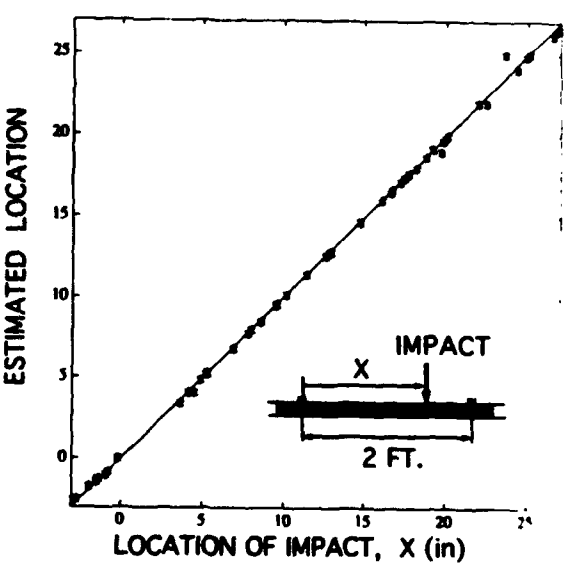

Figure 4 Comparison of impact location between the predictions and the actual measurements.

Dynamic Stresses in Composites at Low Temperatures

Piyush K. Dutta
U.S. Army Cold Regions Research and Engineering Laboratory
Hanover, NH 03755-1290 USA

EXTENDED ABSTRACT

Behavior of polymer composites at low temperature is a neglected area of research, and the dynamic behavior at low temperatures is more so. It is not because that the thermo-physical problems of research at low temperatures are less interesting than the high temperature problems but because that the phenomenal development in technology of composites in the past had been driven by the needs of the aerospace industries which historically have seen more problems with composites at high temperatures than at low temperatures. Of course, it is true that the cryogenic range of low temperature effects on composites have been studied in the past primarily for specific applications, but much wide spread applications of composites through the newly developed land vehicles and water crafts and new applications of composites for civil engineering structures demand a reassessment of the focus of composites research on the dynamic effects at low temperatures.

It is well known that the lowering of temperatures modifies the behavior of composites. The two basic changes that happen in the microstructural behavior of composites are the changes in the elastic modulus of the individual components and secondly in the changes in stress because of mismatched thermal expansion coefficients of these components. Superimposed on these effects will be the effects of high-strain-rate. Figure 1 extracted from Hartwig (1979) shows the dramatic influence of both the low temperature and strain rate on the behavior of the epoxy resin matrix of composites, which would effect the behavior of the composites. The figure shows that low temperature and high strain rate increases the Young's modulus value, E of the polymer matrix. Extending the Rosen's (1965) model of composites failure to tensile loading condition, Dutta (1992) has shown that the maximum critical fiber stress $\sigma_{fcr}(T)$, that would be induced in the composites is given by

$$\sigma_{cr}(T) = 2\left[\frac{V_f E_f (E_m(T_o) + K(T_o - T))}{3(1-V_f)}\right]^{0.5} \quad (1)$$

where E_f = fiber stress, V_f = fiber volume fraction, E_m = matrix modulus, T_o = low temperature, and K is an empirical constant indicative of the new increased modulus of the matrix under the combined effects of low temperature and high strain rate. It is obvious from equation (1) that $\sigma_{cr}(T)$ will rapidly increase to the value of the fiber ultimate strength (Figure 2) if the values of $(E_m(T_o) + K(T_o - T))$ in the numerator increases as a result of temperature decrease, or strain rate increase or both. However, no direct experimental results are currently available to identify the individual effects of these two factors. Currently investigations are underway at CRREL to determine the effects of these two factors separately.

One of the examples of these two combined effects on the composite laminate behavior is seen in the results of the work performed by Dutta, Hui and Altamirano (1991). Figure 3 shows the results of the energy absorption tests by a 30-ply AS4/3502 quasi-isotropic laminated composite when indented by a hemispherical bit under the influence of an incident stress pulse of only 180 microsecond duration. It is seen that in general, at higher velocities of impact, energy absorption increases both at room temperature (21°C) and at low temperature. But at lower velocities where the primary mode of energy absorption, E_c, is by hertzian contact deformation, as outlined by Creszczuk (1982)

$$E_c = (P^{5/3})(4/5)(3\pi/16)^{2/3}\left[(K_1 + K_2)/(R/2)\right] \quad (2)$$

where

$$K_1 = (1-\upsilon_s^2)/(\pi E_s) \quad (3)$$

$$K_2 = (1-\upsilon_z^2)/(\pi E_z) \quad (4)$$

E_s and υ_s are the Young's modulus and Poisson's ratio of the steel indentor, respectively, E_z is the laminate modulus in thickness direction, and υ_z is the laminate's Poisson's ratio. The value E_c clearly decreases with the increased values of E_z as a result of temperature and strain rate.

Similarly, the strain rate dependent behavior of composites in low temperature environment is also important for predicting the crashworthiness of composites used in vehicles or guard rails. It is necessary that serious research effect is undertaken to clearly understand the combined effort of low temperature and high strain rate on composite behavior.

References:

Hartwig, G. (1979). Mechanical and electrical low temperature properties of high polymers. In Nonmetallic Materials and Composites at Low Temperatures (A.F. Clark, R.P. Reed and G. Hartwig, Ed.), New York, Plenum.

Rosen, B.W. (1965). Mechanics of composite strengthening. In Fiber Composite Materials, Am. Soc. Metals Seminar, p 37-75.

Dutta, P.K. (1992). Tensile strength of unidirectional fiber composites at low temperatures. Proc. 6th Japan-US Conference on Composite Materials, June 22-24, Orlando, pp. 782-792.

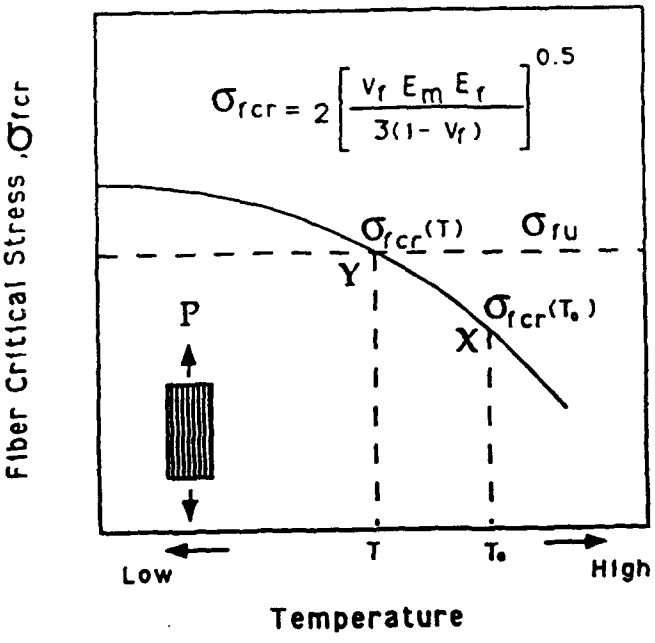

Figure 2. Schematic showing low-temperature induced increase of fiber critical stress.

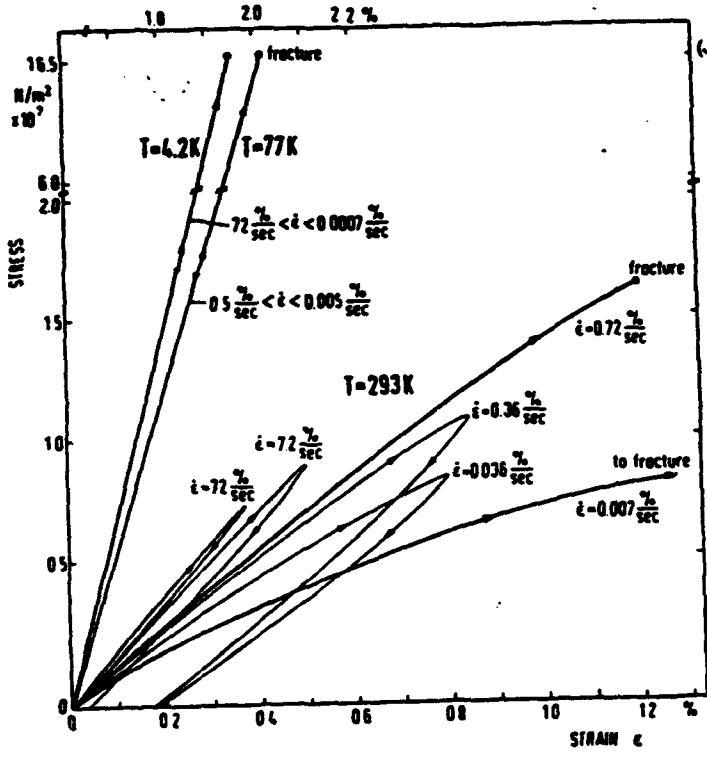

Figure 1. Stress-strain behavior of epoxy resins at different strain rates, $\dot{\varepsilon}$, and temperatures, T (after Hartwig 1979).

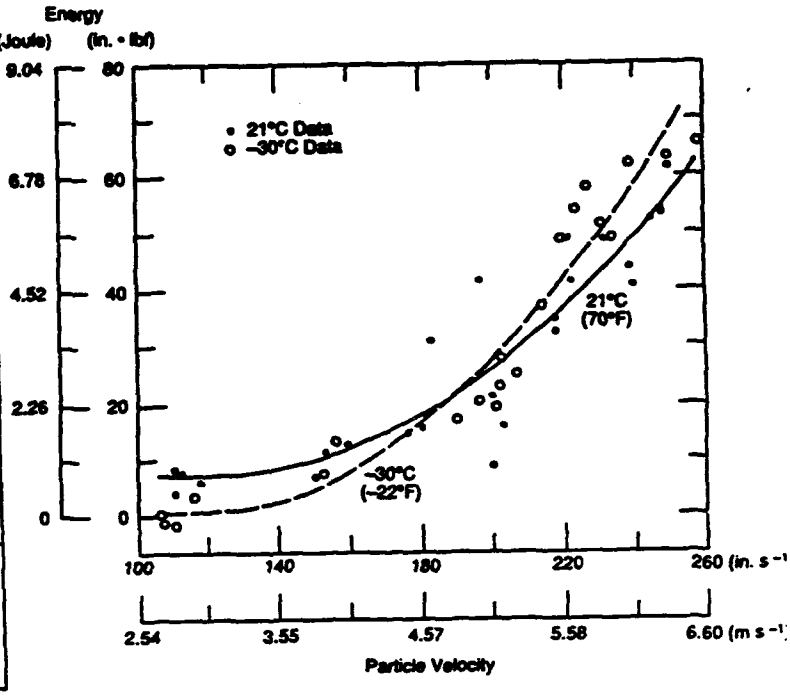

Figure 3. Influence of temperature and velocity on energy absorption.

SAINT-VENANT END EFFECTS IN COMPOSITE STRUCTURES

Cornelius O. Horgan,
Department of Applied Mathematics, School of Engineering and Applied Science,
University of Virginia, Charlottesville, VA 22903

Abstract

Thin-walled structures of interest to the U. S. Army, such as rifle barrels, rocket casings, helicopter blades and containment vessels are often constructed of layers of anisotropic, filament or fiber-reinforced materials which must be designed to remain elastic. A proper assessment of end or edge effects in such structures is of fundamental importance to U. S. Army technology. The extent to which *local* stresses, such as those produced by fasteners and at joints, can penetrate girders, beams, plates and shells must be understood by the designer. Thus a distinction must be made between *global* structural elements (where Strength of Materials or other approximate theories may be used) and *local* elements which require more detailed (and more costly) analyses based on exact elasticity. The neglect of end effects is usually justified by appeals to some form of Saint-Venant's principle and years of experience with *homogeneous isotropic elastic structures* has served to establish this standard procedure. Saint-Venant's principle also is the fundamental basis for static mechanical tests of material properties. Thus property measurements are made in a suitable *gage section* where *uniform* stress and strain states are induced and local effects due to clamping of the specimen are neglected on invoking Saint-Venant's principle. Such traditional applications of Saint-Venant's principle require major modifications when strongly anisotropic and composite materials are of concern. See e.g list of references and the references cited therein. For such materials, local stress effects persist over distances *far greater* than is typical for isotropic materials. In this lecture, we provide a survey of situations in linear elasticity where anisotropy and material inhomogeneity induce such extended Saint-Venant end zones. Both static and dynamic problems are described, although in the latter case relatively few results are known. The implication for the analysis and design of structures using advanced composite materials are addressed.

REFERENCES

Horgan, C. O., and Knowles, J. K., Recent developments concerning Saint-Venant's principle, in *Adv. Appl. Mech.* (T. Y. Wu and J. W. Hutchinson eds.), 23, 179-269, Academic Press, New York, 1983.

Horgan, C. O., Recent developments concerning Saint-Venant's principle: an update, *Appl. Mech. Rev.* 42 (1989), 295-303.

Horgan, C. O., The axisymmetric end problem for transversely isotropic circular cylinders, *Int. J. Solids Struct.* 10 (1974), 837-852.

Choi, I., and Horgan, C. O., Saint-Venant's principle and end effects in anisotropic elasticity, *J. Appl. Mech.* 44 (1977), 424-430.

Choi, I., and Horgan, C. O., Saint-Venant end effects for plane deformation of sandwich strips, *Int. J. Solids Struct.*, 14 (1978), 187-195.

Horgan, C. O., Saint-Venant end effects in composites, *J. Composite Materials*, 16 (1982), 411-422.

Horgan, C. O., and Simmonds, J. G., Asymptotic analysis of an end-loaded, transversely isotropic, elastic, semi-infinite strip weak in shear, *Int. J. Solids Structures* 27 (1991), 1895-1914.

Crafter, E. C., Heise, R. M., Horgan, C. O., and Simmonds, J. G., The eigenvalues for a self-equilibrated, semi-infinite, anisotropic elastic strip, *J. Appl. Mech.* 60 (1993), 276-281.

Fiber Optic Structural Sensing System for a New Road Bridge

R. M. Measures, T. Alavie, R. Maaskant, M.Ohn, S. Karr, S. Huang, D. Glennie, C. Wade*, G. Tadros**, and S. Rizkalla#

University of Toronto Institute for Aerospace Studies
FIBER OPTIC SMART STRUCTURES LABORATORY
4925 Dufferin St., Downsview, Ontario, CANADA
* City of Calgary, Structures and Facilities, Calgary, Alberta, CANADA
** Straight Crossing Inc., 233 - 19th St., N.E., Calgary, Alberta, CANADA
#University of Manitoba, Engineering Bldg., Winnipeg, Manitoba, CANADA

ABSTRACT

The replacement of steel with advanced composite materials represents one of the most significant advances under consideration in the field of Civil Engineering. Since composite materials are unproven in their substitution for steel in concrete structures there is considerable motivation to instrument test structures incorporating these materials in order to gain a through understanding of how well composite materials serve in this new challenging role. We have developed a fiber optic Bragg grating strain gauge that is well suited for embedding within composite structures and has many other attractive attributes. These include the ability to follow the local strain with a very high frequency response while at the same time tracking creep. Lastly, these sensors are immune to electrical interference.

Many civil engineering structures like: bridges, dams, tunnels.... could benefit from a structurally integrated fiber optic sensing system that could monitor the state of the structure throughout its working life. Such an integrated sensing system could also monitor the various structural components during construction, possibly leading to improved quality control. In certain instances this resident sensing system could also provide valuable information on the usage of the structure. For example, in the case of a bridge the sensing system could be used to generate information on the traffic itself.

Two types of carbon prestressing tendons are being tested in a new two-span concrete road bridge that is under construction in Calgary. It was originally planned that UTIAS would instrument six of these girders Bragg grating laser sensors, two with rope, two with Leadline and two with steel.

In the intracore Bragg grating fiber optic sensor the centre (Bragg) wavelength of the reflected signal is linearly dependent upon the product of the scale length of its periodic index variation and the mean core index of refraction. Changes in strain or temperature, to which the optical fiber is subjected, will shift this Bragg wavelength leading to a spectrally encoded optical measurement that can be determined by the simple wavelength dependent ratiometric technique that we have recently developed. We have recently demonstrated that the sensing Bragg grating can be used to control the wavelength of a laser, and for the Calgary bridge project we have developed a 4-channel Bragg grating fiber laser sensor demodulation system. This system involves 4 - independent Bragg grating tuned fiber lasers that are multiplexed in order to be pumped by one semiconductor laser. Each fiber laser is tuned by a connectorized, remote and structurally embedded Bragg grating that serves as a sensor. The measurand controlled wavelength of each fiber laser is determined by a passive ratiometric wavelength demodulation system, pioneered in the UTIAS Fiber Optic Smart Structures Laboratory. The resulting 4-channel Bragg grating fiber laser sensor demodulation system with a laptop computer is rugged, compact and transportable to construction sites where it has been used to undertake measurements on large concrete girders as used for *civil engineering* applications. A schematic of the system is presented as **figure 1.**

To test the performance of the Bragg grating laser strain sensor, Bragg gratings have been adhered to the surface of cantilever beams and the wavelength of the fiber laser measured as a function of the applied strain. Good linearity is observed provided the strain is limited to about 3000 μstrain. Once this is exceeded stress induced birefringence in the optical fiber leads to the appearance of a second peak in the laser spectrum. This undesirable affect can be avoided if polarization maintaining optical fiber is used.

At the University of Manitoba a series of static and fatigue loading tests were performed on concrete girders that were prestressed with the graphite Tokyo Rope and Leadline. Resistive foil strain gauges was adhered to the surface of each of the prestressing cables at roughly their midpoint. Bragg gratings were adhered only to the surface of the prestressing Tokyo ropes, at roughly the same location along the tendon. **Figure 2** shows the the strain, as measured by the Bragg grating laser sensor, plotted against the applied load to the girder.

In the case of the two-span concrete road bridge in Calgary 20 Bragg gratings were embedded into two concrete girders prestressed with steel, two prestressed with Tokyo rope and one girder prestressed with Leadline. In each girder there is at least one Bragg grating temperature sensor and two Bragg grating strain sensors. At the time of writing the bridge is under construction so we hope to provide more details on the use of the Bragg grating fiber laser sensing system in monitoring the strains experienced by the steel and graphite prestressing tendons at theWorkshop itself.

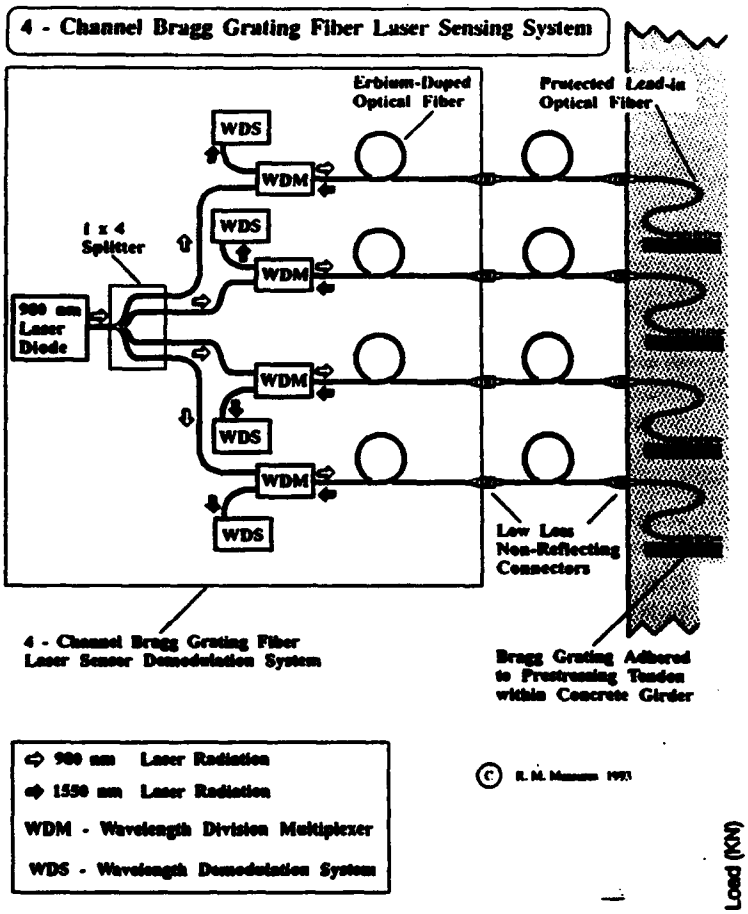

Figure1.

A schematic of the four-channel Bragg grating fiber laser sensor demodulation system used with four Bragg gratings embedded within a concrete structure.

Figure 2.

Variation in the Bragg grating laser sensor strain reading with load applied to test concrete beam prestressed with Tokyo Rope.

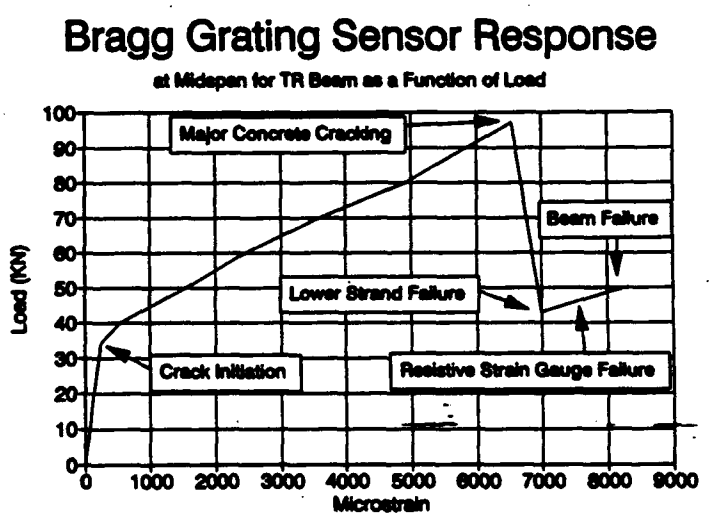

COMPUTATIONAL METHODS FOR PRACTICAL ENGINEERING DESIGN OF THICK COMPOSITE PLATES AND SHELLS

Alexander Tessler
NASA Langley Research Center, Mail Stop 240, Hampton, VA 23681-0001

Design of advanced aircraft, ground-vehicle, and naval structures with multi-layered organic-matrix composite materials requires easy-to-use computational tools which provide accurate predictions of structural response and integrity under mechanical, thermal, and dynamic loads. Unlike metals, composites commonly possess significantly lower strength and stiffness in the direction transverse to the reinforcing fiber as compared to the fiber direction; hence, transverse shear and normal strain and stress effects can significantly contribute to the response and failure of such structures. Consequently, computational tools that are employed in the industrial environment must accurately predict these so-called "secondary" stains and stresses. Conventional shear-deformable theories that are prevalent in commercial codes generally do not provide accurate through the thickness deformations and stresses. Further, nearly all higher-order theories in the literature are impractical for general computational purposes because they do not result in finite elements that are compatible with standard analysis software nor with standard engineering boundary conditions.

The paper first examines recent advances in the area of elastostatic and dynamic analysis of thick laminated composite plates and shells with the specific focus on identifying suitable theories for general-purpose finite element software and industrial applications. Advantages and shortcomings of first- and higher-order theories are discussed both from analytical and computational viewpoints.

A special type of Higher-Order Theory (HOT) for plate and shell analysis which is compatible with existing structural analysis software products and standard engineering boundary conditions is closely examined.[1-3] The theory is based on independent through-the-thickness expansions of displacements, transverse shear strains, and transverse normal stress. Unlike other higher-order theories, it uses a least-squares constraint on the compatibility of deformations and transverse strains which also permits exact satisfaction of upper and lower surface stress equilibrium conditions. The virtual work principle (and, in dynamics, Hamilton's variational principle) is applied to derive the appropriate equations of equilibrium/motion and engineering boundary conditions. As analytical results indicate, the theory is capable of accurately predicting displacements, natural frequencies, mode shapes, and three-dimensional strains and stresses. It yields improved predictions over the first-order theory, particularly for thick laminates and higher vibration frequencies. Moreover, thickness-stretch modes and natural frequencies, which are critical for delamination initiation and which are suppressed in the first-order and many higher-order theories, are accurately predicted.

Figure 1 shows a typical frequency spectra plot for a simply-supported orthotropic square plate where the HOT frequencies for the lowest six modes corresponding to the wave numbers (m,n)=(1,1) are compared with those of three-dimensional elasticity theory (designated as EXACT).

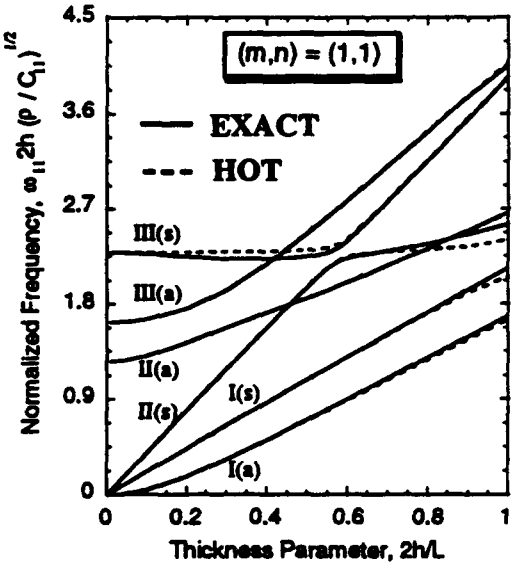

Fig. 1. Frequency spectra for simply-supported, orthotropic square plate for six lowest-frequency thickness modes for wave numbers (m,n)=(1,1).

As can be seen, results agree very favorably with the available exact solutions even in the very thick regime. The corresponding mode shapes for a thick plate are shown in Fig. 2. Though not shown, these modes are also closely correlated with the exact ones.

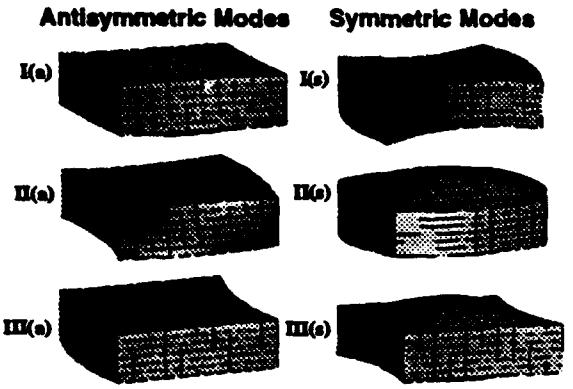

Fig. 2. Six lowest-frequency mode shapes corresponding to wave numbers (m,n)=(1,1) for simply-supported, orthotropic thick square plate (2h/L=0.3).

From the perspective of finite element approximations suitable for general purpose finite element software, this higher-order theory is shown to rely on simple C^0-continuous displacement assumptions that permit efficient and robust finite element formulations. The appropriate approximations for elements of this type are the same as those for conventional first-order elements that have been explored extensively by the author[4] and others. This computational capability enables large-scale analyses of complex multi-layered composite structures, providing improved response and failure predictions using standard engineering software. This is achieved without the additional computational cost that is usually associated with the use of higher-order theories.

A conforming three-node facet shell element and a companion two-node beam element have been formulated and implemented in the general-purpose code COMET (COmputational MEchanics Testbed) so that any structural configuration can be considered. The shell element has also been used in the form of a user-supplied capability in the commercial code ABAQUS.

Additional, 'auxiliary' computational techniques which serve to improve recovery of three-dimensional displacements and mode shapes, strains, and stresses are also discussed, and some of their key features are emphasized. These techniques are generally applied at the post-processing stage of the finite element analysis and address the following areas:

(1) Improved ply-by-ply recovery of displacements and inplane strains and stresses.[5]

(2) Recovery of transverse stresses/strains via integration of three-dimensional equations of equilibrium.

(3) Recovery of physically smooth strain and stress quantities and their partial derivatives by way of the Smoothing Element Analysis (SEA).[6] The latter quantities are required in order to perform integration of three-dimensional equations of equilibrium in (2).

(4) Estimation of residual-equilibrium discretization errors in the finite element analysis in order to guide in adaptive mesh refinement procedures. Such physically meaningful error estimators—which require partial derivatives of stress resultants in plate and shell analyses—are readily computed by way of SEA.

Finally, remarks are offered on the potential use of the aforementioned computational capabilities in the areas of global-local finite element modeling, nonlinear dynamic response, impact damage, and progressive failure in thick composite plate and shell structrures.

REFERENCES

1. Tessler, A., "An improved plate theory of {1,2}-order for thick composite laminates," *Int. J. Solids and Structures*, 30(7), 1993, pp.981-1000.
2. Tessler, A., Saether, E., and Tsui, T., "Vibration of thick laminated composite plates," *J. Sound and Vibration* (to appear, 1993)
3. Tessler, A., "A 10th-order shell theory including transverse shear and normal deformations for elastodynamic analysis of laminated composites," 1st Joint ASCE-EMD, ASME-AMD, & SES Mechanics Conf., Charlottesville, VA (June 6-9, 1993)
4. Tessler, A., "Shear-deformable, anisoparametric flexure elements with penalty relaxation," in *Finite element methods in plate and shell structural analysis*, (eds. T. J. R. Hughes and E. Hinton), Pineridge Press, London (1986).
5. Tessler, A., "Strain and stress computations in thick laminated plates using hierarchical higher-order kinematics," 2nd U.S. National Congress on Computational Mechanics, Washington D.C. (Aug. 16-18, 1993).
6. Tessler, A., Riggs, H. R., and Macy, S., "A variational method for finite element stress recovery and error estimation," *Computer Methods in Applied Mechanics and Engineering* (to appear, 1993).

STATIC AND DYNAMIC RESPONSE OF MODERATELY THICK LAMINATED BEAMS WITH DAMAGE

Ronald C. Averill
Department of Materials Science and Mechanics
Michigan State University
East Lansing, MI 48824-1226

Introduction

The currently available layerwise (or discrete layer) theories provide significant improvements over the equivalent single-layer (or smeared) theories for analysis of thin and moderately thick laminated structures. For practical applications, however, all existing discrete-layer theories give rise to finite element models that are either too computationally expensive or poorly suited for general purpose analysis. In order to take advantage of this powerful class of laminate theories, a new generalized discrete-layer theory and an associated computational model for the analysis of moderately thick laminated beams has been developed[1]. The theory assumes a piecewise linear distribution of the inplane displacements through the thickness of the laminate, and satisfies the stress continuity conditions at the interface between each layer. In this way, the number of degrees of freedom in the theory is made independent of the number of layers in the laminate.

Unlike available theories, the current theory is specially formulated to be ideally suited for solution by the finite element method. A two-noded beam element has been developed that combines the penalty method with an interdependent interpolation scheme, resulting in a simple and efficient C^0 element that is rank sufficient, accurate for both thick and thin beams, and has no apparent defect. The accuracy of the computational model has been demonstrated for static and vibration analysis of thin and thick laminated beams, with and without delaminations and/or ply damage. It has been shown that layerwise variations of the inplane displacements must be taken into account when modelling either the global or local response of damaged laminates.

Approach

In the current theory, the continuity requirements on the displacement variables of the discrete-layer laminate theory of DiSciuva (*J. Sound and Vib.*, Vol. 105, pp. 425-442, 1986) are reduced by momentarily relaxing the condition of continuous transverse shear stresses. Two new degrees of freedom are introduced to replace the expressions in the original theory that give rise to the problematical C^1 continuity requirement. In order to ensure the continuity of transverse shearing stresses, a constraint condition is then added to the statement of the displacement field and its associated functional, so the new form of the theory can be shown to have the same properties as the original theory of DiSciuva. By imposing such a constraint via the penalty function concept, the transverse shear stresses are made continuous without introducing additional degrees of freedom. Furthermore, C^0 continuity of all degrees of freedom is maintained, allowing for a simple, efficient, and accurate finite element model of the governing equations.

The finite element model based on the above laminate theory takes advantage of the interdependent interpolation concept introduced by Tessler and Hughes (*Comp. Meth. Appl. Mech. Eng.*, Vol. 39, pp. 311-335, 1983). As a result, the linear part of the constraint is satisfied identically, the approximation order of the element is effectively increased without adding more degrees of freedom, and the possibility of shear locking is eliminated. The proposed discrete-layer finite element model is thus much more efficient, convenient and widely applicable than any one developed to date.

Numerical Results

A simply-supported (0/d/90/0) beam has been analyzed, where d represents a full-length delamination, modelled as a very thin compliant layer. The normalized center deflection due to a sinusoidal load is plotted versus the span-to-thickness ratio in Figure 1. The center deflections are normalized by those of the exact solution obtained by Pagano (*J. Comp. Mat.*, Vol. 3, pp. 398-411, 1969). For beams with an aspect ratio less than 500, the first-order shear deformation theory (FST) and the third-order theory of Lo, Christenson, and Wu (LCW) do not accurately predict the global deflection behavior, while the current discrete-layer model (ZZ) is nearly exact for all thickness ratios greater than 8.

The reason for the poor predictions of the equivalent single layer theories (FST and LCW) is illustrated in Figure 2, where the inplane displacement at the end of the beam is plotted versus the normalized thickness coordinate

[1] Extension of the theory and computational model to plates and shells is currently underway.

for the case $L/h = 10$. It can be seen in Figure 2 that a piecewise linear variation of displacement through the thickness of a laminate is necessary to adequately model the kinematics of a laminate with a delamination or any type of damage resulting in adjacent layers with greatly different shear stiffnesses. The predictions of the current model are indistinguishable from those of the exact solution of Pagano. Predictions of the through-thickness variation of inplane stress components (not shown) are equally as accurate using the current model.

The layerwise kinematics also affect the dynamic response predictions, as seen in Figure 3. Here, the ratio of the first four natural frequencies of the delaminated beam predicted by FST and ZZ are plotted versus the span-to-thickness ratio. For moderately thick beams, the FST predicts the first four natural frequencies of the beam to be approximately two times greater than those predicted by ZZ. The difference in the predictions increases as the mode number increases, and decreases as the beam becomes thinner.

These results have implications for all post-damage analysis as well as analysis of laminated smart structures.

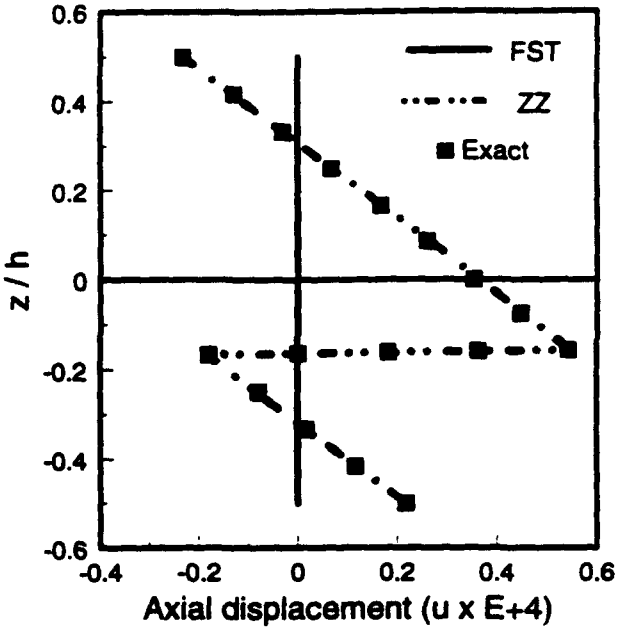

Figure 2.
Axial displacement versus normalized thickness coordinate at the end of a simply supported (0/d/90/0) beam subjected to a sinusoidal load.

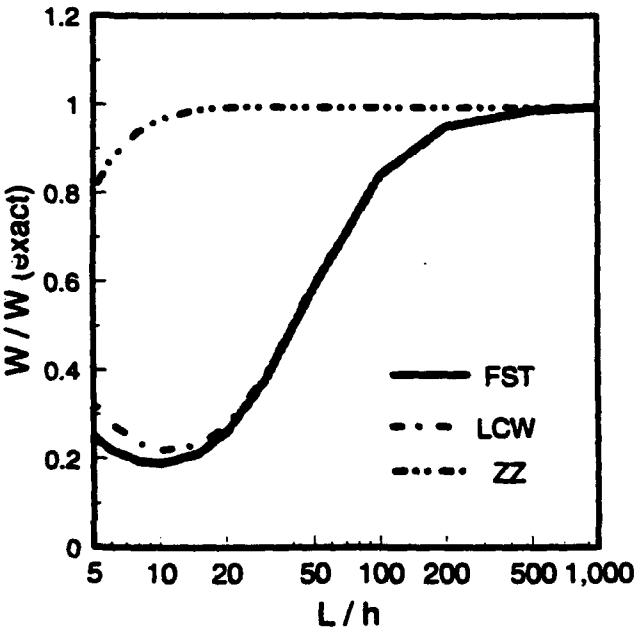

Figure 1.
Normalized center deflection versus span-to-thickness ratio of a simply supported (0/d/90/0) beam subjected to a sinusoidal load.

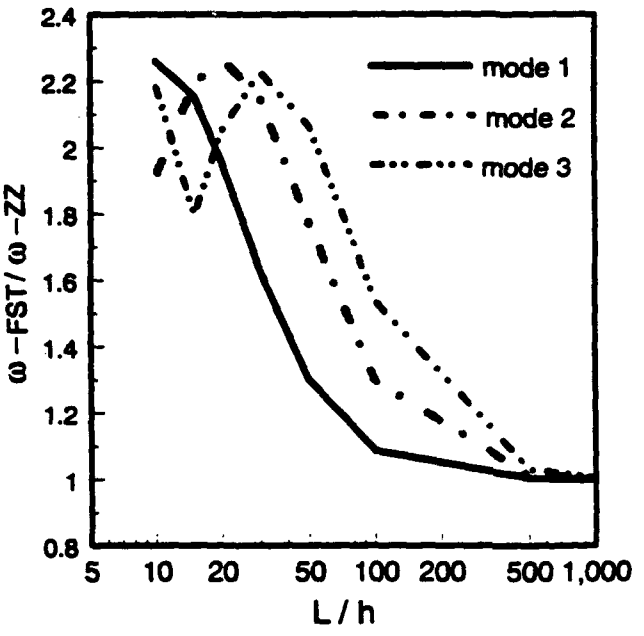

Figure 3.
Ratio of flexural frequencies predicted by FST and ZZ versus span-to-thickness ratio for a simply supported (0/d/90/0) beam.

ACTIVE COMPOSITE TORQUE-PLATE FINS FOR SUBSONIC MISSILES

Ron Barrett
Aerospace Engineering Department, University of Kansas, Lawrence, KS 66045 U.S.A.

A study on the working principles and structural arrangements of active composite torque-plate missile fins is presented. The design evolution from active fin twist to torque-plate design shows that early designs proposed by experimenters like Crawley, Lazarus and Warkentin (1989) provided a valuable starting point for a host of new designs. This early design of adaptive lifting surface was composed of a bending-twist coupled graphite-epoxy plate which had lead zirconate titanate (PZT) piezoelectric sheets laminated on either side of the plate. As the PZT sheets were alternatively contracted and extended to induce a bending deformation, the plate also twisted. The plate was exposed to air loads. Accordingly, small active twist deformations resulted in larger deflections through active aeroservoelasticity.

This first successful design lead to the development of the torque-plate fin configuration. One of the design compromises that was necessary for the bending-twist coupled plate design was to make it thick enough so that bending loads could be carried. Unfortunately, as the thickness was increased, the deflections decreased. So a new design was conceived. This torque-plate fin design alleviates this thickness-deflection design compromise. Fig. 1 shows the evolution to the torque plate design as initially proposed by Barrett (1992[1,2,3]). This design is strengthened in bending by a spar at the quarter-chord and provides much more control than the twisting plate design as the entire aerodynamic shell undergoes a pitch change. If the spar is moved aft, then aeroservoelastic properties may also be used to effectively magnify the pitch deflections.

The torque-plate fin design of Barrett (1992[1,2,3]) used directionally attached piezoelectric (DAP) elements bonded to an isotropic substrate antisymmetrically. The plate was optimized to provide the maximum twist from commercially available stock. However, another design which uses symmetric elements can provide significantly higher twist deflections. An examination of the plate performance using laminated plate theory clearly illustrates the potential of this new arrangement.

Using the analysis techniques outlined by Barrett (1992[1,2,3]), the properties of DAP lamina can be estimated. Fundamentally, they are modeled as having different stiffnesses in the longitudinal and lateral directions, but with equal actuation strains. For a symmetric torque-plate with an isotropic substrate and a main spar that stiffens the plate in bending, the laminate twist can be solved for as shown in equation 1.

$$\kappa_{12} = \frac{D_{22_1}\left(B_{16}+B_{26}\right)_a - D_{26_1}\left(B_{22}+B_{12}\right)_a}{2\left(D_{22}D_{66}-D_{26}^2\right)_1} \qquad (1)$$

If the plate is further constrained so that neither longitudinal nor transverse bending is allowed, then equation 1 simplifies and can be broken down into its components as shown in equation 2.

$$\kappa_{12} = \frac{B_{16a}}{D_{66_1}} = \frac{\left(E_L - E_T\right)\left(t_s t_a + t_a^2\right)}{\frac{E_s t_s}{6}\left(\frac{1-\nu_{LT}\nu_{TL}}{1+\nu_s}\right) + \left(E_L + E_T - 2E_T\nu_{LT}\right)\left(\frac{t_s^2 t_a}{2} + t_s t_a^2 + \frac{2t_a^3}{3}\right)} \Lambda \qquad (2)$$

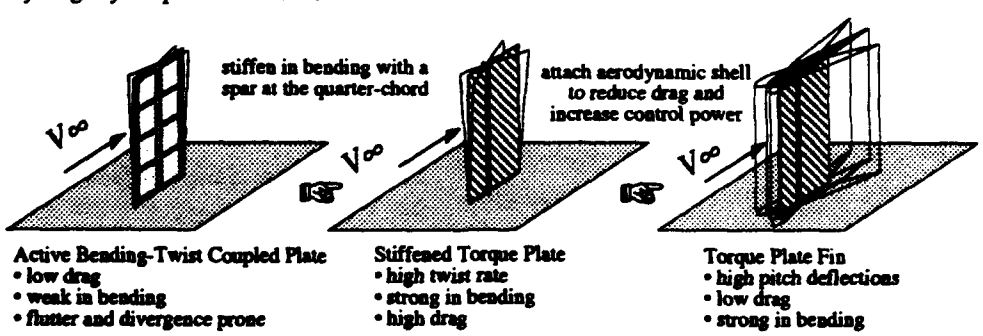

Fig. 1 Design evolution from active plate to torque-plate fin configuration

Similar equations can be derived for other forms of orthotropic actuator elements like piezoelectric fiber composites (PFC). PFCs are similar to DAP elements analytically in that they have differing stiffnesses longitudinally and laterally. However, their active strains are also unequal. For analysis, a nondimensional twist parameter is defined in equation 3 so that the different types of materials may be compared on equal thickness elements, where OR is the orthotropy ratio of the actuator element, AR is the activation ratio, TR is the thickness ratio of the actuator to the substrate, and SR is the stiffness ratio of the actuator to the substrate.

$$TP \equiv \frac{t_s K_{12}}{\Lambda} = \frac{A_R\left[\left(O_R - \nu_{LT}\right) - O_{R\Lambda}\left(1-\nu_{LT}\right)\right]\left(T_R + T_R^2\right)}{\left(\frac{O_R - \nu_{LT}^2}{6T_R S_R\left(1+\nu_s\right)}\right) + \left(O_R + 1 - 2\nu_{LT}\right)\left(\frac{1}{2} + T_R + \frac{2T_R^2}{3}\right)} \qquad (3)$$

Figure 2 shows that TP values approaching 1.5 are regularly attainable using well proven assembly techniques and two-axis bending constraint with a symmetric layup.

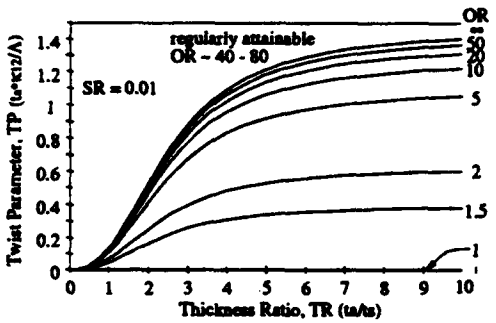

Fig. 2 Twist Parameter for a symmetric DAP laminate with an uncoupled substrate

If PFCs are used to induce twist in a similar manner, then interdigitated electrodes must be used to achieve TP levels approaching that of DAP elements. The interdigitation of the electrodes will induce actuation strains of opposite signs in the actuator plies. As can be seen in Fig. 3, only at very high fiber volume fractions and very large negative strain orthotropies can the PFC laminate surpass the performance of the DAP laminate. However, it should also be noted that if the modulus stiffness ratio, MSR, is increased to 1, then the laminate will resemble a sheet of PZT in stiffness and accordingly, the twist induced by the PFC composite will far surpass that of the DAP laminate.

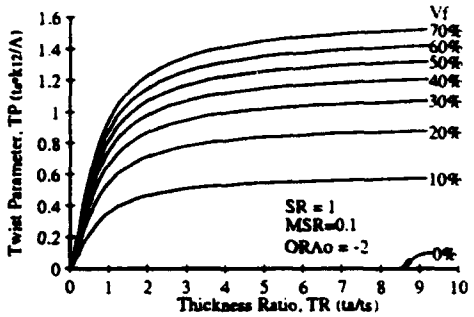

Fig. 3 Twist parameter for a symmetric PFC laminate with an uncoupled substrate

A comparison of the stiffnesses of the two materials shows similar trends. (The stiffness is important in maintaining a high flutter and divergence speed.)

A final examination of the performance gains that are possible through the new structural arrangement is also conducted. This study demonstrates that the amounts of twist deflection obtained by Barrett (1992[1,2,3]) can be nearly doubled and the torsional stiffness may also be increased. This new discovery indicates that aeroservoelastic coupling may no longer be needed for induction of high pitch deflections in missile fins.

REFERENCES

Barrett, R. M. (1992[1]). Wing Pitch Angle Control Device. *Invention Disclosure to the University of Maryland*, UM92-028, Submitted to the U.S. Office of Trademarks and Patents (under review).

Barrett, R. M. (1992[2]). Actuation Strain Decoupling Through Enhanced Directional Attachment in Plates and Aerodynamic Surfaces. Proceedings of the 1st *European Conference on Smart Structures and Materials*, Glasgow, Scotland, pp. 383-386.

Barrett, R. M. (1992[3]). Active Plate and Wing Research Using EDAP Elements. *Journal of Smart Materials and Structures*, Vol. 1, No. 3, pp. 214-226.

Crawley, E.F., Lazarus, K.B., and Warkentin, D. J. (1989). Embedded Actuation and Processing in Intelligent Materials. *2nd Int. Workshop on Comp. Mat'ls and Structures*. Troy, NY.

ARO Workshop on
Dynamic Response of Composite Structures
New Orleans, LA - August, 1993

OPTIMAL VIBRATION CONTROL OF NITINOL-REINFORCED COMPOSITES

A. Baz and J. Ro
Mechanical Engineering Department
The Catholic University of America
Washington, DC 20064

ABSTRACT

Shape memory fibers, made of a NIckel-TItanium alloy (NITINOL), are embedded inside a new class of SMART composite beams in order to control the dynamic characteristics and the damped response of these beams when subjected to external excitations. The NITINOL fibers are tuned by adjusting their initial tension and operating temperature to achieve an optimal balance between the thermal softening of the composite matrix, the stiffening effect imparted by the activated fibers and the enhanced damping of the matrix as it is heated towards its glass transition region.

A finite element model is developed to model the dynamics of damped NITINOL-reinforced composite beams. The model is utilized to compute the natural frequencies, the modal loss factors and the frequency response functions of this class of SMART beams. The frequency responses of the NITINOL-reinforced beams are compared with those of the unreinforced beams in order to emphasize the importance of the NITINOL reinforcement and its optimal tuning in significantly attenuating the vibration of these beams.

1. INTRODUCTION

Considerable attention has been devoted recently to the utilization of the Shape Memory NIckel-TItanium alloy (NITINOL) in developing SMART composites that are capable of adapting intelligently to external disturbances (Baz et al. 1990 and 1991). The emphasis has, however, been placed on stiffening the NITINOL composites through proper activation of the shape memory fibers. Such an emphasis is particularly important when the static characteristics, as the critical buckling loads, are to be controlled. But, when the dynamic response is of concern, the stiffening mechanism alone becomes ineffective in attenuating vibrations resulting from broad band excitations unless it is augmented with a controlled energy dissipation mechanism. Fortunately, NITINOL composites have a unique source of damping which is built-in the composite matrix itself. No attempt has, however, been made to exploit the excellent features of this built-in damping source.

It is therefore the purpose of this paper to simultaneously utilize both the stiffening and the energy dissipation mechanisms to achieve optimal vibration attenuation over broad frequency spectrum. The nature of interaction between the two mechanisms will be investigated and the conditions that ensure optimal balance between them will be determined.

2. DYNAMICS OF DAMPED NITINOL-REINFORCED COMPOSITE BEAMS

The dynamic characteristics of a NITINOL-reinforced beam element, shown in Figure (1), is governed by the following equation of motion:

$$[M_e]\,[\ddot{\delta}] + [K_e]\,[\delta] = [F]. \qquad (1)$$

where $[\delta]$ and $[\ddot{\delta}]$ denote the nodal deflection and acceleration vectors. The stiffness matrix $[K_e]$ of the element are given by:

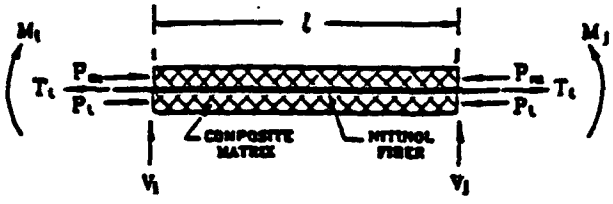

Fig. (1) - NITINOL-reinforced beam element.

$$[K_e] = E_m I_m \int_0^{\ell} [D]^T[D]\,dx - P_m \int_0^{\ell} [C]^T[C]\,dx. \qquad (2)$$

where $E_m I_m$ is the flexural rigidity of the beam element, ℓ is its length, and P_m is the net axial force acting on the element. Also, the matrices [C] and [D] are determined from the transverse displacement function w as follows:

$$w = [A][\delta], \quad dw/dx = [C][\delta] \text{ and } d^2w/dx^2 = [D][\delta]. \qquad (3)$$

The elements $M_e(i,j)$ of the mass matrix $[M_e]$ of the beam element are obtained using the consistent mass formulation as follows:

$$M_e(i,j) = \rho_m A_m \int_0^{\ell} [A_i]\,[A_j]\,dx \qquad (4)$$

where $[A_i]$ and $[A_j]$ are the ith and jth elements of the vector [A] given by equation (3). Also in equation (4), ρ_m and A_m denote the density and cross sectional area of the composite beam. In equation (2), the force $P_m = P_m + P_t - T_t$ where P_m, P_t and T_t denote the axial mechanical loads, the axial thermal load and the total tension developed by the NITINOL fibers respectively. The thermal load $P_t = \alpha\,\Delta\theta\,E_m\,A_m$, is generated by the temperature difference $\Delta\theta$ caused by the activation and de-activation of the NITINOL fibers. Also, α and E_m denote the thermal expansion coefficient of the composite and its modulus of elasticity.

It is important here to note that the activation and deactivation of the NITINOL fibers vary, on one hand, the tension T_t and control the stiffness of the composite and compensate for the softening of the matrix due to the associated heating. On the other hand, it controls the damping characteristics of the composite. This is attributed to the fact that the modulus of elasticity E_m of the composite beam is a complex modulus ($E_m = E'(1 + i\,\eta)$) whose storage modulus E' and loss factor η are controlled by the temperature and frequency of the composite.

3. PERFORMANCE OF DAMPED NITINOL-REINFORCED BEAMS

Materials The characteristics of NITINOL-reinforced beams are determined for a composite beam made of randomly oriented glass fibers embedded in a low cure temperature polyester resin. The beam is 30 cm long, 2.5 cm wide and 0.156 cm thick mounted in clamped-clamped arrangement. The temperature and frequency dependence of the complex modulus of the beam, is shown in Figure (2). Such reduced frequency nomograph is obtained experimentally. The displayed characteristics show typical behavior of structural composites where the storage modulus E' decreases as the operating temperature is increased. It shows also that the damping characteristics of composites increase significantly as their operating temperature is increased towards the glass transition region.

In NITINOL composites, it is possible to compensate for the degradation of the storage modulus of the composite with temperature by tuning the NITINOL fibers properly. The fibers can be tailored to produce their phase recovery forces to counterbalance the softening of the composite matrix with increased temperature. Such an important feature when combined with the enhanced damping at high temperature can be extremely effective in attenuating structural vibrations.

In the present study, four NITINOL 55 fibers that are 0.55 mm in diameter, are embedded inside the beam through vulcanized rubber sleeves that have outer diameter of 0.95 mm.

The characteristics shown in Figure (2) is utilized along with the finite element model to compute the frequency response of NITINOL composites at different temperatures and initial tensions.

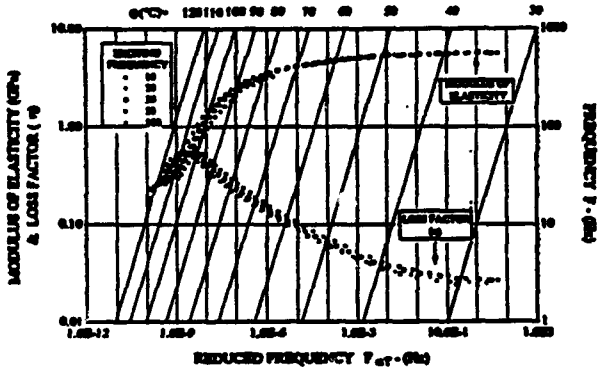

Fig. (2) - Reduced frequency nomograph for the fiberglass/resin composite beam

Vibration control The optimal tuning of the initial tension and operating temperature of the NITINOL fibers is determined in order to minimize the maximum amplitude of vibration of the composite beam when subjected to external excitations. Such amplitude of vibration is measured by the maximum frequency response function (FRF) β_{max} which is determined from:

$$\beta_{max} = \max_{i,j,\omega} \sum_{n=1}^{N} [\phi_n(i)\phi_n(j)] \; / \; [\omega_n^2 - \omega^2 + i\,\eta_n\,\omega_n] \qquad (5)$$

where $\phi_n(i)$, ω_n and η_n denote the mode shape at location i for the nth mode, the natural frequency of the nth mode and the loss factor at the nth mode respectively. The three parameters $\phi_n(i)$, ω_n and η_n are obtained from the solution of the eigenvalue problem of the homogeneous equation of motion of the composite beam which is given by equation (1). In equation (5), ω denote the excitation frequency of a force located at j.

Figure (3) shows the effect of the temperature and initial tension on the maximum FRF indicating that there is an optimal operating temperature for each value of the initial tension. At that temperature, the maximum FRF attains its minimum value. Figure (4) shows the FRF, at beam mid-span due to excitation at the same location, as a function of the excitation frequency for optimally tuned and activated fibers at initial tensions of 13.34 and 31.14 N/fiber respectively.

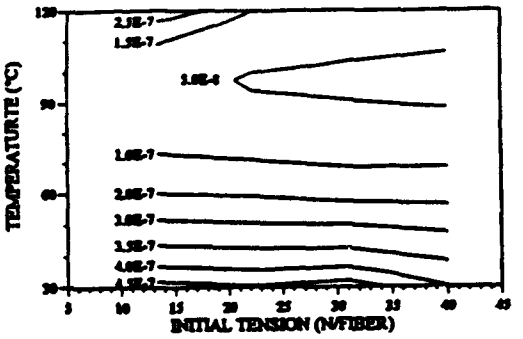

Fig. (3) - Contours of iso-FRF.

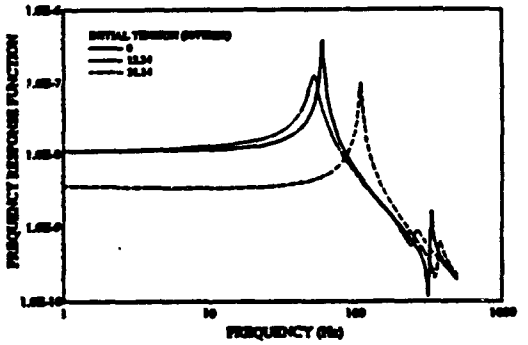

Fig. (4) - Effect of tension & frequency on FRF.

4. CONCLUSIONS

The dynamic characteristics of damped NITINOL-reinforced composite beams have been presented. The fundamental issues governing the behavior of this new class of SMART composites have been introduced. Particular emphasis is placed on the utilization of both the stiffening and the energy dissipation mechanisms, which are inherent to NITINOL composite, to achieve optimal vibration attenuation over broad frequency spectrum. The nature of interaction between the two mechanisms is investigated and the conditions that ensure optimal balance between them is determined.

ACKNOWLEDGEMENTS

This work is funded by a grant from the US Army Research Office (Grant number DAAL03-89-G-0084). Special thanks are due to Dr. Gary Anderson, the technical monitor, for his invaluable inputs.

REFERENCES

Baz, A., et. al., "Active control of of NITINOL-reinforced Composite Beams", in *Intelligent Structural Systems*, ed. by H.Tzou and G. Anderson, Kluwer Academic Press, The Netherland, pp.169-213, 1992.

Baz, A., and J. Ro, "Thermo-dynamic Characteristics of NITINOL-Reinforced Composite Beams", *J.of Composite Engineering*, Vol.2, pp.527-542, 1992.

High-Frequency Composite Beam Dynamics

A.R. Atilgan,[#] V.L. Berdichevsky,[*] C.E.S. Cesnik,[**] D.H. Hodges,[*] and V.G. Sutyrin[***]

School of Aerospace Engineering, Georgia Institute of Technology
Atlanta, Georgia 30332-0150

The classical theory of composite beam vibrations fails to predict a correct dynamical response if high frequencies ($\omega h/\sqrt{G/\rho} \approx 1$, ω - frequency, h - beam thickness, G - shear modulus, ρ - mass density) and short waves ($h/l \approx 1$, l - wave length) are involved. We are developing an improved theory of composite beam vibrations which captures the major phenomena unaccessible to classical theory.

Probably the first attempt to extend the classical one-dimensional beam theory was made by Rayleigh, taking into account the inertia of cross sectional motion to describe the beam behavior more properly under impact load. Then, Timoshenko generalized the classical one-dimensional beam theory by introducing shear deformation to describe the stress state of short waves. Although corrections by Rayleigh and Timoshenko are physically meaningful, quantitative results were usually poor.

A more fundamental base for construction of improved one-dimensional theory was created by Mindlin. He found the key reasoning to improve classical theory: the theory should predict branches of the dispersion curve. The more branches are predicted, the better the accuracy of the theory. Classical theory describes only low-frequency branches. Mindlin suggested a method to incorporate high-frequency branches, but his approach contained some free parameters which should be chosen from fitting the dispersion curves of 1D theory and the exact dispersion curves. Unfortunately, the exact dispersion curves are known only for simplest cases, such as an isotropic homogeneous plate or an isotropic beam with circular cross-section. A method of derivation of 1D theory which automatically guarantees coincidence of dispersion curves of 1D theory and exact dispersion curves has been proposed by V. Berdichevsky about 15 years ago. Later, it was applied to developing an improved 1D theory of isotropic homogeneous (or layered) plate, shells and beams by V. Berdichevsky, Le Khank Chao, M. Riazantzeva and S. Kvashnina. The method has proven to be very efficient. In the study in progress now, we are going to apply this method to developing a 1D dynamical theory of anisotropic inhomogeneous beam. In this talk, some preliminary results are presented.

The key point is to find the cross-sectional modes for high-frequency branches. A code was developed to find these modes numerically for beams with arbitrary anisotropy and inhomogeneity. The big surprise of the first runs is that for some typical types of anisotropy, the first high frequency mode is not the transverse shear mode, as is assumed in Timoshenko's theory, but some in-plane, cross-sectional deformation. That explains why Timoshenko's theory does not work well for composite beams. A parametric study for the first high-frequency modes of a thin strip, anti-symmetric angle ply laminate has been conducted. Four nonclassical modes with the lowest frequencies are shown in Figure 1.

Visiting Scholar. Presently Associate Professor, Mechanics Division, Dept. of Civil Engineering, Istanbul Technical University.

* Professor

** Graduate Student. Fellow of Embraer-Empresa Brasileira de Aeronautica S.A.

*** Visiting Scholar.

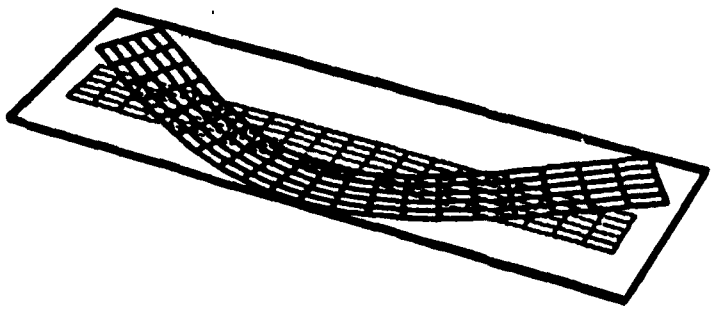

Fig.1 a: Mode 1 – $\theta = 15°$

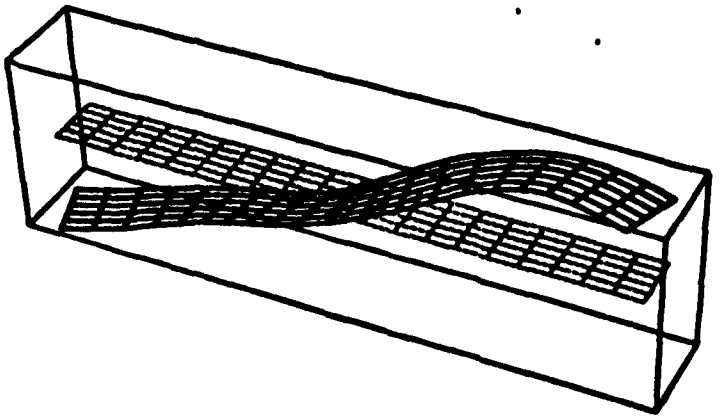

Fig. 1 c: Mode 3 – $\theta = 15°$

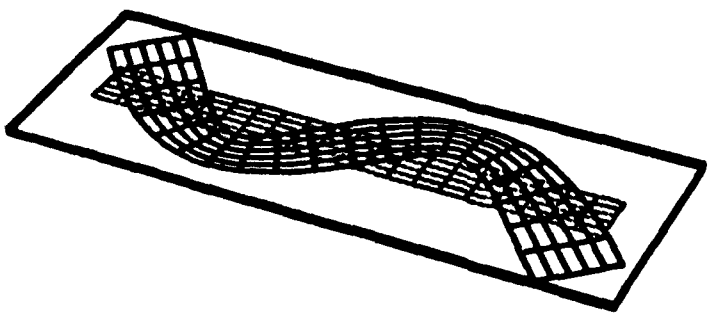

Fig. 1 b: Mode 2 – $\theta = 15°$

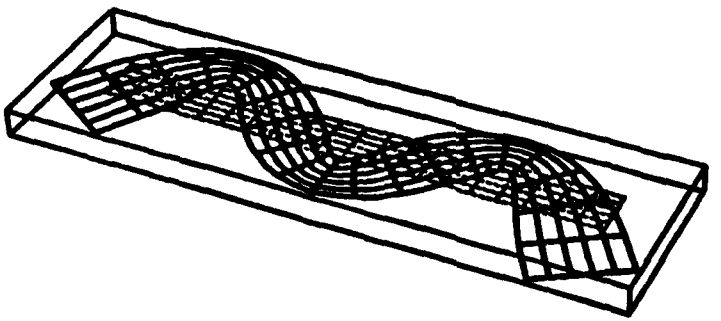

Fig. 1 d: Mode 4 – $\theta = 15°$

Fig. 1: Cross-sectional mode shapes for $[15°/-15°]$

GENERSLIZED STRESS AND FAILURE ANALYSIS OF INHOMOGENEOUS ANYSOTROPIC STRUCTURES

Alexander E. Bogdanovich and Christopher M. Pastore
Textile Material Science, North Carolina State University, Raleigh, NC 27695 U.S.A.

A method of structural analysis based on the spline–sublayer approach is presented. This method was developed to understand the mechanical behavior of inhomogeneous structures, particularly composites, as existing commercial packages do not satisfy the fundamental requirements. In particular, the method is capable of:

- analysis of laminated composite structures providing continuous through the thickness distribution of normal stresses
- analysis of textile composites with elastic properties changing through the volume of the composite
- analysis of progressive damage of composites

For the correct prediction of the behavior of structures both the conditions of continuity for displacements and transverse stresses must be satisfied at each interface of the structure. The continuity of transverse stresses can be satisfied only if transverse strains are discontinuous at each interface, as follows from stress–strain relationships. This leads to the discontinuity of the first derivatives of the displacements. Hence, only those kinematic models which incorporate these discontinuities are correct [1]. Three examples are considered in this paper to demonstrate the power of described technique:

A three–layer [0/90]s graphite/epoxy plate simply supported along its four side edges is considered for progressive damage analysis. The square plate has length a and thickness h. All three layers are of the same thickness. A normal load is applied on the top (z=h) surface as

$$q_z(x,y) = -q_0 \sin(\pi x/a) \sin(\pi y/b) \qquad (1)$$

where $q_0 > 0$. The first step of the initial failure analysis is to define the load, point and mode of initial failure. After a computer "scanning" of the plate volume is applied to all six stress components normalized by corresponding ultimate stress values (and designated further with an asterisk), the greatest is obtained. In this particular example, the maximum stress criterion was first satisfied at q_0=0.779 Msi for the σ_y^* component at x = y = 0.5a, and z=0. Then, in the parallelepiped zone around this point in which the inequality

$$\sigma_y^* > 0.98 \qquad (2)$$

is satisfied, the moduli E_{22}, G_{12} and G_{32} have been reduced (10 times for this particular calculation). Equation (2) defines the damaged zone extending over the region $0.45 < x/a < 0.55$ and $0.45 < y/a < 0.55$, the damaged zone being taken as the bottom layer. The next step in the gradual failure analysis requires one to define the new distribution of the normalized stresses and the dimensions of the zone damaged by that stresses. Then the stiffnesses in this zone have to be reduced. After this is done using the same approaches as in the first step, the new stress distributions are obtained around the new damaged zone. The variation of σ_y^* on z and x coordinates is shown in Figure 1. The stress concentration is higher than after the first step, but is more localized. This indicates that the gradual failure process will stop extending after several steps of the analysis due to decreasing σ_y^* in both x and y directions. In order to continue the analysis, the applied load has to be increased. Then at some step of the analysis another failure mods will be revealed.

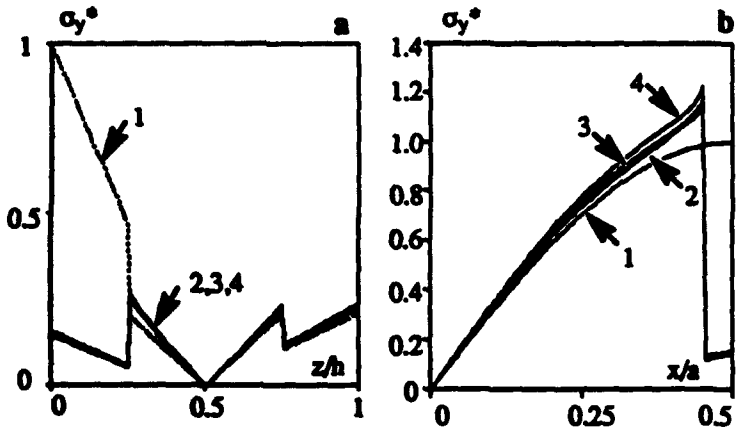

Fig. 1. Variation of the normalized stress σ_y^* along z coordinate at x=0.5a, y=0.5a (a) and along x coordinate at y=0.5a, z=0 (b) for the undamaged plate (curve 1) and the damaged plate (2,3,4) with 3 different discretization meshes

A double box beam spar, exhibiting quasi–unbalanced behavior was considered. It exhibits twist–bend coupling without extension–shear coupling. Both experimental and analytical results have been obtained for twist/bend ratio of the spar for different reinforcement angles. The geometry of the spar was as follows: a = 900 mm, b = 46 mm, h = 48 mm, d = 1 mm. The elastic properties of the Uniweave fabric composite are: E_l = 128 GPa, E_t = 12.1 GPa, ν_{lt} = 0.26, ν_{tt} = 0.2, G_{lt} = 4.56 GPa, and G_{tt} = 5.01 GPa. The analytical and experimental data are compared in Figure 2. The analysis was performed for the length–to–wall thickness ratio 150 (instead of 900), to reduce the number of degrees of freedom employed, while operating at the maximum acceptable element aspect ratio. Despite this simplification of the model, the results match well to the experimental data. Not only are the general trends the same, but also the twist/bend ratio values for the range of reinforcement orientation values are close. It should be pointed out that not one of the previous theoretical models was able to account for a continuous variation of elastic properties around a composite box beam cross section as well as for different "non–classical" effects.

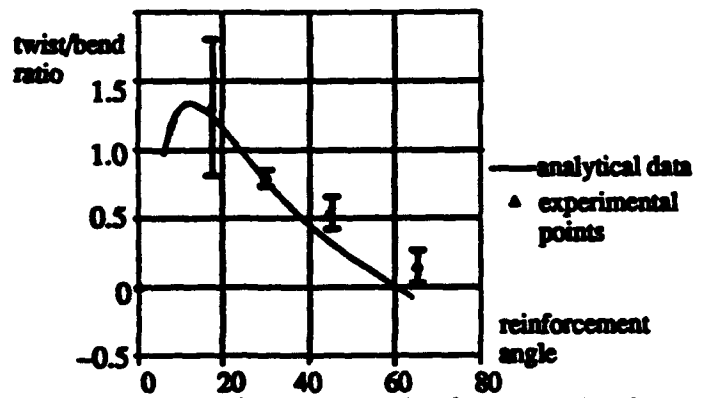

Fig. 2. Analytical and experimental data for the twist/bend ratio at the various reinforcement angles of the box beam spar

As a final example, the analysis of stress fields in a cantilever laminated composite plate under transverse and in–plane loads is considered. A square plate with a/h=5 is composed of three unidirectionally reinforced layers having identical thicknesses and fiber orientation along the x–axis in the top and bottom layers and along the y–axis in the middle layer. Some results for the case of transverse loading (1) are presented in Figure 3. It is seen that longitudinal normal stress σ_x suffers discontinuities at the interfaces between 0 and 90 degree layers, while the transverse stresses τ_{xz} and σ_z don't show any visible discontinuities.

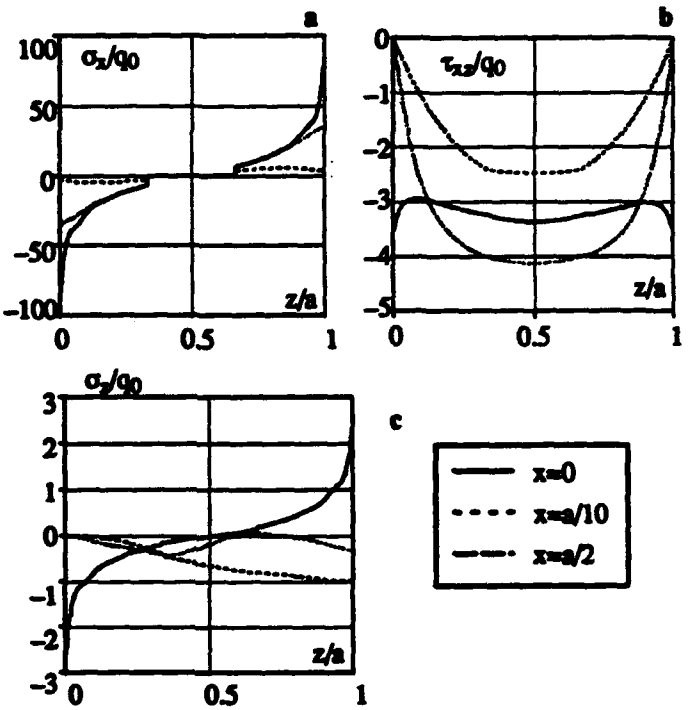

Fig. 3. Variations of σ_x (a), τ_{xz} (b), and σ_z (c) along z for a three–layer cantilever plate under transverse load

REFERENCES

1. Bogdanovich, A.E. (1991). Spline Function Aided Analysis of Inhomogeneous Materials and Structures. Berlin–Heidelberg–New York: Springer–Verlag, 1992, pp. 355–382

Rate Effects in Composite Materials

Wesley Cantwell
Polymers Laboratory, EPFL, Lausanne, Switzerland.

Fiber reinforced composites are presently being used in a wide range of engineering structures susceptible to some form of high speed or dynamic loading. To date, very few systematic studies have been undertaken to assess the rate sensitive fracture properties of fibrous composites and a detailed understanding of these materials response to rapid loading is still lacking. Welsh and Harding (1) used the split Hopkinson bar test to characterize the rate-dependency of the tensile strength and modulus of a number of long fiber reinforced systems. Other workers (2,3) have used the double cantilever beam test to study the influence of loading rate the on interlaminar fracture toughness of thermosetting and thermoplastic-based composite materials.

In this study a fracture mechanics-type specimen geometry has been used to study the influence of loading rate on material toughness and energy absorption. Tests have been undertaken on a wide range of chopped strand mat composites enabling the influence of matrix properties on fracture toughness to be studied in detail. Finally, the relationship between the measured toughness of the material and it's resistance to impact perforation was examined.

The panels were manufactured by a hand lay-up technique involving impregnating three E-glass fiber mats ($300g/m^2$) with either an epoxy-based vinyl ester resin or a polyester resin. Twelve commercially available resins were studied in order to have the widest range of matrix mechanical properties. The nominal thickness of the molded panels was 2mm. Single edge notch bend (SENB) specimens having dimensions 14.5x58mm x thickness were then cut from the panels using a diamond slitting wheel. Notches were then machined at the mid-span using a rotating saw blade. The notches were then sharpened by sliding a fresh razor blade over the tip region. The specimens were supported on two cylindrical rollers positioned 58mm apart and loaded at their mid-points directly above the notch. Tests using crosshead speeds between 0.1 and 100mm/min were conducted on an Instron 1122 machine whereas impact testing was undertaken using an instrumented drop-weight tower. Material toughness was characterized by determining K_C and measuring a work of fracture W_f by simply dividing the energy dissipated by the fracture area.

Fig. 1. Damage zone in a fractured CSM SENB specimen tested at 1mm/minute.

A typical damage zone corresponding to a fractured CM specimen tested at 1mm/min. is shown in Fig. 1. It is clear that energy has

been dissipated over quite a large zone around the principal crack. Figs. 2 and 3 show the variation of K_C and W_f with crosshead speed for an epoxy-based vinyl ester resin CSM composite.

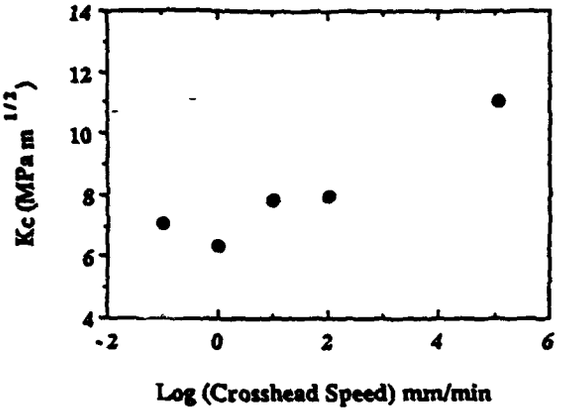

Fig. 2. Variation of Kc with rate for an epoxy vinyl-ester based CSM.

It is interesting to note that both of these parameters indicate that the material is capable of absorbing greater energy at higher rates of strain. Indeed, the work of fracture increases four fold over the range examined. Previous work (1) has shown that glass fibers exhibit a significant rate sensitive response at room temperature. Such effects were investigated in more detail in this study where tests were undertaken on unidirectional glass fiber specimen loaded in flexure. The results of these tests indicated that the tensile strength of the fibers increased by almost thirty percent over the range of loading rates shown in Figs. 1 and 2. It is believed that the trends apparent in these figures result directly from this rate dependent behavior.

A series of drop-weight impact tests were undertaken in order to correlate the energy required to perforate the panels with K_C and W_f. Fig. 4 shows the variation of the perforation energy normalized with respect to specimen thickness as a function of the work of fracture measured under impact loading.

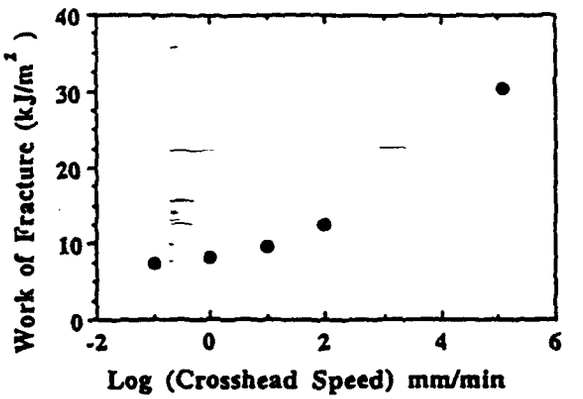

Fig. 3. Variation of W_f with rate for an epoxy vinyl ester CSM.

From the figure it appears that the level of correlation is good. It is interesting to note that those composites having brittle matrices offer the higher work of fractures and in turn superior perforation energies.

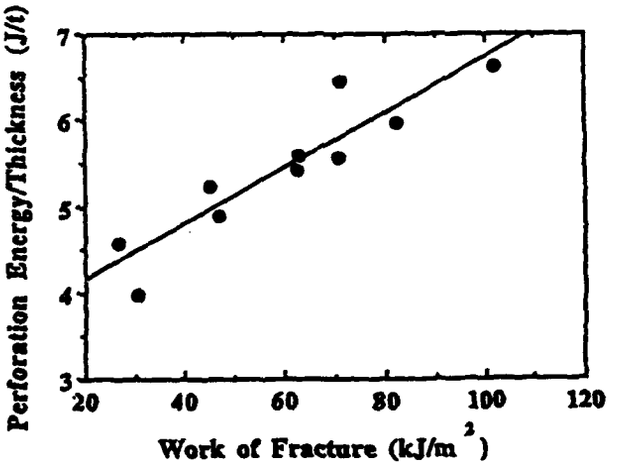

Fig.4. Variation of perforation energy with work of fracture for various composites.

References.
1. L.M. Welsh and J.Harding, Oxford Univ. report OUEL 1579/85.
2. P. Béguelin, M. Barbezat and H.H. Kausch, J. Phys. III France (1991) p1867.
3. S. Mall, G.E. Law and M. Katouzian, J. Comp. Mats. 21 (1987) p569.

AN INNOVATIVE TECHNIQUE FOR MONITORING DAMAGE EVOLUTION IN COMPOSITE MATERIALS WITH FIBER OPTIC SENSORS

by

Greg P. Carman
Mechanical, Aerospace, & Nuclear Engineering
University of California
Los Angeles, California

The use of embedded and surface mounted optical fiber sensors for health monitoring of key structural components in support vehicle systems has begun to evolve in the last decade. These novel sensor systems offer a new methodology to investigate the occurrence of local damage and alert maintenance personnel to the location and progression of damage in composites and homogeneous material systems. While the benefits offered by health monitoring systems represent substantial cost saving in terms of both money and lives, a viable methodology to employ the optical fiber sensors for damage detection and evaluation has not been developed, a detailed study of the sensors robustness to survive in standard operating conditions has not been performed, an adequate technique to embed the sensors has not been presented, and appropriate analytical models depicting the effect of optical fibers on the mechanical properties of the composite has not been developed.

This investigations presents a new technique employing Extrinsic Fabry Perot Fiber Interferometric Fiber Optic Strain Sensor FP-FOSS to measure thermal parameters adequately characterizing damage mechanisms arising in today's advanced materials (e.g. polymeric, ceramic, and metal matrix composites). The monitoring of thermal parameters with FP-FOSS to infer damage accumulation represents the first attempt to employ this methodology in health monitoring applications for composite materials. The information obtained from the embedded and surface mounted FP-FOSS on the damage evolution represents a new approach for determining the health of a heterogeneous material system.

The approach employed in this document is founded upon sound scientific evidence concerning the dependence of a material's fatigue strength on the evolution of certain microstructural damage features, specifically damage networking. The sensitivity of thermal parameters to this significant damage feature is studied in this investigation with the use of metal matrix, ceramic matrix, and polymer matrix composite materials subjected to mechanical and thermal fatigue cycling. The results show that the proposed methodology is a significant improvement over damage evaluation techniques and life predictive methodologies that are presently based on number of fatigue cycles or stiffness reduction measurements. With the use of the proposed characteristic damage metrics, measurement of distributed microstructural damage features is possible and is correlatable with loading profile, fatigue response, and residual strength measurements of a composite.

An analytical model correlating the experimental data obtained from sensor measurements to the damage state present in the material is discussed. This simple model is presently based on classical shear lag techniques. Test data and analytical results are presented for polymeric systems including woven cross-ply Celion G30-500/PMR-15 resin system thermally cycled from room temperature to 450 degrees F and a AS-4-3501/6 quasi-isotropic layup mechanically loaded. Additional test data is provided for a titanium matrix composite system and a silicon-carbide ceramic matrix system subjected to mechanical loads. Experimental and theoretical results obtained from the polymeric matrix system reveal that the thermal parameter changes by as much as 80% over the fatigue life of the composite

(see Figure 1). This further substantiates the supposition that these parameters can be employed to detect damage accumulation in a composite and thus infer remaining strength and life. We show that there is a distinct correlation between damage density and the thermal parameters in these systems, both of which are path dependent. That is, even though two specimens undergo similar load levels the damage evolution are distinctly different in the two specimens. The measurement of the thermal parameters delineates the damage present in each of the specimens.

In this paper we also review various manufacturing techniques employed to construct extrinsic Fabry-Perot Interferometric fiber optic sensors and correlate these processes with measured strength values [1]. We show that if properly constructed the fiber optic sensors strain to failure (i.e. 3%) exceeds that of classical polymeric composite materials. This results suggests that the FP-FOSS should fail after the composite system has failed, at least in quasi-static loading. Test results are also presented on fatigue loaded polymeric composite systems and metal matrix composite systems with attached FP-FOSS. These results demonstrate the longevity of these sensors and the advantages they offer over classical resistance strain gauges with limited fatigue endurance curves.

We also review the effect of embedded optical fibers on a composite materials properties. It has been shown that the compression strength and the transverse tensile strength of a composite material is compromised if the laminate is not properly constructed [2,3]. We have recently developed a working model providing detailed information on appropriate manufacturing techniques of composites containing optical fibers. These analytical models demonstrate fiber optic coatings can be employed to minimize the degradation in a composites transverse tensile strength caused by optical fibers. Guidelines involving the effect of fiber size and orientation in a laminate and the expected degradation on compression strength is also presented.

The information presented in this study has immediate and direct applications in both real time in-situ health monitoring systems and non-destructive evaluation techniques currently under development. The work performed in this investigation employs state of the art measurement techniques to measure the characteristic damage metrics, including optical fiber sensors. The

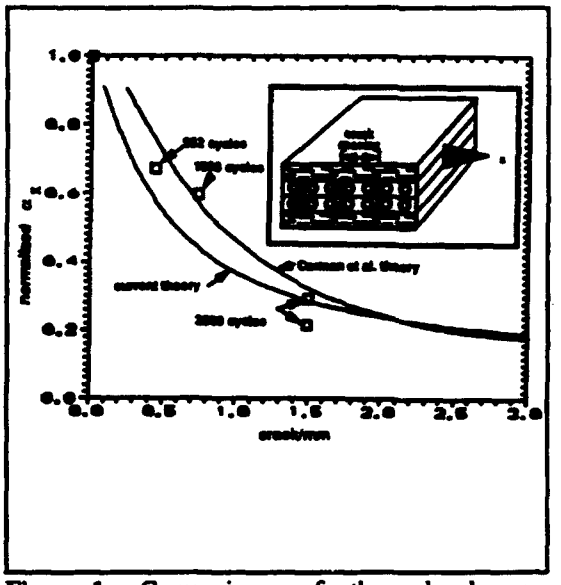

Figure 1: Comparison of thermal damage metrics.

knowledge amassed from this investigation represents the formulation of a new and resourceful approach for accurately characterizing the damage state in a heterogenous material system subjected to fatigue loading. By introducing a new technique for quantifying a composite material's damage state, we provide a fundamental approach not previously embarked upon to unravel the complexities associated with multifarious damage phenomena. The results obtained from this investigation provide essential information to researchers studying composite materials and to engineers designing structural components manufactured from composite materials.

References

1. Carman et al., SEM conf. 1993, pp.1079-1088.

2. Carman et al., J. Int. Mat. Sys. & Struct., V.4 no 1, pp.89-98.

3.Carman et al., J. Int. Mat. Sys. & Struct., to appear 1993.

Nonlinear Structural Design Sensitivity Analysis for Composites Undergoing Elastoplastic Deformation

Aditi Chattopadhyay* and Ruijiang Guo**
Department of Mechanical and Aerospace Engineering
Arizona State University
Tempe, AZ

Introduction

The post-failure mode is a nonlinear phenomenon and is important in the design of crashworthy structures. The material nonlinearities are a consequence of plastic deformation whereas geometric nonlinearities are due to large displacements, nonlinearities in strain-displacement relations and changes in boundary conditions due to possible local buckling. Since the response is dependent on the material and geometric properties of the structure, optimum selection of design variables such as ply orientations, stacking sequences and thicknesses will yield efficient structural design for pre- and post-failure loading conditions. The objective of the current research is to develop a sensitivity analysis procedure which can be used to provide such necessary design trends.

The sensitivity analysis for linear structural problems is a well studied area. Research has also been performed on nonlinear sensitivities[1,2]. However, only isotropic material has been considered. In this paper, a semi-analytical procedure is described for the design sensitivity analysis of composite structures including both material and geometric nonlinearities. A higher order approximation is used in the integration of the rate constitutive equations to improve accuracy. A direct differentiation approach (DDA) is used to calculate the sensitivities. A partial differentiation of the constitutive equations in the inelastic range, is used to calculate the partial derivative of stress with respect to the design variables. The procedure developed is demonstrated through a composite laminated beam problem.

General Theory

Response Analysis: Consider a continuum initially occupying a domain C_0 of volume ${}^0V$ and bounded by the surface ${}^0\Gamma$. At load level t, the configuration deforms to a new configuration with a domain C_t of volume ${}^tV$ and bounded by the surface ${}^t\Gamma$.

A material point ${}^0x = ({}^0x_1, {}^0x_2, {}^0x_3)^T$ in the initial configuration moves to a new position ${}^tx = ({}^tx_1, {}^tx_2, {}^tx_3)^T$ at time t. In the configuration C_t, any volume element d^tV experiences a body force ${}^t\rho\ {}^tb\ d^tV$, where ρ is the mass per unit volume and b is the body force per unit mass, and any oriented surface element $d^t\Gamma = {}^tn\ d^t\Gamma$ experiences a contact force ${}^tt({}^tn)\ d^t\Gamma$, where ${}^tt({}^tn)$ is the surface traction and ${}^tn$ is the unit outward normal on ${}^t\Gamma$. The equilibrium equation at time t may be written in terms of the reference configuration C_r as follows.

$$\int_{rV} {}^t\sigma_{ij}\,\delta\left(\frac{\partial {}^tu_i}{\partial {}^tx_j}\right)\,{}_0^tJ\ {}^rJ\ d^rV = \int_{rV} {}^r\rho\ {}^tb_i\ \delta {}^tu_i\ d^rV + \int_{r\Gamma} {}^t\sigma_{ij}\ {}^tn_j\ \delta {}^tu_i\ {}_0^tJ_\Gamma\ {}^rJ_\Gamma\ d^r\Gamma \qquad (1)$$

where the superscript t on the left denotes time, ${}^t\sigma_{ij}$ is the Cauchy stress, ${}^tu_i$ is the displacement field, δ denotes the variation and ${}_0^tJ = \det\left(\frac{\partial {}^tx_i}{\partial {}^0x_j}\right)$, ${}_0^tJ_\Gamma = \det\left(\frac{\partial {}^tx_i}{\partial {}^0x_j}\ {}^tn\right)$, ${}^rJ = \det\left(\frac{\partial {}^0x_i}{\partial {}^rx_j}\right)$, ${}^rJ_\Gamma = \det\left(\frac{\partial {}^0x_i}{\partial {}^rx_j}\ {}^0n\right)$.

An incremental solution procedure is used to solve the above deformation problem.

Constitutive Models: The procedure being developed is first demonstrated through a nonlinear material model. The constitutive equations are expressed as:

$$\dot{{}^t\sigma}_{ij} = {}^tQ_{ijkl}\ \dot{{}^t\varepsilon}_{kl} \qquad (2)$$

where $\dot{{}^t\varepsilon}_{kl}$ are the infinitesimal strain rates, ${}^tQ_{ijkl}$ are stiffnesses which are functions of the stresses at time t and the design variables, that is, ${}^tQ_{ijkl} = {}^tQ_{ijkl}({}^t\sigma_{ij}, d_1, \cdots, d_n)$ where $d_1, \cdots, d_n$ are the design variables.

Integration of Rate Constitutive Equations: The rate constitutive equations are a set of nonlinear differential equations with the elastic-plastic yield stresses as initial conditions. Solution of this initial value problem for each load level is CPU intensive. A linear approximation of the integration of the rate constitutive equations was used by Tsay and Arora [1]. Here, a higher order approximation of the integration is proposed to increase the accuracy. Integration of Eqn.(2) yields the following.

$${}^t\sigma_{ij} = {}^\tau\sigma_{ij} + \int_{{}^\tau\varepsilon_{kl}}^{{}^t\varepsilon_{kl}} \zeta Q_{ijkl}\, d^\zeta\varepsilon_{kl}$$

---

* Assistant Professor, Senior Member AIAA, Member AHS, ASME, SPIE
** Graduate Research Assistant

This can be approximated as follows.

$$ {}^{t}\sigma_{ij} = {}^{\tau}\sigma_{ij} + {}^{\tau}Q_{ijkl}\,({}^{t}\varepsilon_{kl} - {}^{\tau}\varepsilon_{kl}) + \frac{1}{2}\,(\partial {}^{\tau}Q_{ijmn}/\partial {}^{\tau}\varepsilon_{kl})\,({}^{t}\varepsilon_{kl} - {}^{\tau}\varepsilon_{kl})({}^{t}\varepsilon_{mn} - {}^{\tau}\varepsilon_{mn}) \quad (3) $$

where $\partial {}^{\tau}Q_{ijmn}/\partial {}^{\tau}\varepsilon_{kl} = ({}^{\tau}Q_{ijmn}/\partial {}^{\tau}\sigma_{pq})\,(\partial {}^{\tau}\sigma_{pq}/\partial {}^{\tau}\varepsilon_{kl})$,

which can be expressed in terms of the stresses at time τ and the design variables.

Sensitivity Analysis

Direct Differentiation Approach: Direct differentiation of the equilibrium equation with respect to the design variable d_m yields

$$ \int_{{}^{r}V} \{[(\frac{\partial {}^{t}\sigma_{ij}}{\partial {}^{t}\varepsilon_{pq}}\frac{\partial {}^{t}\varepsilon_{pq}}{\partial d_m} + \frac{\partial {}^{t}\sigma_{ij}}{\partial d_m})\,\delta(\frac{\partial {}^{t}u_i}{\partial {}^{t}x_j}) + {}^{t}\sigma_{ij}\,\delta(\partial(\frac{\partial {}^{t}u_i}{\partial d_m})/\partial {}^{t}x_j)]\,{}_0^{t}J\,{}^{r}J + {}^{t}\sigma_{ij}\,\delta(\frac{\partial {}^{t}u_i}{\partial {}^{t}x_j})\frac{\partial ({}_0^{t}J\,{}^{r}J)}{\partial d_m}\}\,d^{r}V $$

$$ = \int_{{}^{r}V} [\frac{\partial ({}^{r}\rho\,{}^{t}b_i)}{\partial d_m}\,\delta {}^{t}u_i + {}^{r}\rho\,{}^{t}b_i\,\delta(\frac{\partial {}^{t}u_i}{\partial d_m})]\,d^{r}V + \int_{{}^{r}\Gamma} \{[(\frac{\partial {}^{t}\sigma_{ij}}{\partial {}^{t}\varepsilon_{pq}}\frac{\partial {}^{t}\varepsilon_{pq}}{\partial d_m} + \frac{\partial {}^{t}\sigma_{ij}}{\partial d_m})\,\delta {}^{t}u_i + {}^{t}\sigma_{ij}\,\delta(\frac{\partial {}^{t}u_i}{\partial d_m})]\,{}^{t}n_j\,{}_0^{t}J_\Gamma\,{}^{r}J_\Gamma + {}^{t}\sigma_{ij}\,\delta {}^{t}u_i\frac{\partial ({}^{t}n_{j0}\,{}^{t}J_\Gamma\,{}^{r}J_\Gamma)}{\partial d_m}\}\,d^{r}\Gamma \quad (4) $$

In Eqn.(4), ${}_0^{t}J$, ${}^{r}J$, ${}_0^{t}J_\Gamma$, ${}^{r}J_\Gamma$, ${}^{r}\rho$, ${}^{r}b_i$ and ${}^{t}n_j$ are explicit functions of the design variables. Their sensitivities with respect to the design variable d_m are easy to determine. Since the responses are known at time t, the quantities $\partial {}^{t}\sigma_{ij}/\partial {}^{t}\varepsilon_{pq}$ are also known. The quantities $\partial {}^{t}\varepsilon_{pq}/\partial d_m$ can be obtained from $\partial {}^{t}u_i/\partial d_m$. Therefore the unknown quantities are $\partial {}^{t}\sigma_{ij}/\partial d_m$ and $\partial {}^{t}u_i/\partial d_m$. The following section describes a procedure to solve for $\partial {}^{t}\sigma_{ij}/\partial d_m$. Once $\partial {}^{t}\sigma_{ij}/\partial d_m$ are known, $\partial {}^{t}u_i/\partial d_m$ can be solved using Eqn.(4).

Partial Differentiation of Constitutive Equations: Fixing the state variables, partial differentiation of the constitutive equations (2) with respect to the design variable (d_m) yields

$$ d(\partial {}^{t}\sigma_{ij}/\partial d_m) = (\partial {}^{t}Q_{ijkl}/\partial {}^{t}\sigma_{pq})\,(\partial {}^{t}\sigma_{pq}/\partial d_m)\,d\,{}^{t}\varepsilon_{kl} \quad (5) $$

This is a set of linear differential equations in $\partial {}^{t}\sigma_{ij}/\partial d_m$. Their initial values can be known by differentiating the stresses at the yield point with respect to the design variable. This linear problem can easily be solved numerically.

Numerical Example

The above procedure is applied to a $(0^\circ / 10^\circ / 45^\circ)_2$ anti symmetric Glass/Epoxy composite beam with equal ply thicknesses (0.2in) undergoing pure bending. The ply angles are chosen as the design variables. The Tsai-Hill theory is adopted as the yield criterion. In the response analysis, the results of the second order approximation of the integration of the rate constitutive equations are compared with the direct solution of the set of nonlinear differential equations (Table 1). They show excellent agreement in both elastic and plastic ranges. However, the CPU time requirement for the second order approximation is much less than that for the differential solution. In the sensitivity analysis, the results of the direct differentiation approach (DDA) are compared with the those obtained using the finite difference approach (FDA). The sensitivities of curvature with respect to the ply angle θ_3 (20 deg.) are presented in Table 1 and show excellent agreements in both elastic and plastic ranges.

Table 1 Comparison of response and sensitivity analysis

Load	Curvature		Sensitivity of curvature	
x10^5lb-in	Direct Sol	2nd-or Solu	FDA	DDA
0.1	.001309	.001309	.000922	.000922
0.2	.002618	.002618	.001845	.001845
0.3	.003947	.003968	.003458	.003523
0.4	.005584	.005652	.007279	.007436
0.5	.007377	.007453	.010068	.010238
0.6	.009205	.009290	.012938	.013112
0.7	.011062	.011153	.015842	.016013
0.8	.012940	.013038	.018816	.018991
0.9	.014846	.014951	.021935	.022106
1.0	.016775	.016886	.025047	.025212

Acknowledgment

The research was supported by the U.S. Army Research Office. Grant number DAAH04-93-G-0043.

Reference

1. J.J. Tsay and J.S. Arora, "Nonlinear Structural Design Sensitivity Analysis for Path Dependent Problems. Part 1: General Theory," Comput. Methods Appl. Mech. Eng. 81(1990)183-208.

2. J.J. Tsay, J. E. B. Cordoso and J.S. Arora, "Nonlinear Structural Design Sensitivity Analysis for Path Dependent Problems. Part 2: Analytical Examples," Comput. Methods Appl. Mech. Eng. 81(1990)209-228.

VIBRATION ANALYSIS OF FINITE THIN LAMINATED DOUBLY-CURVED PANELS

Reaz A. Chaudhuri, University of Utah, Salt Lake City, Utah 84112

ABSTRACT

Governing partial differential equations and the associated boundary conditions, for the boundary - value problem of large amplitude vibration of arbitrarily laminated (of which symmetric/ antisymmetric cross- ply and angle-ply laminations are special cases) thin doubly-curved panels, that account for von-Karman type geometric nonlinearity, are derived, starting from the method of virtual work. Two numerical solution approaches, based on finite element and global Galerkin methods, are also presented. The latter is restricted to curved panels of rectangular planform. Actual computation of the numerical results is currently underway at the University of Utah, and will be presented in future. Next, the governing partial differential equations and the associted boundary conditions are linearized for the special case of small amplitude vibration, which are solved using two recently developed Fourier type approaches. Details of these solutions to the boundary-value problem of free small amplitude vibration of arbitrarily laminated thin doubly-curved panels of rectangular planform are available elsewhere. Both boundary-discontinuous[1] and boundary-continuous- displacement [2] based double Fourier series approaches, are employed to solve the linear boundary-value problems, involving highly coupled linear partial differential equations with constant coefficients, resulting from CLT (Classical Lamination Theory)-based formulations that also include surface-parallel inertias.

Extensive numerical results that are presented in this study include (i) convergence characteristics of computed natural frequencies, and (ii) effects of length-to-thickness ratio, radius-to-length ratio, fiber orientation angle, lamination sequence, shell geometry and boundary constraints on the response quantities of interest. The accuracy of the solutions are ascertained by comparison with the available FSDT-based analytical and CLT-based Galerkin solutions. Comparisons with the available FSDT (first-order shear deformation theory) -based analytical solutions help in establishing the upper limit (with respect to the thickness-to-length ratio) of validity of the present CLT (classical lamination theory)-based solutions. Also investigated is the highly complex

interaction among bending-stretching type coupling effect, membrane action due to shell curvature, and the effects of surface-parallel (membrane) inertias. It is also concluded that boundary-continuous-displacement based Fourier solutions are superior to their boundary-discontinuous counterparts in their ability to avoid Gibb's phenomenon, in the case of rigidly clamped boundary conditions.

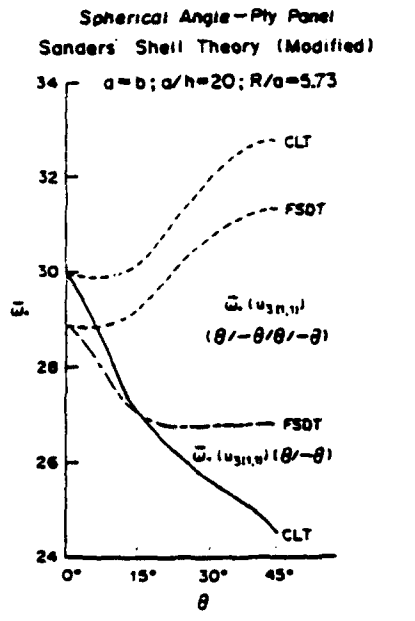

Fig. 2 Variation of normalized fundamental natural frequencies of square relatively deep ($R/a = 5.73$) and relatively thin ($a/h = 20$) antisymmetric angle-ply two- and four-layer spherical panels with θ_0 and comparison with the FSDT.

References:

Chaudhuri, R. A., Int. J. Engineering Science, 27, 1005 - 1022, 1989.

Chaudhuri, R. A., and Kabir, H. R. H., Int. J. Engineering Science, 30, 1647-1664 , 1992.

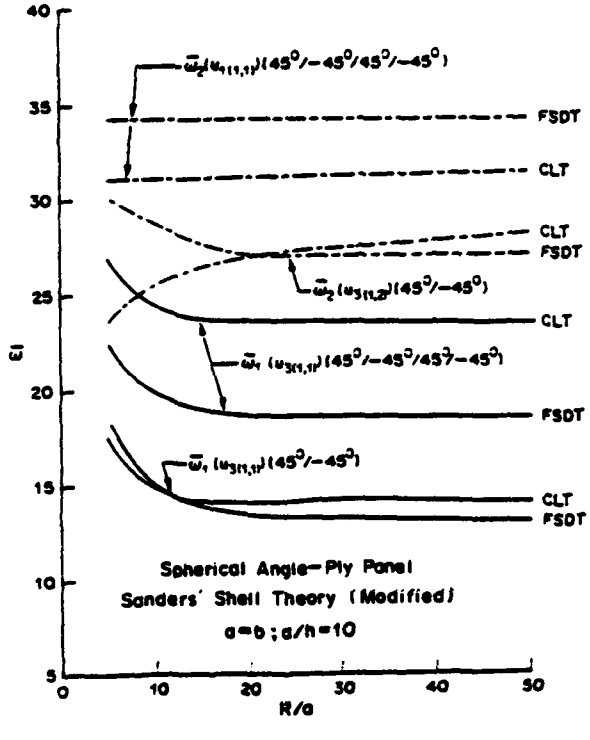

Fig. 1. Variation of normalized fundamental and second (numerically ordered) natural frequencies of square antisymmetric angle-ply two-layer (45°/−45°) and four-layer (45°/−45°/45°/−45°) spherical panels ($a/h = 10$) with R/a ratio, and comparison with FSDT.

ANALYTICAL MODELING OF ELECTRORHEOLOGICAL MATERIAL BASED ADAPTIVE BEAMS

Melek Yalcintas **John P. Coulter**

Intelligent Materials and Manufacturing Laboratory
Department of Mechanical Engineering and Mechanics
Lehigh University
Bethlehem Pennsylvania 18015 U.S.A.

INTRODUCTION

The use of electrorheological (ER) materials in adaptive structures has received much attention recently. Electrorheological materials experience reversible changes in rheological properties such as viscosity, plasticity and elasticity when subjected to electrical fields. These reversible changes are due to chain formation of micron-sized dielectric particles in non polar media under an applied electrical field, resulting in up to several orders of magnitude increases in rheological properties. In essence, ER material behavior transforms from that of a liquid to that characteristic of a solid-like gel when an electric field is applied. Adaptive structures are based on controlling the pre-yield rheology of ER materials.

In this study the dynamic behavior of an ER based adaptive beam was modeled, based on shear configurations. The beam was composed of three layers: an ER material controllable damping layer and surrounding upper and lower elastic plates. The existing models for viscoelastically damped composite three layer beams were examined for their applicability to ER adaptive beams. From the rheological findings it was observed that ER materials exhibit linear rheological behavior similar to many common viscoelastic materials. Based on this similarity in material behavior a modification of existing models used for viscoelastically damped sandwich structures was proposed.

The structural model of the assembly in a transverse continuous vibration mode subjected to simply-supported boundary conditions and actuation at a single point on the adaptive beam surface was analyzed. Theoretical structural natural frequencies, and mode shapes for a 0 -300 Hz. bandwidth range were calculated and the transverse displacement of a specified point on an ER material adaptive beam of the experimental setup is predicted. The earlier experimental results of Don and Coulter (Don, 1993) were used for comparison purposes. The analytical results are compared with experimental results under the same physical conditions. Qualitative agreement between theory and experimentation resulted. In addition an effort was made to reduce the vibration of the structure by selecting the optimum electrical field which yields minimized vibration for each frequency.

MODEL DESCRIPTION

In the Ross-Kerwin-Ungar (RKU) analysis, the transverse vibration equation derived for Euler-Bernoulli beams is considered. The total effective flexural rigidity is found by assuming that all of the layers are composed of ideal elastic materials. Once the expression is obtained for the transverse vibration of the beam, the real modulus in the governing vibration equation is replaced by a complex modulus for the viscoelastic layer only. The final form of the flexural rigidity is expressed in the form of real and imaginary components. A detailed derivation of the complex flexural modulus can be found in the literature (Ross et al., 1959).

The basic model developed by RKU can be further extended by including boundary conditions, an external forcing function, and the controllable nature of ER materials. Structural adaptability is incorporated by assuming that the complex shear modulus of the ER material is a function of electrical field. The Young's modulus of the ER material is considered negligibly small compared to Young's moduli of elastic plates.

The transverse displacement of the adaptive beam was obtained by the use of the expansion theorem. Considering the orthogonality condition of modes, the differential equation of the continous system lead to an infinite set of uncoupled ordinary differential equations which is in summation resulted with the total transverse displacement.

Thus, the extended model is capable of determining natural frequencies, mode shapes and transverse vibrational response at a point on the adaptive beam for an applied point force at a specified location.

RESULTS AND DISCUSSIONS

Theoretical transverse vibration response predictions were obtained and recorded for varying electric field levels from 0 - 3.5 kV/mm with 0.1 kV/mm increments, with a frequency range of 0 - 300 Hz. The transverse vibration amplitude as a function of frequency for electrical fields of 0 kV/mm, 1.5

kV/mm, 2.5 kV/mm, and 3.5 kV/mm is plotted in Figure 1. In this figure the peak values of each curve represent the resonance frequencies of the structure corresponding to that specified electrical field. As the electric field increases, the resonance frequencies shift to higher values while decreasing the general transverse response of the structure. Corresponding experimental results shows the same trend of vibration response. Also the experimental results validate the theoretically predicted controllability of the structure.

The final step taken during the present study was to predict electrical field levels for optimal frequency dependent control of the prototype ER material based adaptive beam. For this purpose the electrical field applied to the ER material damping layer which caused the smallest transverse vibration response of the beam was chosen as optimal. At each forcing frequency, only one electric field level was optimal. Theoretically predicted and experimentally observed optimal electrical field levels are plotted as a function of forcing frequency, Figure 2 illustrates the theoretical predictions. In both cases the optimal electrical field pattern resembled a repeating ramp type curve with a visible period of frequency. If electrical fields higher than 3.5 kV/mm were permitted, the upper limit would be expected to have sharp peaks rather than the flat plateaus shown. The only deviation between the theoretically predicted and experimentally observed optimal electric field levels was the period of this repeating pattern. This deviation could be explained by inaccurate theoretical ER material rheological properties.

CONCLUSIONS

In this study, the theoretical modeling and experimental analysis of ER material adaptive structures based on shear configurations was performed. A model was proposed and tested under varying forcing frequency and applied electrical field levels. The results were compared with experimental tests with an actual ER material adaptive beam. In both cases modal natural frequencies increased and modal vibration amplitude levels changed as the electric field applied to the ER material was increased. This controllable characteristic of ER material adaptive structures is useful when variable performance of the structure is desired.

REFERENCES

Coulter, J. P., Weiss, K. D., and Carlson, J. D., 1993, "Engineering Applications of Electrorheological Materials," *Journal of Intelligent Material Systems and Structures*, Vol. 4, No. 2, pp. 248-259.

Don, D. L., 1993, *An Investigation of Electrorheological Material Adaptive Structures*, Masters Thesis, Lehigh University, Bethlehem, Pennsylvania.

Ross, D., Ungar, E. E., Kerwin, E. M. Jr., 1959, "Damping of Plate Flexural Vibrations by means of Viscoelastic Laminea", *Structural damping*, Section 3, Ruzicka, J. E. ,ed., ASME .

Weiss, K. D., Coulter, J. P., & Carlson, J. D. (1993). "Material Aspects of Electrorheological Systems", *Journal of Intelligent Material Systems and Structures*, Vol. 20, No. 12, pp. 1137-1140.

Yalcintas, M., Coulter, J. P., Don, D. L., " Structural Modeling and Optimal Control of Electrorheological Material Based Adaptive Beams", *ASME Journal of Vibration and acoustics*, submitted for publication.

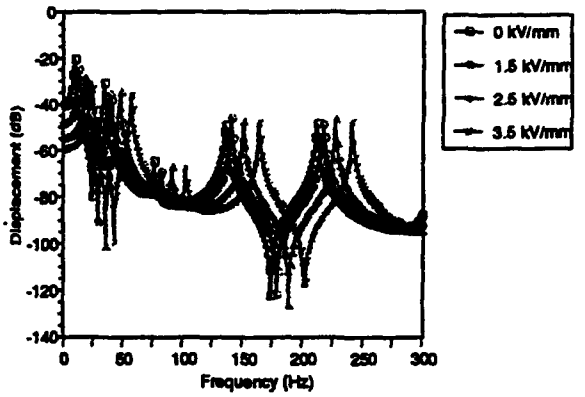

Figure 1 Theoretical frequency response of adaptive beam at Electric Fields of 0, 1.5, 2.5, and 3.5 kV/mm.

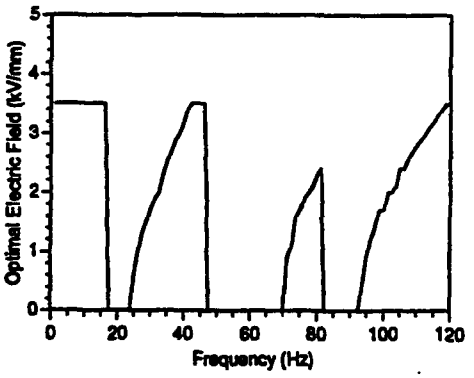

Figure 2 Theoretical Optimal Electric Field Corresponding Each Excitation Frequency.

THE SIGNIFICANCE OF LAMINATE SPALLATION GENERATED BY HIGH-VELOCITY SPHERICAL METALLIC IMPACTORS

Gregory J. Czarnecki
Vehicle Subsystems Division, Wright Laboratory, Wright-Patterson AFB, OH 45433 U.S.A.

Aircraft vulnerability codes rely upon several critical parameters for accuracy of the codes predictions. One such parameter is the ballistic limit (also referred to as the V_{50}). Probabilistic in nature, the V_{50} describes a target's penetration resistance and is defined as the impact velocity where penetration will occur exactly 50% of the time. The V_{50} is commonly determined experimentally (or estimated based on an empirical equation) due to the parameter's variation with changes in projectile or target geometry[1,2,3,4]. Penetrated composite laminates have been observed to eject massive amounts of spall particles, often numbering in the thousands[5]. Composite spall are assumed to exit the laminate over a range of velocities based on the impactor's velocity and the distance of the spall's origin from the shotline. When the energy associated with spallation becomes significant, simplistic equations (such as those to predict the ballistic limit) become confounded.

Experimental data have shown that a nearly linear relationship exists between a projectile's initial (pre-impact) and residual (post-impact) kinetic energies[6,7]. Deviations from linearity are the result of two primary factors. During the penetration event, energy is absorbed within the laminate in the form of delamination, fiber fracture, matrix cracking, and fiber-resin interface failure. Energy absorbed during penetration can also be expected to include target displacement, heat, noise, and even projectile deformation (in the case of semi-rigid impactors). Upon completion of the penetration event, continued deviation from linearity is believed the result of spallation. Although energy absorbed during penetration can easily be assessed and equated to the E_{50} (defined as the kinetic energy absorbed at the V_{50}), the energy associated with spallation remains questionable.

The objective of this study is to determine mass and velocity relationships between spherical metallic penetrators and spall discharged from laminated composites. Of particular interest is defining the critical impact energy requirement to achieve a threshold level of spallation. Also of value is the initial rate of spall mass generation and how latent reductions in this rate affect the average spall velocity.

The target material used in this series of experiments was graphite/epoxy (AS4/3501-6). All experiments were performed on 32-ply $[(0/90/+45/-45)_4]_s$ laminates having a total thickness of 0.180-inch. The projectile's mass was adjusted using 1/2-inch diameter aluminum, steel, and tungsten spheres (6.437×10^{-3}, 18.919×10^{-3}, and 35.231×10^{-3} lbm, respectively). All shotlines were normal to the laminate's surface with impacts occurring in the geometric center of each specimen. Projectile launch velocities were tightly controlled using a light-gas gun. Several tests were performed with each sphere mass at impact velocities near the ballistic limit to establish the on-set of spallation as well as a precise V_{50} velocity. Higher velocity impact tests were conducted to determine the change in spall mass and velocity as a function of impact velocity.

As shown in Figure 1, the relationship between the projectile's initial (E_I) and residual (E_R) energies remains roughly linear over the majority of the energy spectrum of interest. Although the slopes vary slightly for data generated by projectiles of differing masses, all data roughly converges on a single energy required for penetration (between 37.3 and 43.5 ft-lbs). This kinetic energy requirement for penetration (referred to as the E_{50}) is largely independent of the projectile's mass and can be considered constant for the laminate on which it is established. Other parameters such as the projectile's geometry (nose shape and cross sectional area) and target specific parameters (material and lay-up) are expected to influence the E_{50}, but are outside the scope of this paper.

For steel and tungsten impactors, the E_I vs. E_R slope changes from 1.00 to 0.82. This change is hypothesized as resulting from the influence of spallation. A differing slope transition for the softer aluminum impactor (to 0.63) is presumed due in part to the projectile's deformation.

To maintain conservation of energy, the projectile's initial energy must be perfectly transformed into several components upon impact. Data deviating from the theoretical 1:1 slope are the result of many factors, all of which produce a net effect of reducing the projectile's residual velocity. A designated amount of energy (equivalent to the E_{50}) is absorbed by the laminate during the perforation process. After surpassing the penetration threshold, only two major components of kinetic energy remain...that associated with the projectile's residual velocity and with spall particles ejected. Any change of impact energy above the E_{50} must therefore equal the change of the projectile's residual energy plus the spall energy. By setting the x-intercept equal to the E_{50}, the 1:1 relationship between energy "in" and

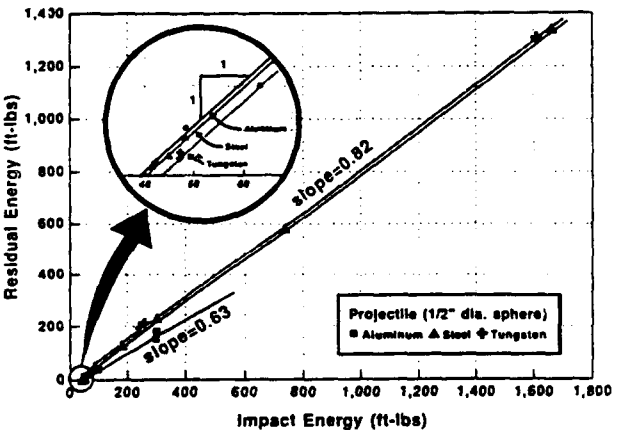

Figure 1. Deviations in the E_I vs. E_R slope as a function of kinetic energy posessed by aluminum, steel, and tungsten impactors.

energy "out" becomes a useful tool for estimating spall energy. The energy associated with spallation (E_s) can therefore be calculated according to the equation $E_s=E_i-E_R-E_{50}$.

Spallation energy is plotted as a function of impact energy in Figure 2. As impact energy increases, the spall energy becomes a significant factor capable of adversely influencing V_{50} predictions.

Figure 3 describes the generation of spall mass as a function of impact velocity. For the rigid steel and tungsten impactors, the critical velocity for spall initiation coincides exactly with the V_{50}. Only for the softer aluminum penetrator does spallation begin at a lower velocity (0.87 times the V_{50}). [Note: The curve shift associated with the change in velocity between 0.87 and 1.00 times the V_{50} (corresponding to 9.3 ft-lbs) is attributed to the projectile's deformation energy.] Although spall initiation coincides roughly with the V_{50}, spallation is not maximized until velocities are in excess of 2.8 times the V_{50}. As impact velocities increase, the slope transitions to zero as the mass subject to spallation attains a maximum limit. For impact velocities below the transition, shear plugging is incomplete, whereas for velocities above the transition, an open hole (roughly the diameter of the projectile) is obtained.

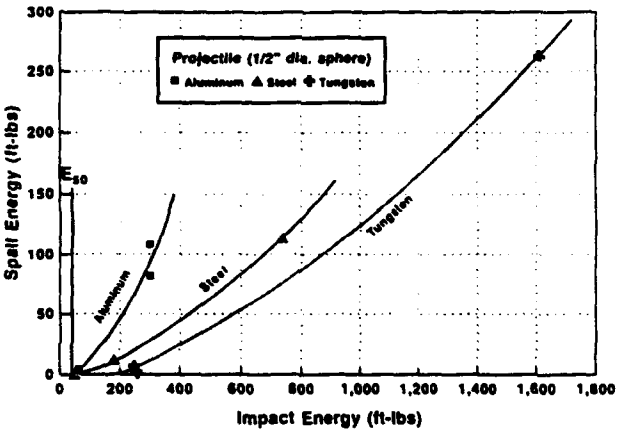

Figure 2. Spallation energy as a function of impact energy using aluminum, steel, and tungsten impactors.

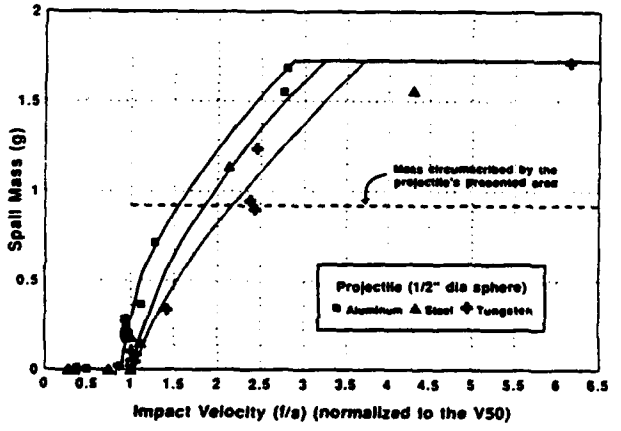

Figure 3. Spall mass generation as a function of the normalized impact velocity using aluminum, steel, and tungsten impactors.

Although not directly measurable, the average spall velocity (V_s) can be estimated according to the equation

$$V_s=[(2)(E_s)(m_s^{-1})]^{1/2}$$

where m_s is the spall mass (equal to the change in target weight). Figure 4 describes the average spallation velocity and projectile residual velocity as a function of the impact velocity. The spall velocity is dependent on the projectile's mass and quickly becomes large for impact velocities above the V_{50}. Note that over the entire impact velocity spectrum, composite spall generated by the aluminum projectile has a velocity identical to that of the projectile's residual velocity. For the heavier impactors (having densities significantly greater than that of the composite spall), the spall velocity deviates significantly from the projectile's residual velocity. Differences between the spall and projectile velocity curves are seen to increase with projectile mass. Low-mass high-velocity projectiles produce a greater spall velocity than high-mass low-velocity projectiles.

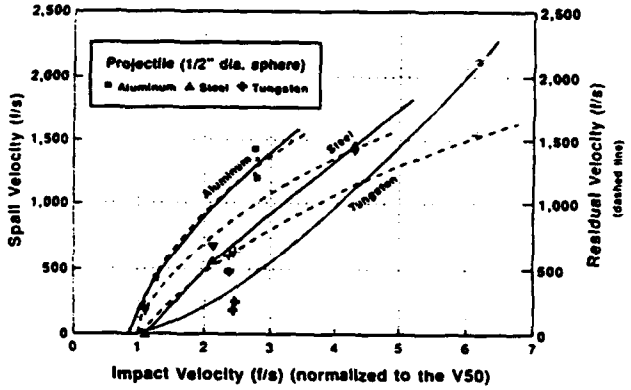

Figure 4. Average spall velocity and projectile residual velocity as functions of normalized impact velocity using aluminum, steel, and tungsten impactors.

REFERENCES

1. Zukas, J.A., Impact Dynamics, "Penetration and Perforation of Solids", pp 155-214, John Wiley and Sons, New York, 1982.

2. "Ballistic Testing of Personnel Armor Materials", Final Report TOP-10-2-506, U.S. Army Aberdeen Proving Ground, 6 January 1975.

3. "Ballistic Tests of Armor Materials", Final Report TOP-2-2-710, U.S. Army Aberdeen Proving Ground, 6 April 1977.

4. Blanas, A.M., "Finite Element Modeling of Fragment Penetration of Thin Structural Composite Laminates", Final Report NATICK/TR-92/019, U.S. Army Natick Research, Development, and Engineering Center, December 1991.

5. Pawlikowski, K., J.T. Lair, and M.A. Samad, Experimental results, Wright Laboratory, Wright-Patterson AFB, OH, May 1992.

6. Lin, L.C., A. Bhatnagar, and H.W. Chang, "Ballistic Energy Absorption of Composites", 22ND International SAMPE Technical Conference, November 1990.

7. Lin, L.C. and A. Bhatnagar, "Ballistic Energy Absorption of Composites - II", 23RD International SAMPE Technical Conference, October 1991.

Natural Vibrations and Waves in Pretwisted Rods

O. Onipede, S.B. Dong
Civil Engineering Dept., University of California, Los Angeles, CA 90024, USA
and
J.B. Kosmatka
Appl. Mech & Engr. Sci. Dept., University of California, San Diego, CA 92093, USA

The behavior of pretwisted rods is distinguished by the ever presence of two coupling effects: (1) extension with twist and (2) bending about one axis with that of the other (even when principal axes are adopted). This paper is concerned with a finite element method of analysis of the natural vibrations in pretwisted rods based on on three-dimensional elasticity. The finite element modeling occurs over the cross-section, which accommodates a cross-section with arbitrary shape, inhomogeneity, mechanical and inertial properties and location of the pretwist axis. The relevant equations from linear elasticity are those in terms of a rotating coordinate system that tracks the cross-sectional geometry along the axis of twist. The cross-sectional finite element modeling leaves the axial dependence ζ and time t undetermined at the outset.

The equations of motion derived by Hamilton's principle are partial differential equations in the axial coordinate and time.

$$[K_1]\{U''\} + [K_2]\{U'\} - [K_3]\{U\} = [M]\{\ddot{U}\} \qquad (1)$$

where primes and dots denote differentiation with respect to ζ and t, respectively. The stiffness matrices $[K_1]$, $[K_3]$ and mass matrix [M] are symmetric and $[K_2]$ is antisymmetric.

Introducing a harmonic wave form, $U = U_o \exp\{i(k\zeta + \omega t)\}$ into Eq. (1), where $k = \pi/\lambda$ is the axial wave number (λ the wave length) and ω the natural circular frequency, results in an algebraic eigensystem in terms of k and ω in the form

$$\left([K_3] - i\,k\,[K_2] + k^2\,[K_1]\right)\{U_o\} = \omega^2\,[M]\,\{U_o\} \qquad (2)$$

Only real k's are considered in this paper, and they represent propagating waves and/or harmonic standing vibrations. Complex eigenproblem (2) can be rendered completely real by combining it with its multiplication by -i to give

$$\begin{bmatrix} K_3 + k^2K_1 & kK_2 \\ -kK_2 & K_3 + k^2K_1 \end{bmatrix} \begin{bmatrix} U_o \\ -i\,U_o \end{bmatrix} = \omega^2 \begin{bmatrix} M & \cdot \\ \cdot & M \end{bmatrix} \begin{bmatrix} U_o \\ -i\,U_o \end{bmatrix} \qquad (3)$$

From symmetry of $[K_1]$ and $[K_3]$ and antisymmetry of $[K_2]$, algebraic eigensystem (3) involves real, symmetric, positive definite matrices, so that all ω^2 are real and positive. Further study of Eq. (3) shows it to consist of two identical subsystems, yielding identical solution pairs. They represent the same wave form except for a $\pi/2$ phase difference in the axial direction.

A computer code prepared was prepared employing 8-node quads and 6-node triangles (both both quadratic interpolations). Isoparametric finite element methodology was used in element matrix formations. Because of the large size of the algebraic eigensystem, subspace iteration was used to extract the lowest subset of the eigendata.

Two examples were given in the full length paper to illustrate the method of analysis and vibrational characteristics, viz., (1) a homogeneous, isotropic bar and (2) a two-layer $\pm 30^\circ$ angle ply composite, both cross-sections with the aspect ratio of ten (width b to height h). Herein, only results for the two-layer composite are presented (see Fig. 1).

The properties of the composite are

$$\frac{E_L}{E_T} = 10 ; \frac{G_{LT}}{E_T} = 0.5 ; \frac{G_{TT}}{E_T} = 0.38 ;$$

$$\nu_{LT} = 0.21 ; \nu_{TT} = 0.3 \quad (4)$$

All frequencies ω were normalized as follows:

$$\Omega^2 = \omega^2 E_T/\rho h^2 \quad (5)$$

where ρ is the unit mass density. Five cases of pretwist were considered for both bars: (1) $\alpha = 0.5°$ about the center; (2) $\alpha = 0.5°$ about the quarter point; (3) $\alpha = 1.0°$ about the center; (4) $\alpha = 1.0°$ about the quarter point; (5) no pretwist. The pretwist angle α refers to a twist rate relative to the thickness h of the bars.

Shown in Fig. 2 are the spectral curves for the lowest six modes of vibrations for cases (1) and (3). In Fig. 3 is shown the cross-sectional modal patterns of the 2nd lowest (torsion-extensional) mode of vibration. These plots reveal the complicated but very intriguing nature of the behavior in pretwisted rods.

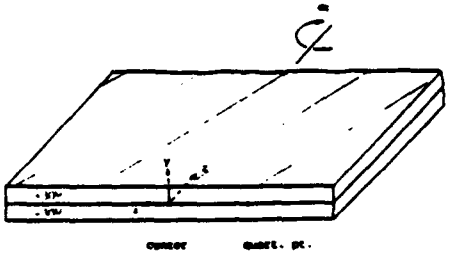

Fig. 1

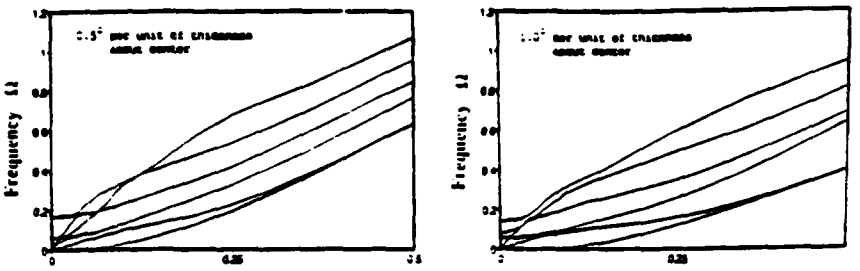

Fig. 2

Case	Real Part		Imaginary Part	
	Axial Disp.	Inplane Disp.	Axial Disp.	Inplane Disp.
no twist	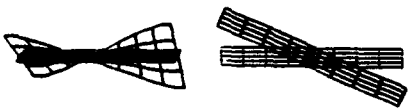			
0.5°/center				
1.0°/center				
0.5°/qt.pt.				
1.0°/qt.pt.				

The axial and inplane displacements may be of different scales

Fig. 3

ANISOTROPIC ELASTIC-DAMAGE MODELS OF COUPLED SOLID DYNAMICS AND HEAT DIFFUSION

E.P. Fahrenthold
Department of Mechanical Engineering
University of Texas
Austin, TX 78712

ABSTRACT

The development of constitutive models for composite materials is motivated in large part by their use in computer-aided structural analysis and design. Finite element methods are by far the most commonly applied tool in such applications. Due to the large CPU time and memory requirements of dynamic, three-dimensional finite element analysis, most micromechanical composite material models see numerical implementation in the form of anisotropic continuum models with internal state variables (Lagoudas and Huang, 1992). The latter form is both compatible with general purpose finite element codes and acceptably computer resource intensive for large scale structural simulations. Typically first order evolution equations for the internal state variables are appended to a displacement-based finite element model in order to simulate the composite structural dynamics.

Although displacement-based finite element methods are well suited to isothermal solid dynamics modeling, many composites engineering applications place a particular emphasis on thermomechanical coupling effects. Included in this category are studies of fabrication processes (Pindera and Freed, 1992), the simulation of high velocity impact dynamics (Drumheller, 1987), and design with shape memory alloys (Gandhi and Thompson, 1992). For mixed energy domain problems of the thermomechanical, thermochemical-mechanical, or thermoelectric-mechanical type, diffusion models or other evolution equations are normally appended to the finite element structural model, in order to simulate the overall system dynamics. Although this method has met with some success, the disadvantages of a somewhat ad hoc or problem dependent modeling approach become apparent as the complexity of the problems of interest increases. Clearly a unified and general purpose approach to the development of numerical models for coupled solid dynamics and diffusion problems is of interest for a significant class of composites engineering problems.

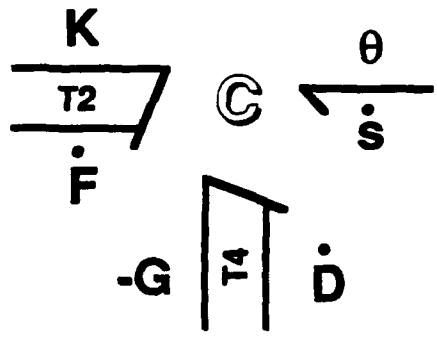

Fig. 1 Bond graph element representing internal energy storage in an anisotropic thermoelastic material with continuum damage.

The bond graph approach (Rosenberg and Karnopp, 1983) to system dynamics modeling offers a unified, energy based method for the formulation of state space models of nonlinear systems, incorporating complex coupling of mechanical, thermal, electrical, chemical, and other energy domains. Although bond graphs have seen extensive application to low order lumped parameter systems, only recently has the method been extended to continuum solid

dynamics of the elastic-plastic (Fahrenthold and Wu, 1988) or thermoelastic (Ingrim and Masada, 1988) type. No previous bond graph work has provided a general modeling approach to the anisotropic, thermoelastic, solid dynamics and heat diffusion problem with internal state variables.

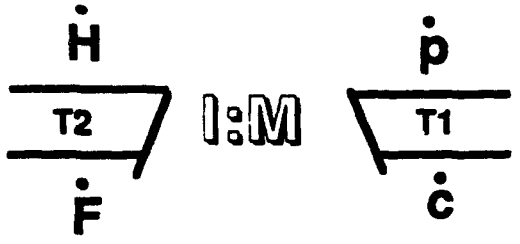

Fig. 2 Bond graph element representing kinetic energy storage in a tetrahedral finite element.

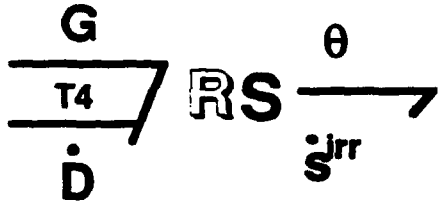

Fig. 3 Bond graph element representing thermomechanical damage evolution in a tetrahedral finite element.

Recognizing the importance of the latter class of problems to composite structural analysis and design, the present paper develops a three-dimensional, state space description of coupled heat diffusion and structural dynamics, for the case of anisotropic thermoelastic materials with continuum damage. Combining bond graph techniques for mixed energy domain modeling with well established finite element discretization methods (Fahrenthold and Wargo, 1992) provides a systematic and thermodynamically rigorous treatment of the thermomechanical problem. The method is well adapted for extension to include electrical, chemical, and other effects of particular interest to composites engineers.

References:

Fahrenthold, E.P., and Wu, A., 1988, "Bond Graph Modeling of Continuous Solids in Finite Strain Elastic-Plastic Deformation," *Journal of Dynamic Systems, Measurement and Control*, Vol 110, No. 3, pp. 284-287.

Fahrenthold, E.P., and Wargo, J.D., 1992, "Lagrangian Bond Graphs for Solid Continuum Dynamics Modeling," *Journal of Dynamic Systems, Measurement and Control*, in press.

Drumheller, D.S., 1987, "Hypervelocity Impact of Mixtures," *Int. J. of Impact Engineering*, Vol. 5, pp. 261-268.

Gandhi, M.V., and Thompson, B.S., 1992, Smart Materials and Structures, Chapman and Hall, New York.

Ingrim, M.E., and Masada, G.Y., 1988, "Bond Graph Representation of Thermomechanical Processes in One-Dimensional Thermoelastic Continua," Automated Modeling for Design, ASME DSC Vol. 8, pp. 1-8.

Lagoudas, D.C., and Huang, C.-M., 1992, "Damage Evolution in the Gauge Theory With Applications to Fibrous Composites," Damage Mechanics in Composites, ASME AMD Vol. 150, pp. 91-102.

Pindera, M.-J., and Freed, A.D., 1992, "The Effect of Matrix Microstructure on the Evolution of Residual Stresses in Titanium Aluminide Composites," Constitutive Behavior of High-Temperature Composites, ASME MD Vol. 40, pp. 37-52.

Rosenberg, R.C., and Karnopp, D.C., 1983, *Introduction to Physical System Dynamics, McGraw-Hill*, New York.

Vibration Damping Characteristics of Thick Composite Structures

S. Jimmy Hwang
3M Center
Bldg. 230-1F-02
St. Paul, MN 55144

Ronald F. Gibson
Mechanical Engineering Department
Wayne State University
Detroit, MI 48202

Abstract

Thick components in structures such as rocket motor cases, pressure vessels and hulls for tanks, ships and submarines are often subjected to vibratory loading, but little is known of the vibration damping characteristics of such components. This is particularly true of thick components made of composite materials.

In general, conventional metallic structures have poor internal damping, and most of the damping in such structures comes from joint friction. The enhancement of vibration damping characteristics of thin metallic panels is typically accomplished by the application of constrained viscoelastic layer damping treatments to the panel surfaces (Nashif, et al., 1985). Such damping treatments have proved to be very effective in improving damping, but at the expense of added weight due to the damping layer and the metal constraining layer. Most of the literature on constrained layer damping deals with thin beams and plates, however, and the effects of thick base structures have not been investigated. While advanced polymer composite materials offer the potential for the development of strong, lightweight and highly damped structures, previous research has again dealt mainly with thin structures with and without surface damping treatments (Mantena, et al., 1991) and not much is known of the damping characteristics of these materials when used in thick structures.

This paper presents the preliminary results of an investigation of the vibration characteristics of thick cantilever beams. The principal objective is to study the effects of increased beam thickness on damping and resonant frequency characteristics of thick structural elements of two types: (1) aluminum beam structures with constrained viscoelastic layer damping treatments, and (2) graphite fiber-reinforced epoxy laminated beam structures without damping treatments.

The analysis of damping was carried out by using a strain energy/finite element approach, which is often referred to as the modal strain energy approach. The theoretical basis of this approach is the Ungar-Kerwin equation (Ungar and Kerwin, 1962) for the total structural loss factor in terms of element loss factors and the fraction of strain energy stored in each element:

$$\eta = \frac{\sum_{i=1}^{n} \eta_i W_i}{\sum_{i=1}^{n} W_i}$$

where η_i is the loss factor of the ith element, W_i is the strain energy stored in the ith element at maximum vibratory displacement and n is the number of elements. Finite element analysis is used to determine the strain energy distribution in the structure, and, in this case, n is the number of finite elements. In general, this equation is evaluated for each mode of vibration, resulting in a modal loss factor for each mode. A previously developed three-dimensional strain energy/finite element analysis (Hwang and Gibson, 1991) based on the fully expanded, three-dimensional version of this equation was used to evaluate the loss factors for the beams in the first bending mode of vibration. The corresponding first mode natural frequencies were determined from the eigenvalue solver in the finite element program.

Experiments have only been done so far on the constrained layer beams, which consist of 2024 alloy aluminum beams of various thicknesses with 3M SJ-2052X constrained viscoelastic layer damping tape of constant thickness on one side of the beam. The viscoelastic adhesive layer is made of 3M ISD-112 acrylic polymer, and the constraining layer is dead soft 1100 aluminum. Unidirectional T-300/934 graphite/epoxy composite beams with fiber orientations of 0^0 and 45^0 were only evaluated analytically, and the corresponding experiments have not been conducted yet.

A previously developed impulse-frequency response technique (Suarez and Gibson, 1987) was used to evaluate damping and frequencies of the beam specimens. This technique is based on the analysis of the frequency response spectrum for a specimen which has been excited by a small electromagnetic impulse hammer. The cantilever beam version of this apparatus is shown in Fig. 1. Displacement response is monitored by a non-contacting eddy current transducer, and a Fast Fourier transform analyzer is used to compute and display the frequency response spectrum. Once the first mode peak in the frequency response spectrum is isolated, damping is determined by the half-power bandwidth method, and the natural frequency is equal to the peak frequency.

Fig. 2 shows the predicted variation in the first flexural mode loss factor of the beams as a function of base layer thickness. High damping is found for thin constrained layer beams due to large shear deformations generated in the viscoelastic layer. As the base layer increases, however, the damping of the constrained layer beam decreases as the effect of the surface damping treatment diminishes. While the damping of the constrained layer beams is greater than that of the composite beams for small beam thickness, the composite beam damping increases and surpasses that of the constrained layer beams as the beam thickness increases. The increase in the composite damping with increasing beam thickness is believed to be due to the frequency dependence of the damping in the epoxy matrix material, and to increased through-thickness shear deformations in the thick composite beams.

Additional results have been obtained regarding the contributions to total damping by the various materials and the different stress components in the beams. For example, shear coupling in the 45° composite beam and the shear stress in the viscoelastic layer of the constrained layer beam are found to be important factors affecting the total damping. Experimental results for the constrained layer beams showed good agreement with predicted values, and the effect of increasing beam thickness on the damping was verified experimentally, as shown in Fig. 3. In conclusion, these results clearly show that, while metal beams with surface damping treatments offer the highest damping for thin beams, composite materials offer superior damping as the beam thickness increases. The implications for real structures having thick components cannot be ignored, and further research on thick plates, thick shells and other thick structures having more complex geometries is warranted.

References

Hwang, S. J., and Gibson, R. F. (1991). The Effects of Three-Dimensional States of Stress on Damping of Laminated Composites. *Composites Science and Technology*. 41, 379-393.

Mantena, P. R., Gibson, R. F., and Hwang, S. J. (1991). Optimal Constrained Viscoelastic Tape Lengths for Maximizing Damping in Laminated Composites. *AIAA Journal*. 29 (10), 1678-1685.

Nashif, A. D., Jones, D. I. G., and Henderson, J. P. (1985). *Vibration Damping*, Wiley Interscience, New York.

Suarez, S. A., and Gibson, R. F. (1987). Improved Impulse-Frequency Response Techniques for Measurement of Dynamic Mechanical Properties of Composite Materials. *Journal of Testing and Evaluation*. 15, 114-121.

Ungar, E. E., and Kerwin, E. M., Jr. (1962). Loss Factors of Viscoelastic Systems in Terms of Strain Energy Concepts. *Journal of Acoustical Society of America*. 34 (2), 954-958.

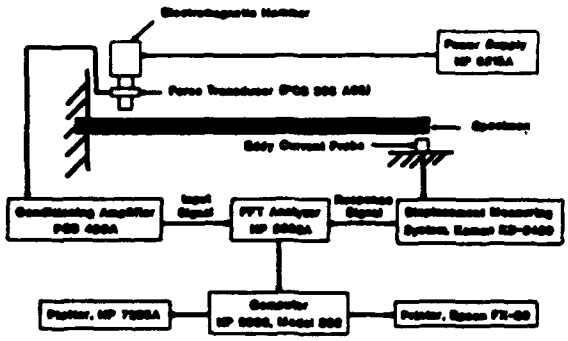

Figure 1. Impulse-frequency response apparatus for measurement of frequencies and damping of cantilever beam specimens.

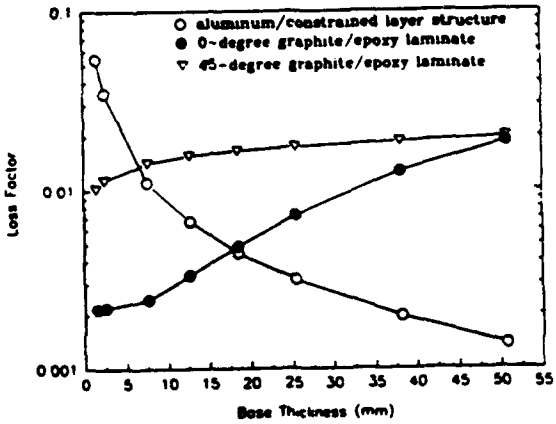

Figure 2. Predicted variation of first mode flexural loss factor with base layer thickness for cantilever beam specimens constructed of aluminum/constrained layer and graphite/epoxy.

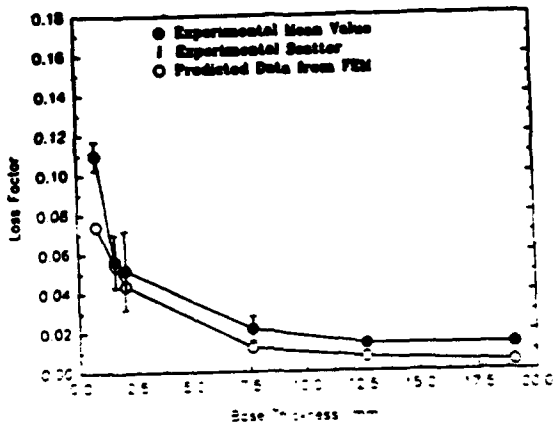

Figure 3. Variation of predicted and measured first mode flexural loss factor with base layer thickness for cantilever beam specimens constructed of aluminum/constrained layer.

A Study of Composite Overwrapped Cylindrical Gun Barrels

David Kokan and Kurt Gramoll
Aerospace Engineering, Georgia Institute of Technology, Atlanta, GA 30332

Thomas Mensah
Clark Atlanta University, Atlanta, GA 30314

This project is a joint research program between Georgia Tech and Clark Atlanta University to investigate the elastic strain and stress response of a filament wound gun barrel during manufacture cure and firing. Included in the project is the actual fabrication of various overwrapped steel tubes with two types of fiber and resin at two fiber tensions. Also demonstrated are the advantages of joint projects between traditional engineering schools and historically black institutions that are strong in science. This project has been funded by the ARMY through the Benet Labs in Watervliet, New York.

This paper will concentrate on the analytical solution of the stress during cure and firing. Numerical results are presented. The results show that a significant residual stress state will exist because of the processing technique. Furthermore, depending on lay-up and cure cycle, large localized stresses can be generated which could cause defects such as longitudinal wrinkles. Also diacussed are several possible solutions.

Large bore gun can be significantly improved by overwrapping the barrel with advanced composite materials. However winding pattern, winding tension, cure cycle, and resin selection are all considered key factors affecting quality and consistency of highly structural efficient filament wound vessels (Lark, 1977). Selecting these is only part of the process. Concerns specific to a particular application must be addressed, both in terms of manufacturing and utilization. This paper will look at the winding tension during fabrication, and then the curing temperature and curing pressure during ramp up and ramp down on the residual stress after cure. Finally, these stresses are examined as a source of wrinkling in the barrels. The basic problem is illustrated in Fig. 1 as a multilayed tube.

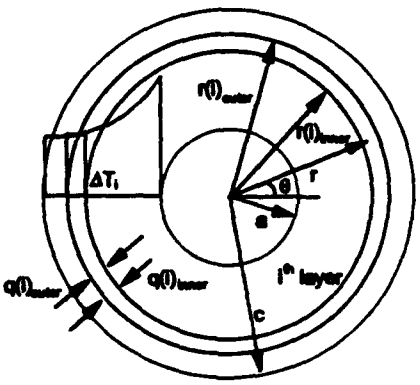

Fig. 1. Basic problem of multilayered cylindrical tube.

One problem with filament winding thick composites is the longitudinal wrinkles that form during the curing process. It is thought that this is due to the bleeding of excess resin as well as fiber compaction. The fibers accommodate the loss of volume by folding over, forming wrinkles (Calabrese, et al, 1987). Even an almost completely dry wind does produce these wrinkles indicating that the problem is more than just resin related. Additional tension applied during the winding could increase compaction and help to reduce wrinkling. Unfortunately, high tension often causes filaments wound circumferentially to cut into lower layers, destroying them. Future work toward solving this problem will involve optimizing the packing of the fibers during the winding process and investigating the effects of the cure cycle.

The stress distribution in a compound cylinder may be found by decomposing the problem into a number of simpler ones, solving each of them, and superimposing the solutions. For each layer, a spatially uniform temperature gradient is assumed. By breaking the cylinder down into a large number of these elements, any general temperature profile can be approximated. Equations have been developed to allow the calculation of stresses and displacements on orthotropic elements. Additional boundary conditions must be enforced at the interface of two layers within the cylinder, such as matching pressure and strains at the interface.

For the winding tension, the method given by Faupel and Fisher (1981) is used to calculate the tension stress on filament wound cylinders.

$$\sigma_r = -\frac{T\left(r^2-a^2\right)}{2r^2}\left(\ln\frac{c^2-a^2}{r^2-a^2}\right)$$

$$(\sigma_\theta)_{composite} = T\left[1-\left(\frac{r^2+a^2}{2r^2}\right)\left(\ln\frac{c^2-a^2}{r^2-a^2}\right)\right]$$

The analysis for an orthotropic cylinder subjected to pressure loads closely parallels that of an isotropic cylinder and is presented in Lekhnitskii (1981). Witherell (1990a), after some simplification of Lekhnitskii's solution, produced the following set of equations for a monolayered orthotropic cylinder under plane strain condition subjected to internal pressure q and external pressure P_o.

$$\sigma_r = \left[\frac{q\lambda^{k+1}-P_o}{1-\lambda^{2k}}\right]\left(\frac{r}{r_o}\right)^{k-1} + \left[\frac{P_o\lambda^{k-1}-q}{1-\lambda^{2k}}\right]\left(\frac{r_i}{r}\right)^{k+1}$$

$$\sigma_\theta = k\left[\frac{q\lambda^{k+1}-P_o}{1-\lambda^{2k}}\right]\left(\frac{r}{r_o}\right)^{k-1} - k\left[\frac{P_o\lambda^{k-1}-q}{1-\lambda^{2k}}\right]\left(\frac{r_i}{r}\right)^{k+1}$$

where

$$k = \sqrt{\frac{\alpha_{11}}{\alpha_{22}}} \qquad \lambda = \frac{r_i}{r_o}$$

For an orthotropic cylinder subjected to a temperature difference, several authors including Hyer (1987) and Witherell (1993) have outlined elasticity solutions for calculating the thermal stresses in multilayered composite tubes. The assumptions are that the stresses and strains are not functions of the axial coordinate and that temperature is spatially uniform

within each layer. This implies that the responses are independent of theta. The equations for these results are somewhat lengthy are not presented here.

For each sub-problem, expressions exist for the radial and circumferential stresses. The last set of unknowns that must be determined are the interface pressures. This is accomplished by requiring that the hoop strain for adjacent layers be equal at their interface. In Witherell's notation, the hoop strain equivalence between layers *i* and *i*+1 is given by

$$\varepsilon(i)^{T}_{\theta,b} + \varepsilon(i)^{pq}_{\theta,b} = \varepsilon(i+1)^{T}_{\theta,a} + \varepsilon(i+1)^{pq}_{\theta,a}$$

where the superscript '*T*' denotes thermal effects and '*pq*' denotes pressure effects. If this condition is enforced for a cylinder with n layers, there will be n-1 interfaces and thus n-1 equations to be solved for the unknown pressures at each interface.

The models described above can be used to determine stresses induced on composite cylinders due to manufacturing or service. In the following section, numerical results are obtained and their impact discussed for a cylinder with a steel liner and a composite overwrap of IM7 as an example. The following material properties (IM7/epoxy) and geometry were used.

Composite Properties	Mandrel Properties
E_θ = 146.8 GPa	E = 200 GPa
E_r = 9.9 GPa	ν = 0.3
E_z = 9.1 GPa	
$\nu_{r\theta} = \nu_{rz}$ = 0.3	Geometry, radius
$\nu_{\theta z}$ = 0.49	inside, a = 34.8 mm
$\alpha_r = \alpha_z = 33.7 \times 10^{-6}/^{\circ}C$	interface, b = 38.0 mm
$\alpha_\theta = -0.0774 \times 10^{-6}/^{\circ}C$	outside, c = 45.7 mm

Although these properties represent a hoop lay-up, the solution technique is not restricted to this type of lay-up. Any orthotropic lay-up can be handled, even ±θ wraps like those produced by the filament winding process, so long as the angle pair is view as a single orthotropic layer.

Winding tension for the IM7 fibers (12K) was set at 6 lb in this study, which equates to a 113.1 MPa tensile stress During the cure, the resin changes from a liquid to a solid plastic capable of transferring load. The stress due to the winding tension, temperature increase in the autoclave, pressure in the autoclave and decrease of temperature in the autoclave are modeled separately and are superimposed to give the total residual stress. As an example, Figure 2 shows the stress state of a cylinder wound with IM7 fibers at a tension of 6 pounds and cured using temperature only. Most authors have assumed that the residual stresses can be estimated by considering only the temperature downramp during cure. This figure shows that these stresses are in fact the dominant ones, but that the other stresses are not negligible It is interesting to note that there exists a significant tensile radial stress at the liner-jacket interface. In the lab, it has been observed that the jacket often separates from the liner because of the thermal mismatch between a steel and composite. It may be difficult to produce an adhesive bond strong enough to handle this large load. The load could be reduced by increasing the winding tension. Other options include autofrettaging, or plastically deforming, the inner liner to force a fit. Conversely, it may be possible to shrink fit the liner by taking it to a very low temperature. It would also be worthwhile to investigate the effect of surface finish on the interface properties.

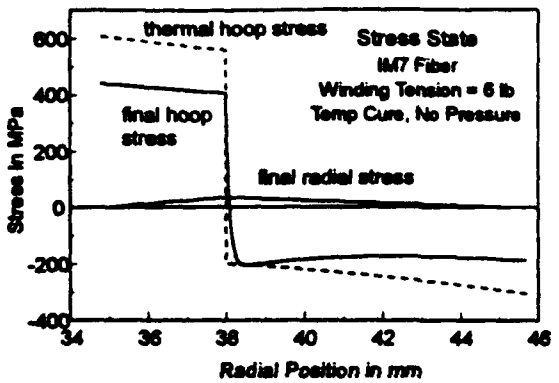

Fig. 2. Final residual stresses from winding and cure.

In conclusion, the equations that have been developed are useful to both the design engineer as well as the manufacturer. Overall residual stress states can be predicted. Just as important is the ability to predict the state of stress during curing to identify the causes of manufacturing problems such as wrinkling. Due to the interaction between the winding tension, the cure temperature, material properties, and cure pressure, it has been found that significant compression can occur on the outer edge of the tubes. In particular, low winding tension, and high cure pressure can result in compress wrinkles on the outside layers. Future work should involve accounting for plastic deformations because of the potential to eliminate the separation problem and to correlate the results with the ongoing experimental phase of this project.

REFERENCES

Calabrese, S.S., Cogdell, J.D., Murray, S.F. and Vollmer, H., 1987, "A Study of High Modulus Graphite/High Temperature Polymeric Matrices - Phase 2," Contractor Report ARCCB-CR-87032.

Faupel, J.H. and Fisher, F.E., 1981, *Engineering Design: A Synthesis of Stress Analysis and Materials Engineering*, John Wiley and Sons, N.Y.

Hyer, M.W. and Rousseau, C.Q., 1987, "Thermally Induced Stresses and Deformations In Angle-Ply Composite Tubes", *J. of Composite Materials*, Vol. 21.

Lark R.F., 1977, "Recent Advances in Lightweight, Filament-Wound Composite Pressure Vessel Technology", Energy Tech. Conf., Houston.

Lekhnitskii, S.G., 1981, *Theory of Elasticity of an Anisotropic Elastic Body*, Mir Publishers, Moscow.

Timoshenko, S.P., and Goodier, J.N., 1970, *Theory of Elasticity*, 3rd Edition, McGraw-Hill, N.Y.

Witherell, M.D., 1990a, "A Plane-Strain Elastic Stress Solution for a Multiorthotropic Layered Cylinder", Technical Report ARCCB-TR-90016.

Witherell, M.D., and Scavullo, M.A., 1990b, "Stress Analysis and Weight Savings of Internally Pressurized Composite-Jacketed Isotropic Cylinders", *Journal of Pressure Vessel Technology*, Vol. 112.

Witherell, M.D., 1993, "A Thermal Stress Solution for Multilayered Composite Cylinders", Submitted for publication, 1993 ASME Pressure Vessel and Piping Conf.

DELAMINATION DYNAMICS AND ACTIVE CONTROL OF DELAMINATIONS

S. Hanagud
School of Aerospace Engineering
Georgia Institute of Technology
Atlanta, GA 30332-0150

To date, most of the efforts that are directed towards controlling the delamination are passive and are focussed on preventing the formation of delaminations. Several passive options that have been proposed include an optimization of the lamina sequence, an introduction of special adhesive layers, and to serrate the fiber - matrix interface. Even when all these passive options are implemented, delaminations do develop in practice. Active control of delaminations is an alternative in such cases. In the rotorcraft technology, some of the applications include delamination control in the flex beam of bearing less rotor system, a composite hub and critical areas of the airframe. The objective of our studies are to explore the feasibility of real time detection of delaminations in a laminated composite structure and use this information to develop active controllers to prevent these delaminations from further growth. Steps that are necessary in achieving this objective are as follows: Techniques are needed to sense and detect the existence, size and location of delaminations. We also need dynamic models for the delaminated system that can be used as the plant model to design controllers. Other items of investigation are structural mechanics foundation for controller design and actuator options.

In this paper, we will discuss our work in the area of delamination detection techniques by using the change of dynamic characteristics due to delaminations. These techniques offer the potential of being used in real time detection techniques. We have developed an analytical dynamic model for delaminated beams. Theoretical solutions of the beam equations that natural frequencies of delaminated beam are different from the frequencies of a non-delaminated beam. The solutions also indicate the existence of an additional frequency and a corresponding mode due to the presence of a delamination. This can be called as an opening mode of the delamination or a delamination modes. We have validated some of our theoretical studies by means of experimental modal analysis. The presentation will include the preliminary work in the area of active control.

BOLTED JOINT STRENGTH OF GRAPHITE/EPOXY LAMINATES SUBJECTED TO BIAXIAL LOADING CONDITIONS

S.V. Hoa

Department of Mechanical Engineering
Concordia University
Montreal, Quebec, Canada H3G 1M8

ABSTRACT

Bolted graphite/epoxy plates were subjected to in-plane biaxial loading. Cruciform shaped samples were used. Testing was performed on a biaxial machine developed and built at Concordia University. Four arms of the cruciform sample were independently loaded. Different lateral loads were applied along one direction. Along the other direction, load was applied on one arm while the opposite arm was held in the grip without applied load. This opposite arm measured whatever load that was bypassed around the constrained bolt hole. Acoustic emission was used to detect the onset of failure. Results show that there is a significant decrease in joint strength with the application of the lateral load. This effect is more severe for plates with smaller size hole (6.35 mm diameter) as compared to plates with larger size hole (19.05 mm).

INTRODUCTION

In designing using composites, it is advisable to avoid the joint as much as possible. This is because the joint is usually the weakest link in a composite structure. However, there are situations where the joint is not avoidable. One example is the case of patching repair of airframes where patches need to be joined to the parent structure. Another example is the attachment of a composite structure to other structural elements, usually by rivets.

The majority of composite structures in airframes are in the form of thin plates or shells. These structures are subjected to biaxial loading conditions in real applications. It is also well known that laminated composites are anisotropic, this means that their response depends on the direction of the loads.

Most work on joints in composite plates or shells have considered only uniaxial loading. The joint is allowed to float freely while loads are applied on the two ends of the assembly until the joint fails. This type of test may produce useful information but it may not produce data that are representative of what the structure is subjected to in real applications.

In this study, joint strength of graphite/epoxy composites under biaxial loading condition is considered. The configuration of the joint has the bolted hole fixed with the loads applied around it. Figure 1 shows a schematic of the load and constraint arrangement.

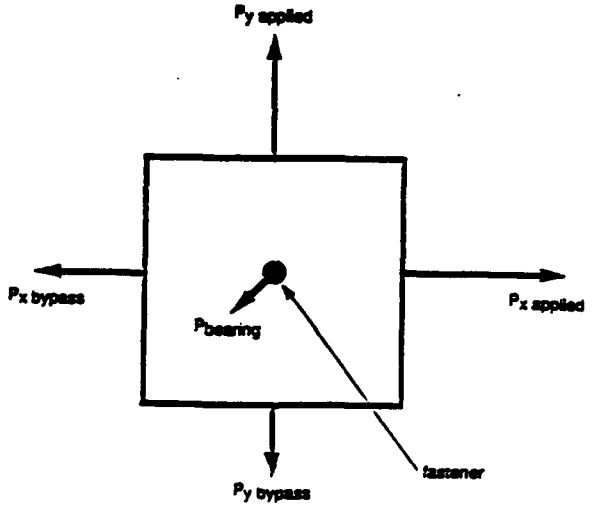

Figure 1: Biaxial bearing/bypass load and constraint arrangement

With the fastener held fixed, different loads can be applied in both the x direction (right hand side) and y direction (upper side) while the x direction (left hand side) and y direction (lower side) are allowed to remain free or are subjected to yet different loads. In other words four different loads can be applied at four loading arms simultaneously. This is possible because the loads can be supported by the fixed fastener.
Depending on the degree of rigidity of the constraint of the fastener, some of the applied loads can be bypassed around the fastener. These are called bypass loads. If the fastener is rigid, there is little or zero bypass load. If the fastener loses its rigidity such as the case after failure at the fastener hole, the bypass load can be larger.

SPECIMEN DESIGN

There appeared to be no form of specimen available for this particular type of test in the literature. It was therefore necessary to design a specimen for this particular test. The development for the design of the cruciform specimen used in this study was given in [1] and [2]. This specimens has the configuration shown in Figure 2.

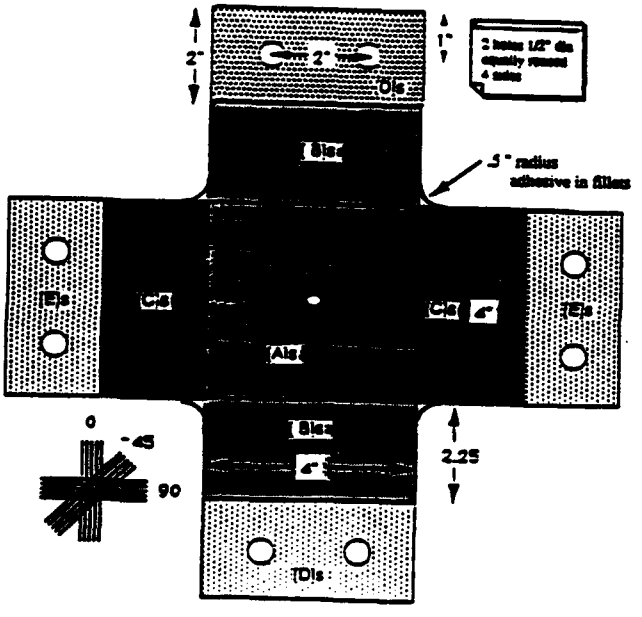

Figure 2: Configuration of biaxial specimen.

RESULTS

Table 1 shows the joint strength results for plates containing of three different hole sizes, five different lateral loads from 0 kN to 30 kN and a case of no clamp load.
Consider first the lateral load as the varying parameter. For plates with small holes (6.35 mm diameter) with a clamp load of 7484 N, as the lateral load is increased from 0 kN to 15 kN, the joint strength decreases from about 48 kN down to about 23 kN, a decrease of more than 50%. This is very significant because it has the implication that design data obtained from uniaxial loading is non-conservative. For the case of plates containing holes of 19.05 mm diameter, as the lateral load increases from 0 kN to 30 kN, the joint strength also decreases but not as significantly as for the case of plates containining a smaller hole.
Consider now the size of the hole as the varying parameter. In this case it is necessary to normalize the hole size by dividing the load by the diameter of the hole. For 0 kN lateral load, the joint strength is 7.56 kN/m for plates with a hole diameter of 6.35 mm and a strength of 3.25 kN/m for plates with a hole diameter of 19.05 mm. There is a reduction of more than 50% of the normalized strength as the hole size is increased. At a lateral load of 18 kN, there is also a reduction in the normalized strength as the hole size is increased from 12.7 mm to 19.05 mm. However, this reduction is not as severe as the case of 0 kN lateral load.
The case where there is no clamp load gives a joint strength of only 20 kN for plates containing 6.35 mm diameter hole. This is the lowest joint strength in all of the plates containing this hole size.

	(6.35 mm)	P/d KN/m	(12.7 mm)	P/d KN/m	(19.05 mm)	P/d KN/m
lateral load	clamp load 7484 N or 26.3 MPa		clamp load finger tight + 1/4 turn		clamp load finger tight + 1/4 turn	
0 KN	47 - 49 KN	7.56			62 KN	3.25
10 KN	38 - 40 KN 32 KN 34 - 36 KN	6.14 5.04 5.5				
15 KN	22 - 24 KN	3.6				
18 KN			45 KN	3.5	62 KN	3.25
30 KN					53 - 60 KN	2.78 - 3.14

0 clamp load 1/4" diameter, 10 KN lateral, failure load at 20 KN

Table 4- Summary of joint strengths.

HIGH-STRAIN-RATE BEHAVIOR OF GR/EP LAMINATE UNDER TRANSVERSE IMPACT

Piyush K. Dutta
U.S.Army Cold Regions Research and Engineering Laboratory
Hanover, NH 03755

and

David Hui
University of New Orleans, New Orleans, LA 70148

Extended Abstract

Much of the early work on the dynamic mechanical response of fiber-reinforced composites used impact bend tests of Izod or Charpy type [1,2]. The complex loading system in such tests does not allow a fundamental interpretation of the data obtained and prevents any simple analysis of the effect of loading rate on the failure processes. For this reason over recent years attempts have been made at the U.S. Army Cold Regions Research and Engineering Laboratory, Hanover, New Hampshire, to develop impact tests for fiber-reinforced composite materials in which a simpler loading system is applied and account can be taken of stress wave effects. Version of the the split Hopkinson's pressure bar apparatus for simple uniaxial compression has been designed and large strain rate effects are being investigated on 48-ply GERP, where mechanical response is strongly rate dependent.

The CRREL Hopkinson Bar Impact Apparatus consists of a short striking bar driven by compressed air and two long, solid, round bars instrumented with strain gauges. The striker's impact on the first bar sets up a compressive stress pulse, whose amplitude depends on the impact velocity and whose duration depends on the striker's length. The test specimen is held between the two bars in a chamber cooled by liquid nitrogen. At the interface, some energy of the stress pulse from the first bar is reflected because of the mechanical impedance mismatch of the bar and the specimen. The rest is transmitted into the specimen, propagates through it, and reaches the second bar's interface with the specimen. At the second interface, part of the stress pulse is again reflected back into the specimen and the remainder is transmitted to the transmitter bar. If the specimen is much shorter than the wavelength of the loading pulse, the wave-transmitting time will be small compared with the duration of the loading stress pulse, and after a few reflections within the specimen, the stress and strain along the specimen become approximately uniform.

Consideration of equilibrium at the interface between the specimen and the transmitter bar shows that the forces in the specimen and in the transmitter bar are equal. The force is determined by measuring the strain on the elastic transmitter bar using strain gauges and the average strain in the specimen is calculated from the displacements at the end of the specimen using equations (1), (2), and (3).

specimen strain $$\varepsilon_s(t) = \frac{-2c}{L_s} \int_0^t \varepsilon_r(t)dt \quad (1)$$

specimen strain rate $$\frac{d\varepsilon_s(t)}{dt} = \dot{\varepsilon}_s = \frac{-2c}{L_s} \varepsilon_r(t), \text{ and} \quad (2)$$

specimen stress $$\sigma_s(t) = E_b \varepsilon_t(t) \quad (3)$$

where

c = wave propagation velocity in the Hopkinson bars

L_s = length of specimen

$\varepsilon_r(t)$ = instantaneous reflected strain

$\varepsilon_t(t)$ = instantaneous transmitted strain

E_b = elastic modulus of the bar material.

Figure 1 illustrates the test system.

Currently an investigation is in progress, supported by U.S. Army CRREL to study the influence of low temperature on the compression impact response of a 48-ply Fiberite 974 epoxy reinforced with T-300 graphite fiber, in an attempt to determine how far the increased strength and energy absorbing potential of different orientations and layers of reinforcements at all rates can be optimized. Figure 2 shows some initial data from high-strain-rate impact on two graphite/epoxy laminates impacted transversely at lower than fracture load in the Hopkinson bar. In the A-1 laminates all plies are oriented in the same direction ($[0]_{48}$). The B-1 laminate also consisted of 48 plies but arranged in six layers as $[0_8/90_8/0_8]_s$. Note that the stress-strain curves, shown in Figure 2(e) and 2(f) for the two types of laminate are significantly different. The average elastic modulus, E_z, of the $[0]_{48}$ laminate is 0.53×10^6 psi (3.66 GPa) and that of the $[0_8/90_8/0_8]_s$ is 0.95×10^6 psi (6.55 GPa). As a result, although both laminates were subjected to nearly the same magnitude of impact stress, 17,500 psi (120.7 MPa), the A-1 laminate, $[0]_{48}$, developed a peak strain of $\epsilon = 30 \times 10^{-3}$ at the strain rate $\dot{\epsilon} = 700$ strains s^{-1}; whereas for B-1 laminate, $[0_8/90_8/0_8]_s$, $\epsilon = 19 \times 10^{-3}$ at $\dot{\epsilon} = 550$ strain s^{-1}. For any particular laminate type the strain rate, $\dot{\epsilon}$, can be systematically increased by increasing the impact velocity or geometry of the specimen. The above results clearly indicate that the impact response of the layered composites is dependent on the ply geometry and ply properties. Since the properties do change under environmental conditions, for example high and low temperatures and humidities, we propose to study these impact responses under the varying environmental conditions for which facilities have been developed at CRREL.

References:

1. Hancox, N.L. (1971). "Izod impact testing of carbon fiber reinforced plastics," Composites, Vol. 1, 41-45.

2. Adams, D.R. and J.L. Perry (1975). "Instrumented Charpy impact tests of several unidirectional composite materials," Fiber Science and Technology, Vol. 8, 275-302.

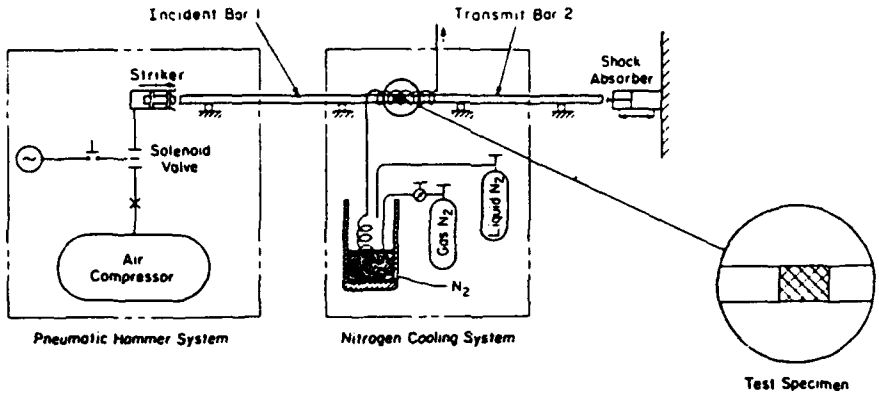

Figure 1. Split Hopkinson pressure bar system schematic.

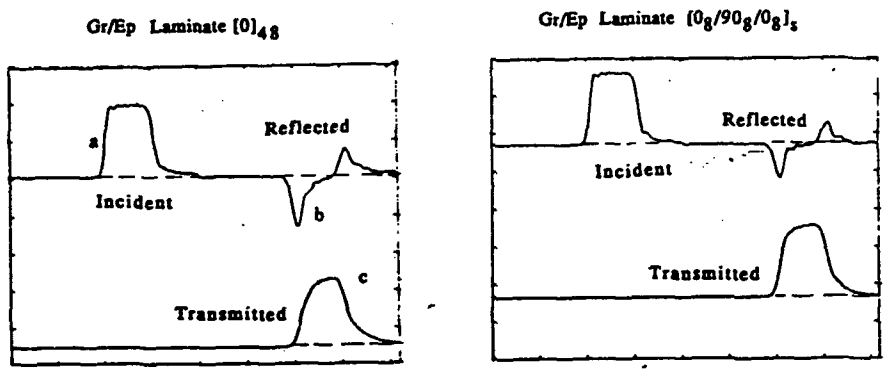

a. Stress waves through the specimen in Hopkinson pressure bar.

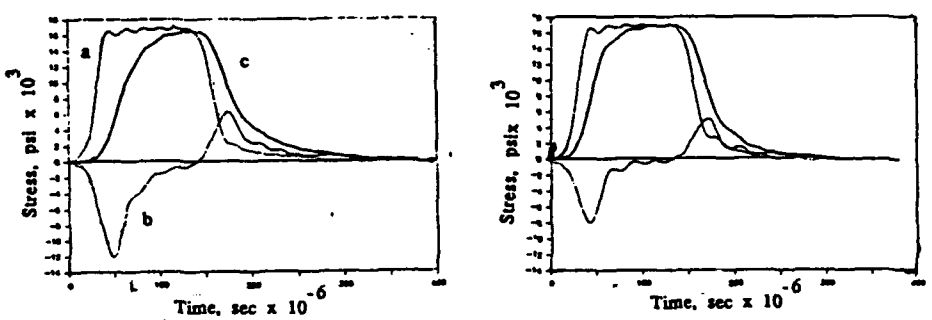

b. Stress waves analysis by superimposition

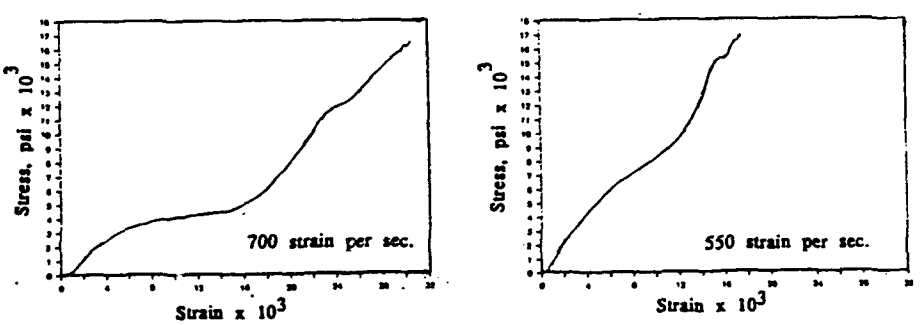

c. High strain rate stress-strain data

Figure 2. High-strain-rate impact test results of two Gr/Ep composites.

Impact of Fiber Composite Laminate Plates: A Percolation View of Perforation and Spallation

Zeev Jaeger[1], Misha Anholt[1], and Arnold H. Mayer[2]
1 Soreq Nuclear Research Centre, Yavne, Israel
2 Wright Laboratory, WPAFB, OH

Abstract

In a series of impact experiments on composite plates which were aimed at testing the conjecture that the perforation threshold represented a critical phenomenon and that Percolation Theory could eventually provide an adequate description of the spallation or fragmentation process accompanying the perforation of anisotropic layered materials, the fragments emerging from a 0/90 layup fiber epoxy plate target were collected and photographed. Image analysis techniques were used to deduce the size distribution of the backside fragments. It was found that the number N of fragments having area S may be represented as a power law $N \sim 1 / S^{J}$. The average exponent for the experiments which were performed at nine different values of impact velocity over the range from 300 to 6000 fps had the value $J = 2.17 \pm 18\ \%$, which lies between the previously predicted theoretical values from Percolation Theory of $J(2D) = 2.05$ and $J(3D) = 2.2$. For the velocity $V_1 = 397$ fps which is close to the perforation threshold velocity, J had the value 2.03, which is surprisingly close to the two dimensional Critical Percolation Limit.

Introduction

The mechanical properties of a composite are severely degraded by impact induced damage. A significant fraction of the projectile kinetic energy is channelled into rival modes of damage,, i.e. delamination, fiber fracture, matrix cracking and fragmentation. Some disintegration appears around and inside the penetration hole, and at the backside of the target spall is produced even at velocities less than the ballistic limit. More energy is consumed above this limit, as intense fragmentation emerges from the target. This process may be studied quantitatively by measuring the fragment size distribution.

Under a short impulse of pressure, a situation typical of either an impact or an explosion is created. The stress acts in a local way and is "unable" to scan the medium for its weakest points. Therefore, many cracks grow simultaneously and independently in different regions of the target. These conditions lead to the well known result (4) that the average fragment size becomes smaller the higher the strain rate. Moreover, they provide the physical justification for using percolation theory in predicting fragment size distributions. (2,3)

Percolation theory (1) has been recognized as a statistical physics model for critical phenomena. By applying it to fracture and fragmentation problems we were able to show that fragmentation (as well as the coalescence of many microcracks forming a macroscopic fracture) is a critical phenomenon. Fragmentation occurs whenever the density of cracks reaches its critical value. That is to say, that when the probability, p, of creating a microcrack achieves the critical value, p_c. For crack densities higher than p_c, the critical density of microcracks, the number of small particles in the population grow at the expense of the reduction of the number of large ones. Consequently, the total surface area of the fragments is growing. It is therfore, expected, that the minimal surface energy required for fragmentation is received at p_c (below p_c a complete shattering of the finite macroscopic piece of material is not possible).

Coming back to impact physics, the determination of the limit velocity below which perforation of a given target by a given projectile is not possible continues to be of much interest. Even the definition of the ballistic limit (5) (the critical value of striking velocity at which the probability of perforation is 50%) suggests that stochastic mechansms are at play. Below the ballistic limit, it is expected that the spalled fragmented zone at the backside of the sample and the shattered and penetrated zone in the front side will be well separated by a zone of delaminated material strong enough to prevent the projectile from perforating the target. In the limit as this intact zone becomes very thin, these two zones will touch each other, and the sample will then become disintegrated throughout its thickness. It is of interest to inquire whether the critical condition for fragmentation supplied by percolation theory is able to yield additional information about the ballistic limit and the physical conditions of its occurrence.

Description of the Experiment

Image Analysis

The population of fragments from each experiment was collected on the inner surface of a cylindrical sheet of paper coated with a sticky adhesive. After the experiment, the cylinder was rolled flat and photographed. Such a procedure has to be carried out with caution in order to avoid any optical noise resulting from shadows, unequal illumination or spurious particles.

The photographs were scanned and a digitized image was obtained. The next step is the division of the digital image into clusters of material (fragments) and the background. This procedure is not easy when the gray levels of the fragments and local background overlap. Also, it is not easy to distinguish two fragments partially overlapping each other. Special data treatments were adopted to reduce distortion and deterioration of the information recorded in the digital picture, which was scanned by a 512 X 512 black and white scanner. Higher resolution of the original photograph, of course, will result in higher final resolution and consequently more data on possible lost information with regard to the very fine fragments.

The measured fragment size histograms vary continuously in an irregular way. In order to overcome the effects of random fluctuations, the results were accumulated in bins having unequal width. Each bin further along on the size axis was made twice as large as the preceding one. The total number N of occurences in a bin was divided by the bin width, to obtain the average distribution density of size S. A linear least squares fit of log N against log S was performed in order to deduce the parameters of the expected power law relationship.The results are presented in Figure 1. The slopes and intercepts of the linear fits are presented in Table 1 for each velocity.

The role of strain rate in controlling fragmentation was recognized by Grady [3] in the early eighties. The highest strain-rate found during an impact may be estimated by the ratio of the projectile to its radius, $de/dt \sim V_p / R_p$. Strain rates at the backface may be estimated by multiplying this value by some attenuation function for the particle velocity. In any case, it is expected that the higher the impact energy is, the smaller will be the average fragment size. It is not surprising therefore that the trend of intercepts in Table 1 really represents the fraction of fine particles in the distribution. The behavior of the slopes needs further consideration. The mass of a fractal structure having a length L (L>>1) is given by $M(L) \sim A L^D$ where D is the fractal dimension. At the critical point, $p = p_c$, the value of D is known. For homogeneous percolation in the plane, D = 1.9 (2D). In three dimensional space D = 2.5 (3D). An additional result of percolation theory [1] is that the number n_s of clusters having s sites (per site) is given by $n_s \sim 1 / S^J$, where J = (d+D) / D, and where the exponent J has the value J = 2.05 in two dimensions and J= 2.2 in three dimensions (d=3). All the slopes in Table 1 are around these values with an error not exceeding about 20%. Furthermore, in the introduction, a possible relation between the perforation threshold and critical fragmentation was conjectured. The lowest velocity in Table 1 is not far from the perforation threshold found experimentally [6], namely V_0 = 375 fps. The slope of the corresponding fragment size distribution is extremely close to the theoretical value of J for the two dimensional case. If the fragments of the impacted composite plate have a fixed thickness (as would be the case if it they resulted from the fragmentation of previously delaminated plies), then the measured area distributions would represent, in fact, two dimensional mass distributions. In a laminated material with planar weaknesses between the plies, such a hypothesis appears plausible. In general isotropic solids, a true three dimensional behaviour is expected with J = 2.2. It is interesting to check whether fragment size distributions from impacted brittle soldis also behave in the same way near the perforation limit. More work is needed in order to correlate other statistical Physics features either with dynamical predictions or with experimental data.

References

(1) D. E. Grady, J. Appl. Phys. 53,322 (1982)

(2) R. Englman, N. Rivier and Z. Jaeger Phil. Mag B56, 751 (1988)

(3) M. Anholt, R. Englman and Z. Jaeger, "Percolation Approach to Locally Caused Fragmentation", Centre de Physique, Les-Houches, France, D. Beysems et. al. Eds, April 12-17 1993

(4) D. Stauffer "Introduction to Percolation Theory", Taylor and Francis, London 1985

(5) J. A. Zukas, "Penetration and Perforation of Solids", chap.5 in "Impact Dynamics", J. A. Zukas, T. Nicholas, L. B. Gresczuk and D.R. Curran Eds, Wiley N.Y. (1982)

(6) G. J. Czarnecki, "A Preliminary Investigation of Dual Mode Fracture Sustained by Graphite/Epoxy Laminates Impacted by High Velocity Spherical Metallic Projectiles" MS Thesis, University of Dayton, OH (1992)

Impact Dynamics and Damage initiation in Laminated composites

S. P. Joshi, University of Texas at Arlington; Klaus Friedrich and Jozsef Karger-Kocsis, University of Kaiserslautern; Alexander Bogdanovich, Latvian Academy of Sciences

Low velocity impact induced damage assessment requires knowledge of contact behavior, transient elastic wave propagation, crack nucleation, and propagation and interaction. The initial crack formation takes place in and near the contact region and therefore is sensitive to the indentation behavior. A detailed dynamic stress field based on the realistic contact laws [1] provides information about highly stressed zones in the undamaged target composite structure. These zones can be identified as crack initiation domains. The stress field in these crack initiation domains is used to identify the stress components responsible for cracks nucleation. Once the crack nucleation is recognized, propagation can be studied with the help of the fracture mechanics principles. However, it should be recognized that the dynamic stress field at every stage of propagation is very complex and therefore intractable to detailed study. It is clear that the elastic stress field, although complex, is well defined up to the point of initial fracture. Joshi and Sun [2,3] presented a simple study incorporating the above mentioned notions of the impact-induced damage initiation in laminated composites.

The impact damage in laminated composites has been an active research area for a long time which is evident from the vast amount of literature available in this area. The purpose of this paper is to discuss some important features of contact behavior, transient incident energy propagation and crack nucleation with the help of numerical and experimental results.

Determination of spatial and temporal distribution of contact traction is important in impact studies. It is apparent that the traction distribution over the contact area can have a profound influence on the nature of the near contact stress field. For example, compare the Boussinesq stress filed [4] in a half space subjected to point load to a Huber stress field [5] with distributed load according to Hertz analysis. The spatial distribution of the impact load should not be ignored when studying impact-induced fracture initiation occurring in the near-contact region.

The temporal characteristics of the impact loading are also important. The difference in rates at which the incident energy is imparted to the structure and propagated away from the impact point is responsible for the high stress build-up in the near-contact region. The contact area and the traction distribution changes with change in resultant contact load with time. In a dynamic contact, spatial and temporal characteristics of the contact are coupled. The use of static indentation laws may be considered and is justified under the following assumptions:

1. The total contact duration is a order of magnitude longer than the time taken by the longitudinal waves to travel through the thickness of the target composite, assuming thickness is the smallest dimension.

2. The rate of change of contact area is a order of magnitude smaller than the characteristic inplane longitudinal wave velocity.

3. The impactor dimensions are comparable to the thickness dimension of the target or it is very stiff compared to the target. This rules out effect of elastic wave propagation in the target.

The numerical results in this study are obtained by incorporating static indentation laws in conjunction with the plate and impactor dynamics. The temporal distribution of contact force is obtained by employing a plate finite element analysis [5] with the static experimentally obtained indentation laws [6]. The effect of spatial variation of the impact load on through-the-thickness distribution of stresses is captured by considering a plane strain problem of an infinitely wide plate impacted by a rigid cylindrical impactor. The contact length during the impact is calculated by modified Hertzian indentation law, providing elliptical force distribution over the contact length. The previously obtained (from the plate analysis) temporal distribution is implemented as resultant impact load in the cylindrical impactor problem. The quantitative information about the loading is lost in doing so,

while the qualitative nature of the impact loading is retained. The contact length, obtained using the Hertzian law, is scaled to match the experimentally obtained contact. The spatial distribution of the load is assumed to be elliptical and is applied as consistent nodal forces within the contact length. The nodal forces are modified at every time step integration, depending on the contact length and resultant impact load.

Elastic waves travel at different phase speeds in different directions because of anisotropic material properties of the target. The initial stress field in the vicinity of impact is solely due to incident energy if the geometric boundaries are sufficiently away from the impact point. The relative importance of reflected energy (geometric boundary conditions) in initiating damage may be resolved by comparing the time taken by the dominating frequency component of the initial pulse to reach the impact region after reflection within the impact duration itself. It should be noted that interference between initial pulse and the reflected pulse can be constructive or destructive. We will restrict the discussion to non-interference cases.

We expect three dimensional stress field in the vicinity of the impact center (a region with dimensions of the order of maximum contact length) and two dimensional (plate or shell type) stress field in the far-region. The thickness dimension plays an important role. The Near-Impact-Stress-Field (NISF) is considerably different in thick and thin laminated composites. The NISF is also altered by the boundary conditions on distal surface (free surface or surface resting on rigid support etc.) which is the nearest surface from impact point. The transverse normal stress in NISF has to satisfy compressive normal traction on the contact surface and zero traction on the rest of the proximal surface and the distal surface; this surface is free in most of the practical problems. In general, the impact duration is far greater than the time taken by a longitudinal wave to travel through the thickness and, therefore, the through the thickness distribution of the transverse normal stress will not be altered by the reflection from the distal surface. This means that the problem is quasi-static in the thickness direction which also justifies use of static indentation laws. These two attributes of the NISF (boundary conditions and quasi-static nature) restricts transverse normal stress from becoming significantly tensile.

Crack nucleate in region of high stress concentration. These stress produced cracks orient themselves perpendicular to the maximum tensile principal stress direction in the brittle isotropic material by a smooth impactor is experimentally verified [7]. In case of anisotropic solids, it is necessary to take into account the orientation dependence of both elastic constants and surface energy. Clearly, in composites with strong directional cleavage tendencies, the anisotropy in surface energy will govern. In general, though, we expect some compromise between the tendencies for cracks to be orthogonal to maximum tensile stress and weaker cleavage planes. Each ply of the laminated composite plate may be considered as transversely isotropic, with plane of isotropy being orthogonal to fiber orientation of the ply. Therefore, the crack will nucleate orthogonal to the major component of tension in the isotropic plane of the ply. Initial impact damage can be explained with the help of this hypothesis.

Representative numerical and experimental results will be included in the full length paper to substantiate the arguments and elaborate on the various aspects of the low velocity impact presented above.

This research is partially funded by NATO grant No. CRG 920 125.

REFERENCES

1. Tan, T.M. and Sun, C.T., NASA CR-168057, December 1982.
2. Joshi, S.P. and Sun, C.T., J. of Composite Materials, Vol. 19, No. 1, 1985, 51-66.
3. Joshi, S.P. and Sun, C.T., J. of Composites Technology and Research, Vol. 9, No. 2, 1987, 40-46.
4. Lawn, B.R. and Swain, M.V., J. of Material Science, Vol. 10, 1975, 113-122.
5. Lawn, B.R., J. of Applied Physics, Vol. 39, 1968, 4828-4834.
6. Chen, J.K., Ph.D. Dissertation, Purdue University, 1984.
7. Yang, S.H. and Sun, C.T., NASA CR-165460, July 1981
8. Mikosza, A.G. and Lawn, B.R., J. of Applied Physics, Vol. 42, 1971, 5540-5545

GEOMETRICALLY NONLINEAR IMPACT RESPONSE OF THIN LAMINATED IMPERFECT CURVED PANELS

Rakesh K. Kapania* and Tom-James G. Stoumbos**

Department of Aerospace and Ocean Engineering
Virginia Polytechnic Institute and State University
Blacksburg, VA 24061, USA

An analytical study is conducted to predict the nonlinear transient response of thin imperfect laminated curved panels subjected to impact loads. Although a large number of studies dealing with impact response of flat laminated plates has been conducted in the past, relatively little work seems to be available on impact of laminated curved panels. The imperfect panels are modeled using a doubly-curved thin plate/shell element capable of modeling arbitrary geometric imperfections. The element was previously presented by Kapania and Yang (1986) and was later extended to study the large-displacement behavior of laminated anisotropic plates and shells (Saigal et.al., 1986) and the buckling, postbuckling and nonlinear vibrations of imperfect plates (Kapania and Yang, 1987).

The element is quadrilateral in shape and has four nodes, one at each corner. Each node possesses 12 DOFs: u^1, $\partial u^1/\partial\xi$, $\partial u^1/\partial\eta$, $\partial^2 u^1/\partial\xi\partial\eta$ and similar quantities for u^2 and u^3, where u^1, u^2 and u^3 are the displacement components in Cartesian coordinates x^1, x^2 and x^3, respectively, and ξ and η are the curvilinear orthogonal coordinates on the middle surface of the shell.

Linear and nonlinear transient responses are obtained using the modal superposition method (MSM) and a reduction method based on Ritz vectors (R-R), both in conjunction with direct integration schemes (Wilson-θ or Newmark methods) (Kapania and Byun, 1993). The effect of the number of modes used is also discussed. A modified contact law is incorporated to evaluate the impact loads due to a projectile. Different non-dimensional shell radii $[r/h]$ are used in order to study the effect of the non-dimensional shell radii $[r/h]$ on the impact response of laminated curved panels. The effect of geometric imperfections on linear and nonlinear transient response under sudden impact loads is also analyzed.

* Associate Professor.

** Graduate Research Assistant.

The laminated composite curved plate considered is a 20-layered $[0°/45°/0°/-45°/0°]_{2s}$ laminate. The plate dimensions α and β are 15.24 cm and 10.16 cm, respectively. The thickness of the plate, denoted by h_0, is 0.269 cm. The curved plate is assumed to be impacted at the center by a spherical steel impactor of diameter 1.27 cm with an initial velocity (v_0) of 3 m/s as shown in Figure 1. The mass density of the impactor is $7.96 \times 10^{-5} Ns^2cm^{-4}$. The boundary conditions are simply supported and immovable in the planes along the plate's edges. The material properties of a graphite/epoxy lamina are assumed to be: $E_1 = 120\ GPa$, $E_2 = 7.9\ GPa$, $\nu_{12} = 0.30$, $G_{12} = G_{23} = G_{13} = 5.5\ GPa$, and $\rho = 1.58 \times 10^{-5} Ns^2cm^{-4}$.

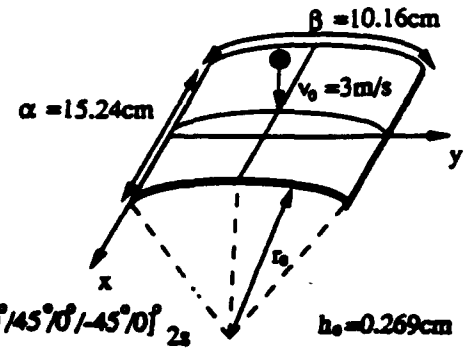

Fig. 1. A laminated curved plate subjected to impact load at the center

The finite element mesh used in this analysis is an 8×8 finite element mesh (for the whole plate). The contact force histories and central deflections of the curved plate were obtained by using both the modal superposition (MSM) and the Ritz reduction (R-R) methods for three different shell radii. The nondimensionalized shell radius defined as r_0/h_0 was used. The contact force histories and central deflections of the curved plate were obtained using a time step of $2\mu s$.

From the comparison between the two methods it was found that both show good agreement in the contact force and displacement histories of a laminated curved plate subjected to impact loads. In

the present iterative procedure for impact response analysis, the time increment needed to be very small in order to get accurate contact forces. For linear analysis, the Rayleigh-Ritz reduction method based on Ritz vectors required less CPU time than the mode superposition method although the results were very similar.

Both methods required a large number of basis vectors to account for the impact load which has high-frequency characteristics. Furthermore, for the nonlinear analysis, the mode superposition method required less CPU time as shown in Table 1. It should be noted that since most of the time is spent on the calculation of the internal nodal force vector the use of reduction methods in performing nonlinear impact response analysis may not result in significant reduction in CPU time. The need for development of an efficient way of handling the calculation of the internal load vector is apparent. Also note that basis updating should be performed properly in order to obtain accurate results for nonlinear impact response studies.

Table 1 Comparison between the CPU time required for the modal superposition method (MSM) and the Ritz reduction method (R-R) (nonlinear analysis).

Non-Dimensional Shell Radius	Number of Modes	CPU Time ($\times 10^4 sec$)	
		MSM	R-R
4000	40	0.5237	1.6185
	60	0.5297	1.8960
1000	40	0.5245	1.6403
	60	0.5333	1.9056
250	40	0.5265	1.6343
	60	0.5285	1.8953

With the reduction of the non-dimensional shell radius $[r/h]$ the curved plate appeared to be stiffer. The non-dimensional shell radius $[r/h]$ for values less than 1000 caused significant changes in the impact response of the laminated curved plate. Figure 2 shows a comparison between the central deflection histories for three different non-dimensional shell radii $[r/h]$. The introduction of geometric imperfections led to similar conclusions, that is a stiffer structure as shown in Figure 3.

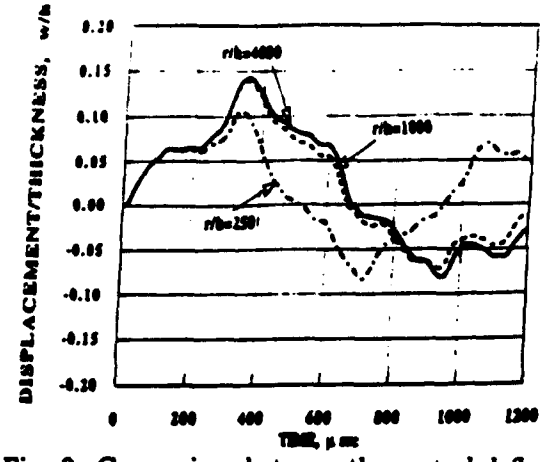

Fig. 2. Comparison between the central deflection histories for three different non-dimensional shell radii (r/h) (plate thickness: 0.269cm).

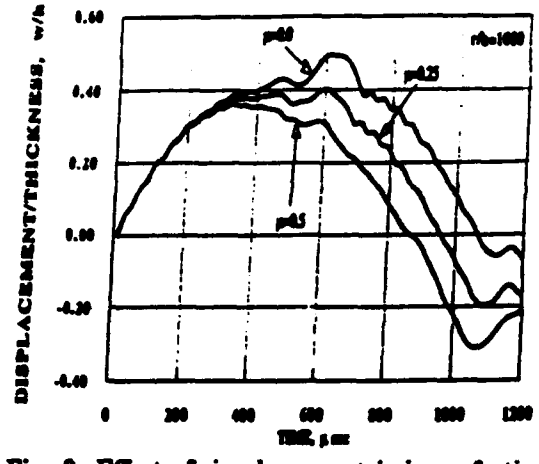

Fig. 3. Effect of simple geometric imperfections on central deflection for non-dimensional shell radius (r/h)= 1000 (plate thickness: 0.1345cm).

REFERENCES

Kapania, R. K., and Byun, C., "Reduction Methods Based on Eigenvectors and Ritz Vectors for Nonlinear Transient Analysis," *Computational Mechanics, An International Journal*, Vol. 11, No. 1, 1993, pp. 65–82.

Kapania, R. K., and Yang, T. Y., "Formulation of an Imperfect Quadrilateral Doubly-Curved Shell Element for Post-Buckling Analysis." *AIAA J.*, Vol. 24, No. 2, 1986, pp. 310–311.

Kapania, R. K., and Yang, T. Y., "Buckling, Postbuckling, and Nonlinear Vibrations of Imperfect Plates," *AIAA J.* , Vol. 25, No. 10, 1987, pp. 1338–1346.

Saigal, S., Kapania, R. K., and Yang, T. Y., "Geometrically Nonlinear Finite Element Analysis of Imperfect Laminated Shells," *Journal of Composite Materials*, Vol. 20, March 1986, pp. 197–214.

Control Designs for Smart Structures and Their Experimental Validation

Farshad Khorrami
email: khorrami@pueel.poly.edu
Control/Robotics Research Laboratory
School of Electrical Engineering & Computer Science
Polytechnic University, Six Metrotech Center
Brooklyn, NY 11201

I. Introduction

Due to earth-based and space-based applications, and with the promised advent of light-weight high-strength composite materials, much attention has been given to modeling and control of large flexible structures and weapon pointing systems. Another class of systems, for which vibration suppression is of great importance, is high speed positioning devices such as probes for electronic circuit boards, robotic manipulators, and machine tools. Utilization of smart or intelligent materials in control of systems exhibiting flexibility is receiving increased attention recently. Research and development of completely integrated structures with embedded actuators, sensors, signal processing, and control systems are of prime interest. Different electroactive materials such as piezoceramics, shape memory alloys, electrorheological fluids, polymer biomaterials, magnetorestrictive materials are being considered for active control purposes.

Several control design strategies for flexible mutlibody systems, large flexible structures, and smart structures are briefly outlined in this paper. To complement our theoretical studies of these systems, several experimental setups have been and are being developed at CRRL. The emphasis of the experimental research in CRRL is on control of flexible mechanical structures, smart structures, and robotic systems. In the next section, two of the experimental setups developed at the CRRL are described. Control objectives for these experiments range from ***nonlinear controllers to fuzzy logic and neural network control systems for active vibration suppression to slewing and pointing***, and combinations thereof. Furthermore, ***system and parameter identification for control*** is another primary objective in the development and utilization of these experiments.

II. Experimental Setups

A. A Two-Link Flexible Manipulator

A two-link robot arm with replaceable links has been developed at the CRRL. Different configuration (i.e., rigidity) can be studied by varying the lengths and the thickness of the arms. Figure 1 shows a picture of the experimental setup. The actuator for the first link is a direct drive DC motor and the second link is actuated by a geared DC motor through anti-backlash gears. The second joint has been designed to be light-weight; however, the joint and the tip are supported on an air bearing on a granite table. Each arm is instrumented with a piezoelectric type accelerometer at its tip and several pieces of piezoceramics along the links.

Figure 1: The two link flexible arm at CRRL.

B. A Slewing Truss Structure with Active Members

A slewing truss structure has been developed (Figure 2). The struts and the nodes for the structure are the same as the ones used in NASA's and JPL's setups. One of the nodes is attached to a direct drive motor through a hub assembly. An active member is being installed in the truss setup by replacing one of the struts by a piezo type linear actuator. This will provide an active member for vibration suppression along the truss. We are also instrumenting the truss by various sensors.

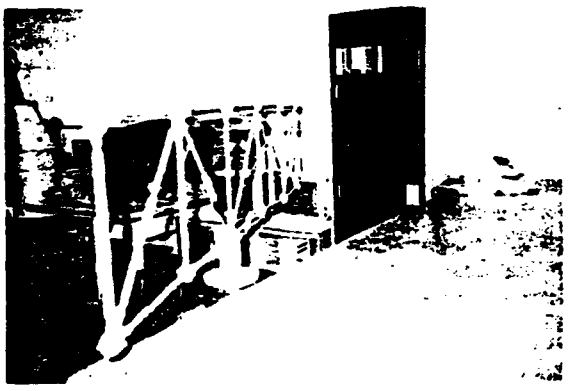

Figure 2: The slewing truss structure with active members.

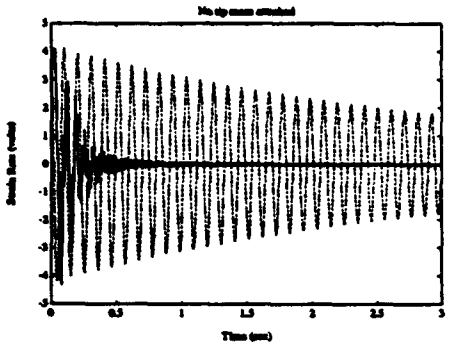

Figure 3: Open and closed-loop responses.

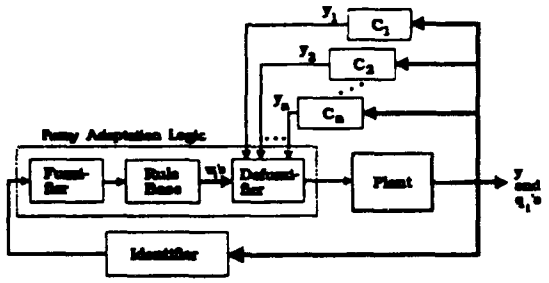

Figure 4: Architecture of the fuzzy adaptive controller.

III. Control Design Methodologies

A. *Adaptive Nonlinear Control*

Flexible articulated structures are nonlinear distributed parameter systems. It is well known that the vibrational frequencies of such systems are geometric configuration dependent. Therefore, linear based control designs tend to be conservative to accommodate for such variations. We have developed nonlinear based control designs to significantly reduce the frequency variations due to geometric configuration. This scheme is based upon asymptotic expansions on the nonlinear distributed parameter dynamics. Furthermore, nonlinear adaptive controllers have been considered to guarantee robust performance in presence of parametric perturbations.

B. *Decentralized Control*

By definition of a smart structure, sensors, actuators, signal processing, and control algorithms are embedded in a smart structure. We will refer to a collection of sensors and actuators and the associated signal processing and control algorithm as a "smart patch." In envisioned smart structures, many smart patches may be utilized to perform different tasks and therefore these systems will exhibit a decentralized information structure. Therefore, it is highly desirable to have decentralized control strategies meaning that each smart patch in the system will have its own decision making rules and algorithms. This is highly desirable for the following reasons: 1) No need for information transfer among "smart patches," 2) Fault tolerant, i.e., failure of one "smart patch" does not cause the failure of the overall system, and 3) Ease of real-time computational load on each subsystem.

We are currently pursuing decentralized control strategies for the systems under consideration. A typical response of the advocated controllers to suppress vibrations of a slewing beam is given in Figure 3. The beam has surface-mounted piezoceramics as sensors and actuators.

C. *Fuzzy Logic Adaptive Control*

Fuzzy controllers are based on three well known stages: 1) the fuzzification stage, 2) the rule base stage, and 3) the defuzzification stage. First, the partitioning of the fuzzy input space is carried out and the corresponding membership functions of the fuzzy sets are assigned. Thereafter, the system parameters involved must be identified and their membership values in the fuzzy input sets evaluated (fuzzification). We have developed a technique utilizing a fuzzy rule base to switch among several controllers designed for different operating regimes and/or different parameter sets. The technique utilizes a real-time system identification algorithm during the fuzzification step. Any parameter estimation method may be employed to obtain the unknown parameters or variables. The overall structure of the scheme is depicted in Figure 4.

D. *Neural Network Control*

Artificial Neural Networks (ANNs) have shown great potential for adaptive control applications due to their capability to learn the unmodeled system characteristics through nonlinear mappings. This feature is desirable in the smart structures due to the inherent nonlinearities of the system. We are currently utilizing a multi-layer feedforward neural network with a Trajectory Pattern Method (TPM) for identification and trajectory tracking of nonlinear systems (especially non-minimum phase systems). The TPM utilizes specific time functions for generation of feedforward signals. The neural network is advocated to reduce the trajectory error by *optimizing* the appropriate parameters such as base harmonics in the TPM. The training algorithms used for the networks are the back propagation technique and the genetic algorithms.

IV. Acknowledgement

This work is supported in part by the U.S. Army Research Office under grant # DAAH04-93-G-0209.

PROGRESSIVE FAILURE ANALYSIS OF COMPOSITE STRUCTURES MADE OF THERMO-ELASTIC SOLIDS

MARIO E. PACHAJOA, KUNG-YAN LEE, JAMES D. LEE

Department of Civil, Mechanical and Environmental Engineering,
The George Washington University,
Washington, DC 20052

Extended Abstract

Since "Desert Storm" in 1990, interest in military high technology has came to an all time high, especially in contemporary weapon systems that use electronics and composite materials.

The potential for significant weight reductions in weapon system through the use of advanced composites was first reported on a broad scale in the Air Force project "Forecast" conducted in 1963. This observation was based on the then recent development of high-modulus, high-strength, low density fiber and the superior mechanical properties that could be developed when these fibers were converted into composites laminates.

In military aircraft, composites offer improved performances. A number of aircraft design and construction programs are in progress involving major use of advanced composites. For example, the European Fighter Aircraft (EFA) is designed using composite wings and forward fuselage. The use of composite materials will result in an approximately 35% weight reduction as compared to that of conventional materials. Another example is the construction of the AV-8B MK. 5 Harrier II airframe, where the use of composite materials give rise to a 25% weight saving in the airframe compared to an all-metal construction.

Recent efforts to increase ballistic protection and reduce the weight necessary for this protection have led to a new focus in composite materials among the armor community. A vital aspect of armor design is an understanding of the properties which control anti-ballistic performance. Unfortunately, for these new materials, the fundamental research necessary for this understanding has only recently received attention. This is mainly a consequence of the fact that the processes occurring during the projectile penetration are at extremely high strain rates.

As armor-vehicle designers are forced to reduce weight and increase protection, fibers are being combined with ceramics, metals and plastics to create more effective armors. For example the M1A1 Abrams MBT Chobham armor, and the M2/M3 Bradely LAV (Light Armor Vehicle) interior spaced laminate armor, are constructed of these composite materials. The principle advantage of fibers is their high-strength-to-weight ratio. Other properties such as tensile modulus, elongation, energy absorption and sound speed have proven to be important in characterizing impact. Impact, however, is a complex problem and one should not rely on any single property as a predictor; often combinations of properties are the key.

Other products made of composite materials in the military include the KE-EP lightweight helmet and the KE-EP protective vest.

However, very likely the most important application can be in the next generation "Rail Gun" weapon system, of which the "rail" part that plays a critical role could be made of composite.

The increasing use of composites in the military field , as well as in the aerospace, marine, and automotive fields, has spurred great interest in developing numerical tools to optimize designs made of composite materials. Laminated composites, by their nature, are heterogeneous and anisotropic. This makes the failure characteristics of the composite materials more complicated than that of the isotropic materials. Only in the most recent years, the finite element technique together with the high capacity and high speed of modern computers have made it possible to analyze fiber reinforced composites in detail.

Some well-known commercial finite element codes are capable, to a limited degree, of analyzing composite structures. However, few programs attempt to perform a complete thermo-mechanical failure analysis of composite structures. Recently, under a grant from the NASA Goddard Space Flight Center, a general purpose thermo-mechanical finite element program, called COMPASS (COMPosite Analysis of Structural Systems), was developed for the analysis of composite structures. Three main solution sequences are offered by the code, namely: 1) non-linear-static stress analysis, 2) delamination growth analysis, 3) progressive failure analysis.

Focus of this work is on the progressive failure analysis which is the third case available within COMPASS. All elements assume linear stress-strain-temperature relations. Failure of a composite element is determined by using Hashin's failure criterion, while the failure of an isotropic elements is determined by using the von Mises failure criterion. The solution process involves increasing the original load until an element fails. The element that failed is classified as being isotropic or composite. Furthermore, composite element failure is identified as being in fiber or matrix mode. The stiffness, the heat conductivity, and the thermal expansion matrices of that element are then altered according to the mode of failure. As a consequence, the stresses and the temperature in the entire structure are redistributed. The structure is then analyzed with the set of matrices to determine if any further failure is induced. If further failure does not occur, the load is increased to the level needed to cause the next element to fail. This incremental process continues until catastrophic failure occurs. The ultimate load carrying capacity of the structure is then determined.

The constitutive relations of anisotropic thermo-visco-elastic solid, the failure criteria and post-failure material behavior, and the finite element formulation of composite structures made of thermo-mechanical solids are presented. Also, for illustrative purpose, the procedures and the numerical results of the progressive failure analysis of a composite plate are discussed in detail.

Paper for Army Research Office Workshop on:

DYNAMIC RESPONSE OF COMPOSITE STRUCTURES

ABSTRACT

Title: Damage and Energy Exchange From Impact At Super-Perforation Velocities On Carbon Fiber Epoxy Composite Plates By Rigid Sphere Projectiles

Author: Arnold H. Mayer, Flight Dynamics Directorate, Wright Laboratory, WPAFB, OH

Summary

An extensive experimental program to investigate the damage and energy exchange which accompany the ballistic impact and penetration by rigid spherical steel projectiles of carbon fiber epoxy composite plates above their penetration threshold has been conducted . New significant findings concerning these impact phenomena are described. Preliminary applied mechanics analyses that serve for their explication or correlation are derived.

Description of the Experimental Program

The experimental program consisted of firing one-half inch diameter rigid spherical steel projectiles at carbon fiber epoxy matrix composite plates which were clamped between steel plates containning a 3 inch diameter circular hole with the design impact point located at its center. The composite target plates were 32 plies thick layed up in balanced quasi-isotropic stacking arrangements consisting of 0, 45, and 90 degree fiber orientations and also in balanced spiral staircase layups in which the fibre direction increased in increments of 90, 45, 22.5, or 11.25 degrees from ply to ply. Ten inch diameter rigid plastic cylinders with axes coincident with the shotline were lined with adhesive paper and placed flush with the front and rear target support plates in order to catch spall fragments emanating from the target plate. Circular end plates containing a small central hole to permit uninterrupted passage of the projectile were also covered with adhesive paper to catch fragments travelling with velocity vectors contained within a small cone of the axis. Projectile velocity was measured ahead of the target plate by means of a set of fine trip wires of known separation distance by noting the instants of break of electrical continuity and behind the target by two sets of induction coils of known location along the pipe axis which were wrapped around the outer cylindrical surface of the plastic pipe. Thus the energy imparted by the projectile to the target material could be computed. Some experiments were performed without the adhesive paper and the loose fragments collected in the plastic pipe were swept together and weighed and compared with the weight loss of the target plates. A single set of plates consisting of plates which had been penetrated at different velocities were stained with Gold Chloride, pyrolyzed in an air oven, deplied with a scalpel, mounted on a rigid backing and subjected to measurement of the areas of the penetration hole and of the envelope of surrounding gold-stained delaminated area. This was done with the aid of automatic image analysis equipment. It was thus possible to obtain the shapes and distribution of hole and delaminated areas on each ply of panels penetrated at different velocities over the range of 200 to 6000 feet per second. An additional novel measurement was made of the total surface and internal fracture area which communicates with the surface by employing a surface area measurement apparatus based on the gas adsorbtion technique with Nitrogen as the adsorbent gas.

Principal Findings

1. Energy exchange between

projectile and target.
The fraction of the original kinetic energy associated with the projectile after completion of the impact event at first increases with increase in the initial impact velocity and then appears to approach a constant asymptotic value. Logically, this asymptotic value must vary with the thickness of the target plate, being unity for a plate of vanishing thickness and zero for one of semi-infinite thickness.

2. Type, morphology and distribution of the damage.
The observed damage consisted of a generally irregularly shaped perforation hole, fragmented material which originated from the region of the hole, and a delaminated region surrounding the hole located between each pair of plies in which there was a change in fiber orientation.

3. Extent and variation of the total delaminated surface with impact velocity.
The curve depicting the variation of the total delaminated area with incident velocity of the projectile possesses a bathtub-like shape. The area enclosed by the outer envelope of the delaminated area at first decreases with increasing projectile velocity from its value at the penetration threshold, and then, after passing through a minimum value, increases steadily with further increase in velocity.

Relevance, Utility and Value of the Research Findings to the interests of the Armed Services

The initial objectives of the reported research are tied to the increased presence of manmade or composite materials of the general kind investigated in this study in the construction of military vehicles and weapon platforms as a result of now well recognized structural efficiency advantages such as strength to weight ratio and potential tailorability of strength in required directions to accommodate the directionality of imposed loads. Decisions to employ new materials in the construction of military materiel entail a responsibility to understand the associated repairability issue that stems from their susceptibility to realistic types and magnitudes of damage from impact by ballistic projectiles, and the effect on vulnerability as a result of their influence on the performance of the engaged projectile and of the degree of strength retention in the presence of realistic types and magnitudes of damage. The investigation thus far has uncovered three much sought after items of information concerning the interaction of spherical projectiles with composite plates. In particular, the first finding that the degree of damage is bounded from above by the damage incurred at the perforation threshold is considered a useful piece of knowledge for maintenance personnel. A second relevant finding is the understanding gained from the present investigation that enables one to infer the form of the momentum interchange with projectiles in general and which consequently allows correlation of the thresholds for various types of functioning. Thirdly, the finding concerning the asymptotic value which is rapidly approached by the fraction of initial kinetic energy retained by the projectile after penetrating a composite panel is an important piece of information to aid in assessment of potential for additional damage by a spherical projectile which has penetrated a multiplicity of panels to structure located farther along the trajectory, or in the design of a single plate capable of yielding a specified degree of attenuation of the incident energy of an incident steel sphere.

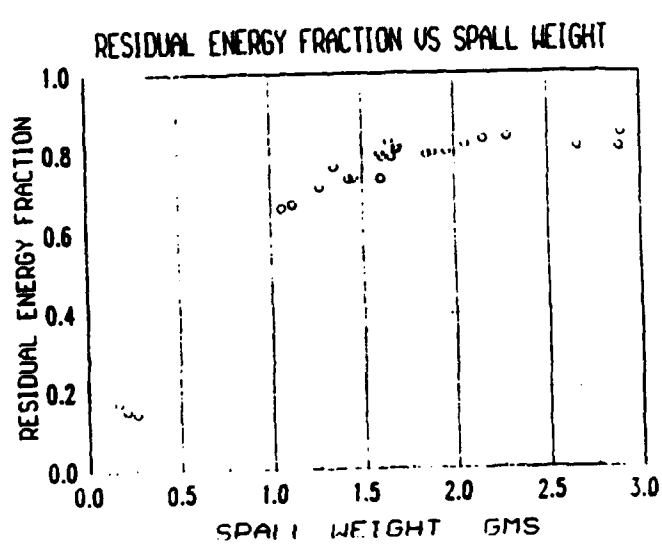

THE DYNAMIC RESPONSE OF THICK ANISOTROPIC COMPOSITE PLATES

Adnan H. Nayfeh, Department of Aerospace Engineering and Engineering Mechanics
Univ. of Cincinnati, Cincinnati, OH 45221

and

Timothy W. Taylor, General Electric Aircraft Engines, Evendale, OH 45215

We develop the analysis and numerical calculations for the response of thick anisotropic elastic plate strips subjected to transient loadings. Problems associated with the vibration of mechanical systems have long been of interest in structural applications. Most of the available work deals with various aspects of plates constructed of only isotropic materials. Even here, mostly approximate results are available which are based on classical bending theory of plates. Typically, the plate is assumed to be "thin" so that variations of displacements and stresses through the plate's thickness are neglected and that the plate is of infinite extent, as presented by Chow (1971) for an orthotropic laminated plate.

Comparatively speaking, however, only a limited number of results have appeared on free vibration of thick bounded plates, especially thick anisotropic plates. Much less work is available on the response of such structures to transient loading conditions.

Specifically, our resulting structural component, made-up of multioriented unidirectional fiber composite laminates, is an anisotropic plate having monoclinic symmetry. Special combinations of orientations of such laminates may result in higher than monoclinic symmetry. However, no combinations of such laminates would lead to less than monoclinic symmetry. Thus, the problem we deal with encompasses all classes of symmetry greater than triclinic symmetry.

The analysis of the plate strip of Fig. 1 is conducted in two steps.

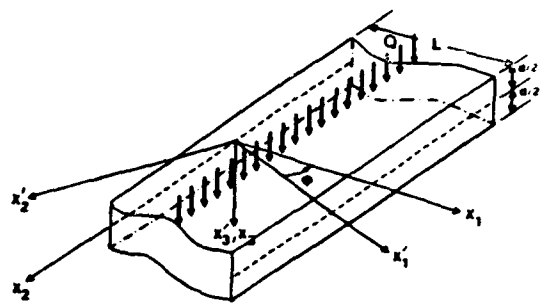

Fig. 1 Plate strip model with applied load

In the first step, the characteristic free vibrational modes of the strip are derived. Linear transformations are utilized to derive the sixth degree characteristic equation and the secular equation for this case in closed form. We subsequently isolate the mathematical conditions for symmetric and antisymmetric wave mode propagation in completely separate terms, as developed by Nayfeh and Chimenti (1988)

$$D_{11}G_1\coth(\gamma\lambda_1) - D_{13}G_3\coth(\gamma\lambda_3) + D_{15}G_5\coth(\gamma\lambda_5) = 0, \quad (1a)$$

$$D_{11}G_1\tanh(\gamma\lambda_1) - D_{13}G_3\tanh(\gamma\lambda_3) + D_{15}G_5\tanh(\gamma\lambda_5) = 0. \quad (1b)$$

We use the two secular equations (1a,b), together with the charateristic equation, to obtain the proper combinations of λ and γ for valid solutions. In the second step, the applied loads are expanded in terms of these normal modal functions, and the response of the plate is obtained by linear superposition of the appropriate components. Material systems of higher symmetry, such as orthotropic, transversely isotropic, cubic, and isotropic are contained implicitly in our analysis.

We write the formal solutions (Jones (1971)) for the displacements

$$(u_1,u_2) = \sum_{n=1}^{\infty}\cos(\beta_n x_1)\sum_{q=1}^{6}(1,V_{nq})U_{nq}e^{(\lambda_{nq}x_3+i\omega_n t)} \quad (2a,b)$$

$$u_3 = \sum_{n=1}^{\infty}\sin(\beta_n x_1)\sum_{q=1}^{6}W_{nq}U_{nq}e^{(\lambda_{nq}x_3+i\omega_n t)}. \quad (2c)$$

An example of our modal calculation is given in Fig. 2 for a plate composed of an orthotropic material with elastic constants given in MPa by C_{11}=128, C_{12}=7, C_{13}=6, C_{22}=72, C_{23}=5, C_{33}=32, C_{44}=18, C_{55}=12.25, C_{66}=8 and ρ=2g/cm^3.

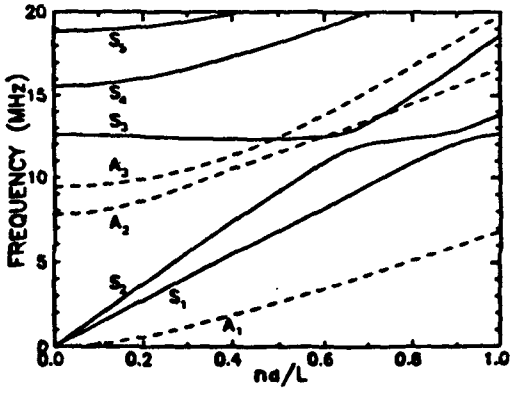

Fig. 2 Natural frequency versus nd/L, ϕ=45°

In this figure, we present a plot of natural frequency versus the nondimensional quantity nd/L (discrete wave number) for a plate with ϕ = 45°. Lines labeled A_i and S_i correspond to the ith antisymmetric and symmetric natural modes, respectively. A surprising feature of this plot is the crossing of the second and third antisymmetric modes by the third symmetric mode.

Finally, we develop the transient response of the plate when subjected to an impulsive line loading applied along the x_2-axis.

$$u_i(x_1,x_3,t) = \sum_{n=1}^{\infty}\sin(\frac{n\pi}{2})\sum_{m=1}^{\infty}\{\frac{Q}{\omega_{mn}M_{mn}}[\sum_{q=1}^{6}W_{mnq}U_{mnq}e^{\lambda_{mnq}\frac{d}{2}}]u_{imn}(x_1,x_3)\sin(\omega_{mn}t)\}, \quad n \text{ odd}. \quad (3)$$

REFERENCES

Chow, T. S. (1971). On the propagation of flexural waves in an orthotropic laminated plate and its response to an impulsive load. J. Comp. Mat. 5, 306-319.

Nayfeh, A. H. and Chimenti, D. E. (1989). Free wave propagation in plates of general anisotropic media. J. Appl. Mech., 56, 881-886.

Jones, A.T. (1971). Exact natural frequencies and modal functions for a thick off-axis lamina. J. Comp. Mat., 5, 504-520.

Strength Evaluation of Composite Laminates with Various Holes under Bending

Y. Zhao, S.S. Pang, and C. Yang
Louisiana State University
Baton Rouge, Louisiana

Introduction

Fiber-reinforced composites have been used in many applications of Army service to replace exotic alloys due to their lightweight, corrosion-resistance, and high strength. While the strength of notched structures under various loadings has always been of concern to the Army, satisfactory evaluation approach has not been available due to the limitation of existing theories. The discovery of hole size effect made it clear that the classical design based on the stress concentration factors may no longer be acceptable for notched composites. Mainly for this reason, great efforts have been made since the early 1970's to evaluate the notched strength of laminated composites with cutouts. As a result, several models have been developed so far including the linear elastic fracture mechanics model (LEFM), finite stress distribution models, damage zone model, and progressive failure model. The finite stress distribution model drew more attention than other models. Whitney and Nuismer (1974) proposed "point stress criterion (PSC)" and "average stress criterion (ASC)" in the study of orthotropic laminates containing a circular opening or a crack under tensile loads by assuming that the strength of a notched plate was controlled by the normal stress adjacent to the circular hole. These models have been extended by many researchers since then.

Almost all of the previous studies in this area were limited to the in-plane loadings. Although composite laminates with cutouts under bending have many applications, very few studies have been reported. The main reason is the difficulties in stress analysis. In this study, a simplified approach has been used which combines the experiments and finite element analysis to evaluate the notched strength of laminates under bending. This notched strength depends on many factors such as the geometry of the opening, width and thickness of the plate, material properties, fiber angles, and stacking sequence. This paper is the first part of a series of investigation and focuses on the laminates with elliptical holes under bending. Further studies will include laminates with various holes under different loadings and the effect of stacking sequence.

Notched Strength Evaluation

For an isotropic laminate under in-plane tension, the normal stress is uniformly distributed across the laminate thickness. But when the laminate is subjected to a bending load, the stress varies in the thickness direction. This difference also exists in the laminated plates. For a cross-ply laminated plate under the in-plane tensile load, all of the 0° plies are in the same stress level, and all the 90° plies are also in the same stress level. If the stress in one 0° ply (or 90° ply) reaches the ultimate strength, all the 0° plies (or 90° plies) will fail simultaneously. But for the cross-ply laminates under bending, each 0° ply or 90° ply is in the different stress level. The stress at one point or the average stress over a length may not represent the stress level or stress concentration of the laminate. Therefore, these criteria may not be directly applied to the case of bending. It is more reasonable to include the stress variation across the laminate thickness in the failure models. By this consideration, the following failure models were presented to evaluate the notched strength of laminates under bending.

Modified Point Stress Failure Model - This model extends Whitney and Nuismer's point stress model by defining the "point stress" as the average stress of the plies with same fiber angle across the laminate thickness. For the laminates other than on-axis unidirectional or cross-ply, the maximum stresses usually will not occur along a radial line parallel to the applied bending moment but at some angles. Thus the modified point stress criterion should be applied along a path which encloses the elliptical opening, as shown in Fig. 1.

$$\frac{2}{h_\alpha}\int_0^{h/2}(\sigma_\alpha)_{dz}\frac{x^2}{(a+a_1)^2}+\frac{y^2}{(b+a_1)^2}-1\,dz=\sigma_u \qquad (1)$$

where σ_α is the stress of the ply with fiber angle α, h_α is the total thickness of the plies with fiber angle α, h is the total thickness of the laminate, σ_u is the ultimate strength of the material along or perpendicular to the fiber direction, and a_1 is a characteristic parameter to evaluate the failure strength of the laminate.

Modified Average Stress Failure Model - In the case of in-plane loadings, the average stress criterion includes the contribution of the stress distribution along the radial direction in the vicinity of the hole edge. For notched laminates under bending, the contribution of stress distribution along the thickness direction should also be considered. Mathematically, this modified model can be written as

$$\frac{2}{a_2 h_0}\int_{R}^{R+a_2}\int_{0}^{h/2}\sigma_x(\theta, r, z)\,dr\,dz = \sigma_0 \qquad (2)$$

where R is the radial distance from the edge to the center of the hole, θ is the location of the section where maximum stress occurs, and a_2 is another characteristic parameter to predict the failure strength of the laminates under bending.

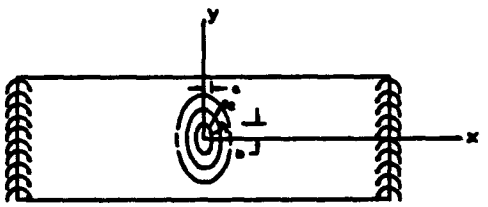

Fig. 1 A Laminate with an Elliptical Hole under Bending

As discussed earlier in the introduction, a theoretical/analytical solution to the problem of notched laminate under bending would be extremely complicated and very difficult to achieve. Finite element method seems to be the best alternative to serve the purpose. This has been realized by many investigators when studying tensile failure of notched laminates. In this current investigation, a simplified approach was utilized which combines the sample experiments and finite element stress analysis. A brief description of this procedure is given as follows:

- Conduct 4-point bending test and record the "load vs. deflection" curve.
- Obtain "first ply failure load" from "load vs. deflection" curve for each sample.
- Calculate the strength reduction factors for plates with different holes.
- Apply modified PSC or ASC to the plate without hole to determine the failure load of the plate.
- Determine failure loads for plates with different holes using strength reduction factors.
- Conduct finite element stress analysis by applying the failure loads to the notched composite laminates.
- Apply modified PSC and ASC to each case to determine the parameters a_1 and a_2.

Experimental Study

A four-point bending test was performed to determine the failure load of laminated composites containing an elliptical hole under bending. A dial gauge was attached to the bottom surface of the sample to measure the deflection. Scotchply laminated samples containing an elliptical hole were tested. Each sample was a 9"× 3"× 1/8" $[(0/90)_3/\bar{0}]_s$ laminated plate. Five different elliptical hole sizes were used. To determine the failure loads for each sample, "load (force) vs. defection" curve was plotted during the experiment and was later be used to calculate the strength reduction factors.

Stress Analysis

The finite element method was utilized in the stress analysis of composite laminates with different holes under bending. The software COSMOS/M, which is capable of handling laminated composites, was used. A finite element code was also developed by the authors to compare the numerical results. The results from COSMOS/M and the developed code are consistent. The stress distributions for each case were obtained.

Results and Discussions

With stress distribution provided by finite element analysis and strength reduction factors from experiments, the characteristic parameters a_1 and a_2 were obtained by applying modified PSC and modified ASC. The parameters a_1 and a_2 evaluate the notched strength of laminate under bending in two ways. The parameter a_1 focuses on the intensity of stress at one point in the vicinity of the opening, while a_2 considers the stress distribution in the radial direction near the hole. It was found that for an elliptical opening, the larger the aspect ratio, the smaller the strength reduction factors. It was also found that both a_1 and a_2 are reduced as the aspect ratio increases.

References

Nuismer, R.J. and J.M. Whitney, 1975, "Uniaxial Failure of Composite Laminates Containing Stress Concentrations," *Fracture Mechanics of Composites*, ASTM STP 593, 117-142.

Tan, S.C., 1987, "Notched Strength Prediction and Design of Laminated Composites under In-Plane Loadings," *J. Composite Materials*, 21, 750-780.

Whitney, J.M. and R.J. Nuismer, 1974, "Stress Fracture Criteria for Laminated Composites Containing Stress Concentrations," *J. Composite Materials*, 8, 253-265.

Optimal Control of Infinite-Order Smart Composite Structural Systems Using Distributed Sensors

Vittal Rao and Robert Butler
Department of Electrical Engineering and
Intelligent Systems Center
University of Missouri-Rolla, Rolla, MO. 65401

ABSTRACT

The salient features of smart structures are the generation of internal forces for suppressing vibrations, mode shape control and the spatially distributed nature of the actuators and sensors. In the conventional control design methodology, the spatial distribution of sensors and actuators is not taken into consideration. Recently, a number of researchers have proposed designing distributed control schemes for infinite-order structural systems using distributed sensors and actuators. The main advantages of distributed control are (i) the ability to control all modes of the structure thus eliminating spill-over problems, (ii) trade-offs between gain margin and bandwidth of the controllers, and (iii) the use of displacement, rotation and strain measurements as feedback signals in the infinite-order systems. The design and implementation of optimal control strategies for infinite-order smart structures present challenging problems. One is the computational effort required to design optimal controllers for infinite-order structural models, and the other is the development of optimally shaped distributed sensors and actuators. A procedure for sensor shape optimization and the design of controllers for simple cantilever beam test article has been developed and discussed in this paper.

The smart materials polyvinylidene fluoride (PVDF) and shape memory alloys can be utilized in the development of customized distributed sensors. These sensors can be shaped to control the desired response of the structural system. For the implementation of optimal control strategies, we need to develop sensor shape optimization techniques. In this paper, a method for the design of controllers for infinite-order structural systems is examined that uses finite dimensional approximations to desired curvature and curvature rate kernels. These kernels are used for generating the shapes of PVDF distributed sensors. The output of these spatially distributed sensors will be utilized directly as the control signal for suppressing the structural vibrations.

A method for the calculation of distributed sensor shape functions was presented by Miller and van Schoor in 1991. A finite element model (FEM) of the system was used to obtain a state space model of the structural system. With the use of the FEM interpolation function, shape functions representing a continuous approximation to the discrete linear quadratic regulator (LQR) solution were determined. The shape functions were then transformed into the appropriate shape functions required for the implementation with PVDF distributed sensors. This method is computationally intensive and requires covering the entire structure with two distributed sensors for the implementation of the optimal control solution. Also, only the LQR control design solution was demonstrated and the shape functions were not verified with simulations.

In order to verify the design method discussed above, simulations using the distributed sensors were necessary. Initial simulations of the LQR controller using the state space model of the structural system were performed. The results of this simulation were considered to be the standard by which the performance of the system with the

distributed sensors was evaluated. A second simulation of the system was performed to evaluate the distributed sensors. This was done by using the FEM interpolation function to calculate the distributed parameters of the structure and the resulting response of the spatially continuous distributed sensors. The comparison of the two simulations confirmed the shape function calculation of the distributed sensors.

The calculation of the sensor shape functions is a mathematically and computationally intensive process. In this procedure it is required to calculate displacement and displacement rate kernels. These kernels are then transformed into the desired kernels by the appropriate mathematical operations. For the PVDF sensor implementation, this requires a double integration of the displacement kernel to obtain the curvature kernel and a double integration of the displacement rate kernel to obtain the curvature rate kernel. A method is presented for the direct calculation of the curvature and curvature rate kernels. This reduces the computation time required for the distributed sensor shape optimization.

Completely covering the members of a structure with two distributed sensors may be possible in a laboratory setting, but it may not be practical for a large structure with many structural elements and physical components. A solution to this problem was found by using a relatively small part of one of the distributed sensors along with an observer. The output of the resulting distributed sensor provides a portion of the desired control signal. The observer may be driven by the output of the implemented sensor providing the states of the state space model. The states may then be used to generate the missing part of the control signal that would be provided by the full sensor. This method increases the amount of computation that must be done by the control system, but it does allow for the implementation of the desired control with a distributed sensor covering a part of the structure. The usefulness of a single relatively small customized PVDF film sensor along with an observer to provide full state feedback information for the entire structure is examined. The complexity and performance of the proposed control scheme is compared with the original distributed sensor implementation.

Since smart structures exist in a variety of sizes and shapes and in various applications, it is desirable to have many different control design algorithms available to the control design engineer. For many of the potential applications, controller design methods other than the LQR may provide superior performance. As a first step, a pole placement controller was designed to determine if shape functions for this controller could be calculated for the distributed sensors. The shape functions obtained were satisfactory indicating that state space controllers other than the LQR may be implemented with the distributed sensors.

In summary, we have developed an alternate method for computing curvature and curvature rate kernels in the development of optimized sensor shape functions and proposed a procedure for utilizing a partial distributed sensor along with an observer for the implementation of controllers. We have also examined various control methodologies for designing distributed controllers. The usefulness of a single relatively small customized sensor along with an observer to provide full state feedback information is demonstrated with simulation studies. We are in the process of implementing these sensors and control algorithms on a simple cantilever beam test article.

ELECTRO–THERMO–MECHANICS OF SPRING–LOADED CONTRACTILE FIBER BUNDLES WITH APPLICATIONS TO IONIC POLYMERIC GEL AND SMA ACTUATORS

Mohsen Shahinpoor

Intelligent Materials, Structures & Systems Laboratory

College of Engineering

University of New Mexico

Albuquerque, New Mexico 87131

ABSTRACT

A mathematical model is presented for the dynamic response of contractile fiber bundles embedded in or around elastic springs that are either linear helical compression springs or hyperelastic springs such as rubber–like materials. The fiber bundle is assumed to consist of a parallel array of contractile fibers made form either contractile polymeric muscles such as polyacrylic acid plus sodium acrylate cross–linked with bisacrylamide (PAAM) or polyacrylonitrile (PAN) fibers. The proposed model considers the electrically or pH–induced contraction of the fibers which may include resistive heating of the fiber in case of shape–memory alloys. The theory then branches out to two different description of such processes for ionic polymeric gel fiber bundles and shape–memory alloy fiber bundles.

INTRODUCTION

Intelligent material systems and structures have become important to all defense and civilian sectors of the society (see Ahmad, Crowson, Rogers and Aizawa [1]). Accordingly, based on such materials, structures and their integration with appropriate sensors and actuators, novel applications, useful for all defense and civilian programs, have emerged. Numerous examples may be cited as can be seen from key reference articles such as [1] and Crowson and Anderson [2]. In the present paper a mathematical model is presented for the dynamic response of contractile fiber bundles embedded in or around elastic springs that are either linear helical compression springs or hyperelastic springs such as rubber–like materials. The proposed theory presents two different description of such processes for ionic polymeric gel fiber bundles and shape–memory alloy fiber bundles.

For the case of ionic polymeric gel fibers the model consists of an encapsulated hermetically sealed, helical compression spring–loaded cylindrical linear actuators containing a counterionic solution or electrolyte such as water+acetone, a cylindrical helical compression spring and a collection of polymeric gel fibers (polyelectrolytes) such as polyvinyl alcohol (PVA) polyacrylic acid (PAA) or polyacrylamide. Furthermore, the helical spring not only acts as a compression spring between the two hermetically sealed circular end–caps but contains snugly the polymeric gel fiber bundle and also acts as the cathode (anode) electrode while the two actuator end–caps act as the other cathode (anode) electrodes. In this fashion, a DC electric field of a few volts per centimeter can cause the polymer gel fiber bundle to contract (expand). This causes the compression spring to contract and pull the two end–caps closer to each other

against the elastic resistance of the helical spring. By reversing the action by means of reversing the electric field polarities the gel is allowed to expand while the compression spring is also expanding and helping the linear expansion or the actuator since the polymeric gel muscle expands due to the induced alkalinity along the helical spring body. Thus, electrical control of the expansion and the contraction of the linear actuator will be possible. A mathematical model is presented based on the proposed composite structure that takes into account all pertinent variables such as the pH of the gel fiber bundle, the pH of the surrounding medium, the hyperelastic parameters of the fiber bundle, the electrical variables of the gel, the electric field strength, the pH field strength and all pertinent dimensions followed by some numerical and experimental simulations and data.

For the second model, we consider the fiber bundle of SMA to be either circumscribed inside a helical compression spring with flat heads or in parallel with a number helical compression springs, end–capped by two parallel circular plates with embedded electrodes to which the ends of the SMA fibers are secured. Thus, the fibers can be electrically heated and subsequently contracted to compress the helical compression spring back and forth. Design details are first described. In essence the dynamic behavior of the actuator depends on the interaction between the current supplied to the wires and the heat transfer from the wires. Further, a mathematical model is presented to simulate the electro–thermo–mechanics of motion of such actuators. The proposed model takes into account all pertinent variables such as the strain ϵ, the temperature of the fibers $T(t)$ as a function of time t, the ambient temperature T_0, the martensite fraction ξ, the helical compression spring constant k and the overall heat transfer coefficient h. Numerical simulations are then carried out and the results are compared with experimental observations of a number of fabricated systems.

ACKNOWLEDGMENT

This research is supported by Army Research Office. Thanks are due to Dr. Gary Anderson, Dr. Andy Crowson, Dr. Wilbur Simmons and Dr. Ed Chen for valuable discussions and for their encouragement and support of this research.

REFERENCES

1–Ahmad, I., A. Crowson, C.A. Rogers and M. Aizawa, editors : Proceedings of "US–Japan Workshop on Smart/Intelligent Materials and Systems," March 19–23, Honolulu, Hawaii, (1990), Technomic Publishing Company, Lancaster–Basel, Pa, (1990)

2–Anderson G.L., and A. Crowson, "ARO Smart Structures Program," Proceedings US–Japan workshop on Smart/Intelligent Materials and Systems," ref. (1) pp. 38–339, (1990).

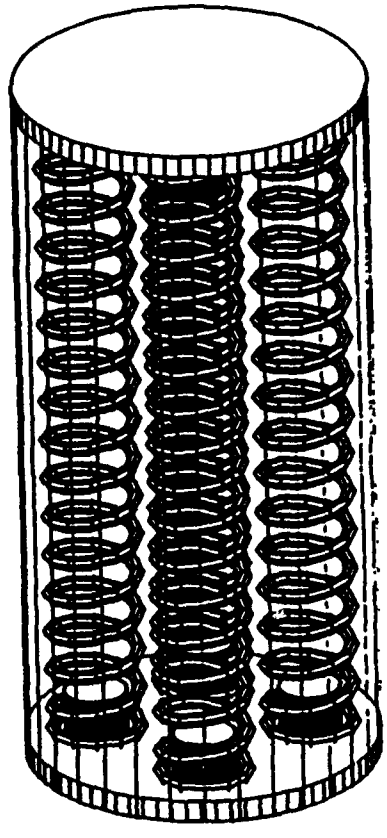

Figure 1– Composite Fiber–Bundle Structure

BUCKLING AND COLLAPSE OF SUDDENLY LOADED STRUCTURES

George J. Simitses

Aerospace Engineering and Engineering Mechanics
University of Cincinnati, Cincinnati, Ohio 45221

Problems which deal with stability (or instability) of motion have concerned researchers for many years in many fields of engineering. In structural mechanics, dynamic stability or instability has received considerable attention in the past 40 years. Several studies have been conducted by various investigators on structural systems which are dynamically loaded (sudden loads, periodic loads or nonperiodic time-dependent loads). In these studies, several attempts have been made to define critical conditions and to develop methodologies for estimating critical conditions. In reviewing these efforts one easily concludes that, in structural mechanics, "dynamic stability" encompasses many classes of problems, and many physical phenomena. It is not surprising then, that the term finds several uses and interpretations, among structural mechanicians.

Problems of parametric resonance, follower force problems, and fluid-structure interaction problems are all listed under the heading of "dynamic stability", among others. See the review article of Herrmann (1967).

Finally, a large class of structural problems that has received considerable attention and does qualify as a category of dynamic stability is that of impulsively loaded configurations and configurations that are suddenly loaded with loads of constant magnitude and infinite duration. These configurations under static loading are subject to either limit point instability or bifurcational instability with an unstable postbuckling branch (violent buckling). The two types of loads may be thought of as mathematical idealizations of blast loads of (1) large decay rates and small decay times and (2) small decay rates and large decay times, respectively. For these loads, the concept of dynamic stability is related to the observation that for sufficiently small values of the loading, the system simply oscillates about the near static equilibrium point and the corresponding amplitudes of oscillation are sufficiently small. If the loading is increased, some systems will experience large-amplitude oscillations or, in general, a divergent type of motion. For this phenomenon to happen, the configuration must possess two or more static equilibrium positions, and escaping motion occurs by having trajectories that can pass near an unstable static equilibrium point. Consequently, the

methodologies developed by the various investigators are for structural configurations that exhibit snap-through buckling when loaded quasi-statically. See the book by Simitses (1989) and the cited references.

In addition, there is considerable work reported in the literature that deals with suddenly loaded columns and plates. The beginning of the study of these problems can be traced to the investigation of Koning and Taub (1933) who considered the response of an imperfect ("half-sine" initial shape), simply supported column subjected to a sudden axial load of specified duration. Since these geometries under static loading exhibit bifurcational buckling with stable postbuckling strength (smooth buckling) their behavior is different from that of geometries which exhibit violent static buckling. Therefore, the concepts, criteria and estimates of critical conditions are different. In all cases of geometries which are subjected to sudden loads the ultimate interest is whether or not dynamic buckling will lead to collapse. This is a very important design consideration. For more references see Simitses (1987).

The presentation will deal with concepts, criteria and estimates of critical conditions for this class of problems. Moreover, examples of systems which are subject to this type of loading and therefore subject to dynamic buckling will also be presented. These include shallow arches and spherical caps, frames, cylindrical shells, and many others. These configurations are representative of domes, submarine hulls, aircraft fuselages and jet engine casings. In addition, the presentation will address such important effects as those of duration time, static pre-loading and damping. The emphasis will be placed on identifying problems in search of a solution and future research directions.

In this task, special consideration will be given to structural configurations made out of fiber reinforced composites, such as laminated plates and shells.

REFERENCES

Herrmann, G. (1967), Stability of equilibrium of elastic systems subjected to non-conservative forces, *Appl. Mech. Rev.*, **20**, 103-108.

Koning, C. and Taub, J. (1933), Impact buckling of thin bars in the elastic range hinged at both ends, *Luftfahrtforschung*, **10**(2), 55-64 (translated and published as NACA TN 748 in 1934).

Simitses, G.J. (1987), Instability of dynamically loaded structures, *Appl. Mech. Rev.*, **40**(10), 1403-1408.

Simitses, G.J. (1989), *Dynamic Stability of Suddenly Loaded Structures*, Springer-Verlag, New York.

A TEST METHOD FOR DYNAMIC PROPERTIES OF COMPOSITES UNDER INTERIOR BALLISTIC CYCLES

Jerome T. Tzeng and Ara S. Abrahamian
US Army Research Laboratory
Weapon Technologies Directorate
Aberdeen Proving Ground, MD 21005-5066

For fiber reinforced composite materials, the matrix dominated properties (i.e. shear and transverse tensile) increase with strain rate. Fibers such as graphite and glass fibers are in general not rate-sensitive materials; however, the fiber dominated properties may increase due to the effects of strengthening matrix. This is especially true for compressive strength and modulus since a rigid and strong matrix can provide lateral supports increasing the buckling strength of fibers. Dynamic behavior of materials is typically obtained from standard testing machines up to strain rates of 1-10 /sec and from Hopkinson Bar experiments at strain rates greater than 100 /sec [1,2,3]. This generally leaves a gap in strain rates effects in the 10-100 /sec band, precisely the zone of interest for launching of projectiles. In addition most current testing is performed at a constant strain rate up to failure of the specimen. While this procedure does give a good picture of the increase of yield and ultimate stress with increasing strain rate for rate sensitive materials, it is unclear as to whether this increase in strength at failure can be effectively used to prevent failure of materials subjected to short, high rate, impulsive loads under interior ballistic cycles.

This investigation proposed a experimental set-up and procedures including an Air Gun system, design of test fixtures and data acquisition. The experiments will be able to simulate the loading condition of tank gun and artillery projectiles during launching. The Air Gun system consists of a series of various diameter tubes (2,3,4,and 7 inches) of great lengths. Figure 1 shows an overall layout of the Air Gun system. The breech area of the gun is located on the right hand side where a projectile is loaded. The gun barrel is then evacuated to 1 Torr and the projectile is released. The bird is accelerated by atmospheric pressure (or slightly augmented) and travels for several hundred feet (up to 300 feet for the 7 inch gun) to the catch-box area in the terminal velocity.

After muzzle exit, the bird impacts a mitigator which is fabricated from honeycomb material and can be geometrically tailored for specific loading rates. The momentum exchange mass (MEM) is a piece of heavy steel to absorb the residual energy from impact. Figure 2 illustrates the mechanism of impact tests. By careful engineering of theses features, it is generally possible to create realistic interior ballistic loading rates, pulse shapes and durations during the deceleration of the bird. The specimen is held by a fixture between mitigator and MEM and an extra mass may be added in front of the fixture to adjust the force in the specimen. The speed of projectile and force acting on each component of the system can be predicted from modeling of dynamic response during impact.

Fixtures are designed and fabricated to hold the specimen in correct alignment during impact and provide uniform stress transfer into the specimen. The gage length is adjustable and test results can be compared to those from standard static test fixtures such as IITRI or Celanese configurations by ASTM Standard D 3410 [4,5]. A 0.5 inch gage length is used for this specific investigation. The composite test coupons is about 1.00 inch wide and 0.09 inch thick with a layup construction of $[(0/45/-45/0)_4]$. Im7/8551-7 composite prepreg was used for fabrication . Figure 3 shows a typical failure of specimen after an impact test.

Measurements of displacements and deformations were performed by a streak cameras. A strip pattern was printed on the surface of specimen and a high speed camera was aimed at the strip constantly during impact. Figure 4 shows a streak film taken by the camera with speed of 120 ft/sec. The total impact duration of this particular test is about 5 mil second. The parallel white/black strip in the film is the image of the strip pattern. It is noted that the movement of strip is a rigid body motion of the specimen while the contraction of strip is compressive deformation due to impact. The streak film was then digitized and analyzed by using a high resolution PDS 1010A micro-densitometer and PDS 2300C data acquisition system. Accordingly, the deformation state in terms of time was obtained and the strain due to impact could be calculated. Figure 5 shows the strain as a function of time. A very sharp drop occurs at end of impact (about 4 msec) where material failed. The ultimate compressive strain is about 1%.

An accelerometer was placed on the MEM surface to record the acceleration in terms of impact time. The force in the specimen is assumed to be equal to the force acting on the MEM. Therefore, stress in the specimen can be derived and is equal to the product of the acceleration and the mass of MEM. The force as a function of impact time is illustrated in Figure

6. The zigzag pattern in the curve is due to a stress wave travelling in the MEM. The maximum stress in the specimen can be calculated to be 220, 165 and 122 ksi at points A, B and C, respectively. The static ultimate strength was measured to be 115 ksi by using ITTRI test method with same gage length.

Strain rate effects on compressive properties of composite are clearly observed. In fact, the tested specimen shows the failure is initiated by transverse delamination then followed by fiber buckling (Figure 3). Since the polymer matrix is highly rate dependent material, the dynamic strength increases as strain and loading rates increase.

References

1. Kolsky, H. "An Investigation of Mechanical Properties of Materials at Very High Rates of Loading," Proc. Phys. Soc., London, 62-B, pp.676-700, 1949.
2. Nicholas, T. and Bless, S. J., "High Strain Rate Tension Testing," Metal Handbook, 9th Ed., Amer. Soc. Metals, Vol. 8, pp.208-214, 1985.
3. Staab, G. H. and Gilat A., "A Direct-tension Split Hopkinson Bar for High Strain-rate Testing," Experimental Mechanics, pp.232-235, September, 1991.
4. Adams, D. F. and Odom, E. M.,"Influence of Test Fixture Configuration on the Measured Compressive Strength of a Composite Material",J. of Composite Technology & Research, Vol. 13, No. 1, pp.36-40, Spring 1991.
5. Adams, D. F. and Lewis, E. Q., "Influence of Specimen Gage Length and Loading Method on the Axial Compressive Strength of a Unidirectional Composite Material", Experimental Mechanics, pp.14-20, March, 1991

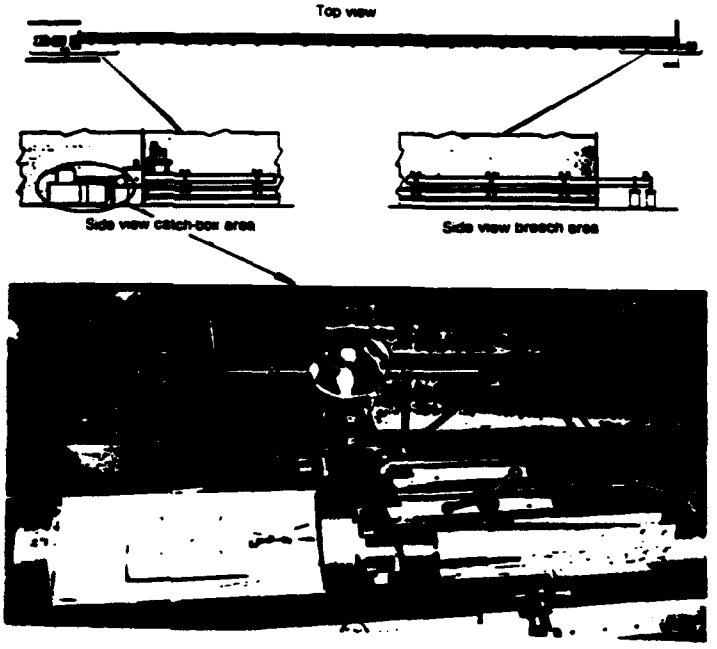

Figure 1. Air Gun System

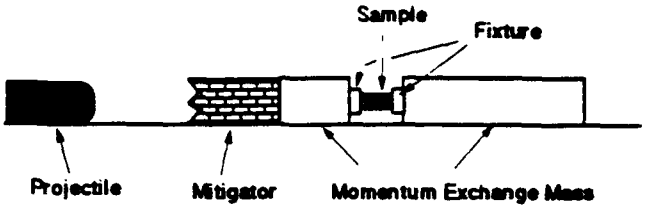

Figure 2. Schematic of test set-up

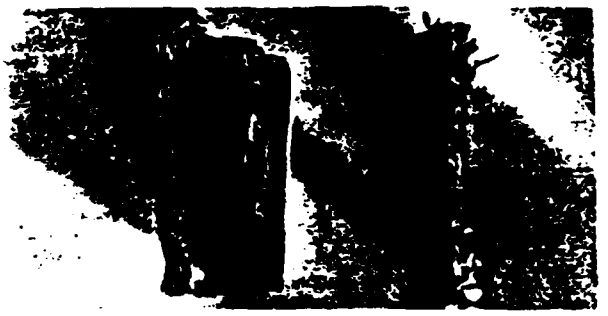

Figure 3. Specimen after impact

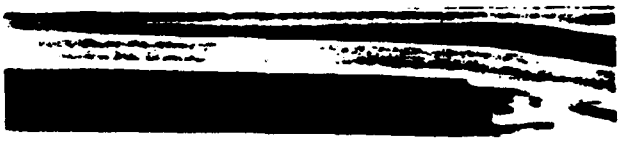

Figure 4. Streak film

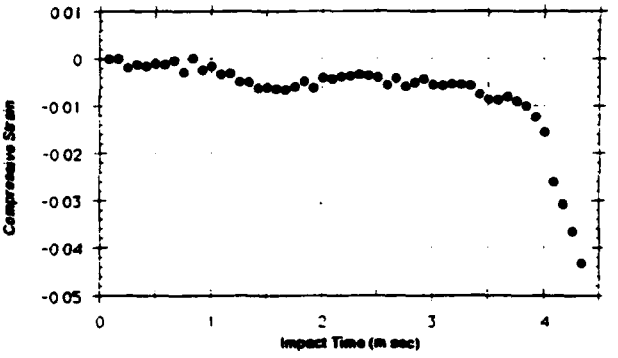

Figure 5. Compressive strain in the specimen during impact

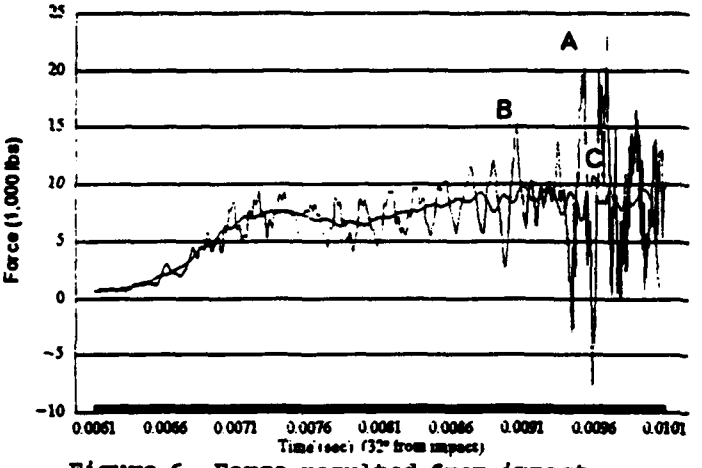

Figure 6. Force resulted from impact

Technology Programs in Composite Structures at the U.S. Army Missile Command

by

Terry Vandiver
Structures Directorate
U.S. Army Missile Command

The U.S. Army Missile Command has a number of projects in the areas of advanced composite structures. Each project has the ultimate goal of improving weaponry for current and future military systems. Most of the projects described below span the FY93-95 time frame.

One ongoing project at MICOM is 3-inch bottle testing used to determine ultimate strengths used in design of composite structures. The method used for fabricating mandrels is tedious and time consuming. This program will develop a more efficient method of fabricating bottles in quantities consistent with program needs.

Proof testing of composite structures is currently the method used at MICOM to determine the quality of rocket motorcases and launch tubes. Taguchi methods will be utilized to determine the effects of the rate of pressurization, the rate of proof load to burst pressure, and the fiber/resin combinations on composite test vessels.

Incorporation of optical fibers into a composite structure for strength, pressure, and temperature measurement is currently underway at MICOM. Optical fibers will be incorporated into the 3-inch pressure vessels to determine practicality. The specimens will then be hydroburst tested to determine if structural integrity is compromised due to the optical fiber. Analysis on the microstructure will be performed to determine effects on the matrix.

An effort is underway in the area of service life predictions. A literature search will be performed to obtain data on long term exposure of composites. A series of similar test specimens will be fabricated and exposed to similar conditions at accelerated times. The specimens will be tested in the same manner as those seeing long term exposure and a correlation between the two tests will be developed.

The determination of critical fiber length in resin transfer molding is a program underway at MICOM. Specimens will be made and tested in tensile and flexure modes. The test specimens will be of simple geometry and consist of various chopped fiber lengths mixed with resin and injected

into a mold. Data from the tensile and flex tests will be plotted (load vs. fiber length) thus determining a "critical fiber length" for an anticipated load condition.

Another program underway at MICOM is thermoplastic coatings for use on composite and metal substrates as a substitute for CARC paint. A series of both metal and composite substrates will be flame sprayed using selected thermoplastics. The coating and material combinations undergoing successful application will be tested for coating integrity to environmental exposure, adhesion and flexibility. ASTM tests will be used.

A high use temperature composite structures program is underway at MICOM. Polyimide resins and phenolic triazine are the primary candidates that have been manufactured to date. The MICOM Advanced Kinetic Energy Missile System composite booster motorcase and centerbody sections have been manufactured by four contractors and are currently being tested for bending and ultimate strength at MICOM.

A technology effort is underway at MICOM on low impact damage of graphite/epoxy composite structures. Taguchi methods are being utilized to determine design enhancements which can be used to mitigate impact damage and increase the survivability of a variety of composite structures such as motorcases and launch tubes. Additional layers, either filament wound or braided will be added to a baseline structure. The structures will then be impacted at different levels of energy and hydroburst to determine ultimate strength.

A composites adhesive program is underway that characterizes adhesives via rapid heating rates. Double lap shear joint test specimens will be fabricated with incorporated thermocouples near the adhesive joints. Tests will be performed at both high heating and loading rates to simulate environements that adhesives encounter when used in missile systems.

Each one of the above described programs is being performed jointly by Government, universities and industry to encompass all the areas of expertise to assist in solving problems encountered in the completion of the tasks.

DAMAGE MECHANISMS IN METAL MATRIX COMPOSITE PLATES

George Z. Voyiadjis, Anthony R. Venson and Peter I. Kattan
Department of Civil Engineering
Louisiana State University
Baton Rouge, LA 70803

ABSTRACT

Damage mechanics is used to investigate the various damage mechanisms in loaded metal matrix composite plates. These structural components are widely used in the Army's vehicles and installations. They are constantly subjected to different types of loads which give rise to the initiation and growth of various damage mechanisms. These mechanisms range in scope from matrix-related to fiber-related. In addition, certain damage mechanisms arise due to the effect of the interaction between the matrix and fibers. In general, these include void growth and coalescence, microcrack initiation, crack propagation, fiber fracture, debonding and delamination.

The damage model is based on the concept of effective stress introduced by Kachanov (1958) and the recent work of Murakami (1988) . A new damage tensorial variable is introduced to model crack initiation and propagation. The definition of this tensor is based on experimental measurements of the crack density at mutually orthogonal cross-sections of the damaged component. The damage model is coupled with existing material model to formulate an integrated damage characterization constitutive model for metal matrix composite plates. The resulting coupled material model is capable of analyzing both elastic and elasto-plastic metal matrix composites. However, in all cases, the brittle fibers are assumed to be elastic.

The measured crack densities are normalized with respect to the crack densities at the failure load. The results are shown in terms of stress-strain curves for the damaged components. In addition, damage curves are shown representing plots of the damage variable components versus the strain. Certain conclusions and recommendations are made based on the results. In particular, the critical state of damage is located and identified.

Two approaches are considered in the formulation of the damage model with respect to the damage of the matrix and fibers as shown in Figure 1. The first approach is termed "overall" in the sense that one damage variable is used to characterize damage in both the matrix and fibers (Kattan and Voyiadjis, 1993). The second approach is termed "local" in the sense that two damage variables are used to model the damage mechanisms in the matrix and fibers; one for each constituent (Voyiadjis and Kattan, 1993). Each approach has its own advantages and disadvantages. In the first approach, utilizing one damage variable has the benefit of capturing all damage effects in the system. However, this approach lack a detailed description of each damage mechanism as it lumps them all into one

variable. On the other hand, the local approach has the advantage of considering "local" or "constituent" damage mechanisms as it uses an independent variable for each. However, its weak point lies in the characterization of interfacial damage; that is it cannot describe properly the damage arising due to the interaction of the matrix and fibers, like decohesion and debonding.

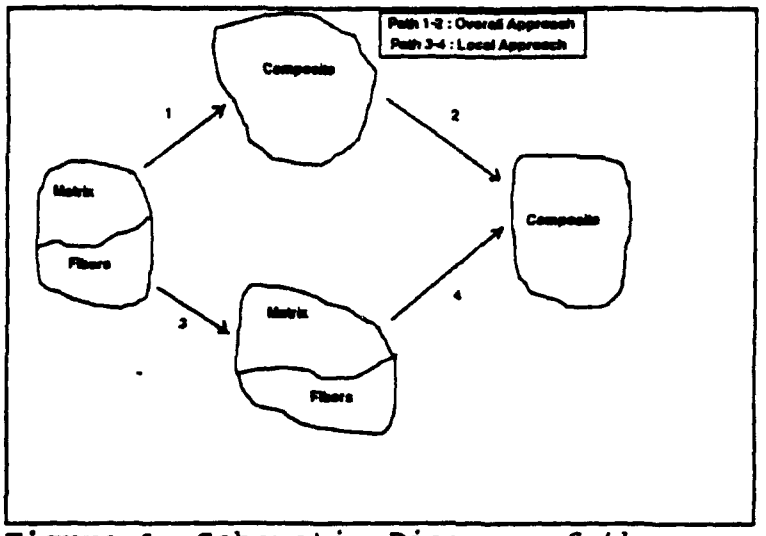

Figure 1 Schematic Diagram of the Overall and Local Approaches.

In the derivation of the constitutive model, it is shown that for the elasto-plastic model, an anisotropic yield function is derived for the damaged composite system. This results from the consideration a von Mises type yield function for the undamaged matrix material with elastic fibers. In a similar fashion, it is also shown how the flow rule for the plastic strain is non-associated for the damaged composite system, where an associated flow rule is assumed for the undamaged matrix material.

In order to validate the theoretical predictions, a number of uniaxial tensile loading experiments are performed on titannium aluminide SiC-reinforced metal matrix composite specimens. Two different laminate layups are considered: $(0/90)_s$ and $(\pm 45)_s$. Only one of each orientation was loaded to failure. The remaining specimens were loaded at up to certain percentages of the failure load. The damaged specimens are then analyzed using image analyses techniques. Crack densities are measured for all the damaged sepcimens. The damage tensor is computed based on these measurements and the results are compared with the theoretical models.

REFERENCES:

Kachanov, L. M. (1958). On the Creep Fracture Time. *Izv Akad. Nauk USSR Otd. Tekh.* .Vol. 8, pp. 26-31 (in Russian).

Murakami, S. (1988). Mechanical Modeling of Material Damage. *Journal of Applied Mechanics*. Vol. 55, pp. 355-360.

Kattan, P. I. and Voyiadjis, G. Z. (1993). Micromechanical Analysis of Damage in Uniaxially Loaded Unidirectional Fiber-Reinforced Composite Laminae. *International Journal of Solids and Structures*. Vol. 30, No. 1, pp. 19-36.

Voyiadjis, G. Z. and Kattan, P. I. (1993). Local Approach to Damage in Elasto-Plastic Metal Matrix Composites. *International Journal of Damage Mechanics*. Vol. 2, No. 1, pp. 92-114.

THE EFFECT OF WIDTH ON THE FREE VIBRATION OF ANISOTROPIC LAMINATED BEAMS

J. M. Whitney
Professor of Graduate Materials Engineering
University of Dayton
Dayton, Ohio

ABSTRACT

Beams are well recognized as a basic structural element. Engineering students are introduced to classical beam theory in conjunction with sophomore strength-of-materials which traditionally deals with homogeneous metals. Increased use of composite materials in engineering applications has induced the need to develop analytical models applicable to laminated, anisotropic beams.

Initial development of laminated beam theory can be found in elementary strength-of-materials where beams constructed of different materials are considered. In this context laminated beams are analyzed within the framework of classical beam theory. In particular, each layer is assumed to be under a state of one-dimensional stress (i.e. axial normal stress and transverse shear stress are the only non-vanishing stresses). For materials with similar Poisson ratios, this assumption is valid. However, for highly anisotropic materials with a severe mismatch of Poisson ratios from ply-to-ply a serious *transverse strain incompatibility* results. This issue has been initially addressed by considering bidirectional laminates under uniaxial tension loading (Dietz, 1949). Classical strength-of-materials framework has also been utilized for analyzing laminated, anisotropic beams by Vinson and Sierakowski (1986) and more recently by Vasiliev (1993).

Other approaches to laminated beam theories have enforced transverse strain compatibility. However, confusion exists in these one-dimensional approaches between cylindrical bending and a beam theory. The difference between the two models is analogous to the difference between plane stress and plane strain in classical theory of elasticity and is clearly distinguished by Whitney (1987). Cylindrical bending has been confused with beam theory. A valid laminated beam theory should reduce to classical beam theory for the case of a homogeneous material. This does not occur with cylindrical bending.

Width effects produce additional difficulties with laminated composite beams due to the large width-to-thickness ratio of many applications, including current *flexure test specimens. In particular*, laminated beams are closer to a narrow plate than to a classical beam. Shear coupling produced with the inclusion of angle-ply layers in the laminate make one-dimensional assumptions less valid (Kedward, 1972).

In the current paper the effect of length-to-width ratio and width-to-thickness ratio on the response of anisotropic laminated beams is investigated. The parameter under consideration is the fundamental free vibration frequency. Exact solutions are obtained for the case of specially orthotropic thin plates with two opposite edges simply-supported and the two adjacent edges free. Minimum length-to-width ratios compatible with one-dimensional beam assumptions are established for laminates having a high major Poisson's ratio under bending. In order to consider angle-ply laminates within the framework of specially orthotropic plates, stacking geometries with very weak bending-twisting coupling are investigated.

The effect of cross-section width is investigated by considering long narrow plates with various width-to-thickness ratios. In this case it is necessary to modify the thin plate theory to include transverse shear deformation in the width direction.

Beam Theory versus Cylindrical Bending

Consider a laminated plate having *infinite length* in the y-direction with uniform boundary conditions along the edges (see Figure 1). If any surface or inplane loads are independent of y, then the displacements and the corresponding force and moment resultants are independent of y. This theory is not compatible with classical beam theory as force and moment resultants are induced relative to the y-direction.

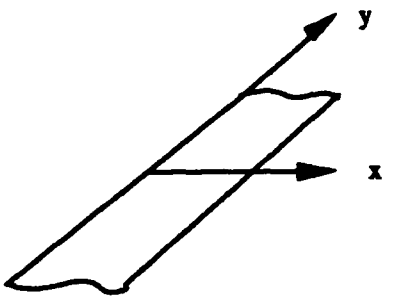

Figure 1. Cylindrical bending.

A classical beam is characterized by a plate having a high width-to-thickness ratio with the long sides free as illustrated in Figure 2. In this case the force and moment resultants relative to the y-direction vanish. The inplane stresses within the plies, however, are two-dimensional in nature.

Free-Vibration Analysis

Using classical laminated plate theory based on the Kirchhoff assumptions, an exact solution can be obtained for a specially orthotropic laminated plate with opposite sides simply-supported and the adjacent edges free. Numerical results are obtained for $[\pm 45°]_{8S}$ and $[\pm 45°/0°_2]_{3S}$ laminates with ply properties which are typical of contemporary graphite/epoxy laminates.

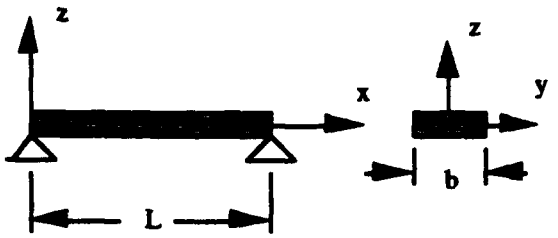

Figure 2. Classical beam.

Both of these laminates contain bending-twisting coupling which induces the laminate to behave as an anisotropic plate rather than a specially orthotropic plate. However, the coupling is very weak for these laminate stacking geometries and the fundamental vibration frequency can be accurately obtained by treating the plate as orthotropic. The solution is obtained by seperation of variables. An iteration scheme in conjunction with a transcendental equation is required in order to obtain the fundamental vibration frequency.

Numerical results are shown in Figure 3 for the $[\pm 45°]_{8S}$ with ω^* denoting a normalized fundamental frequency.

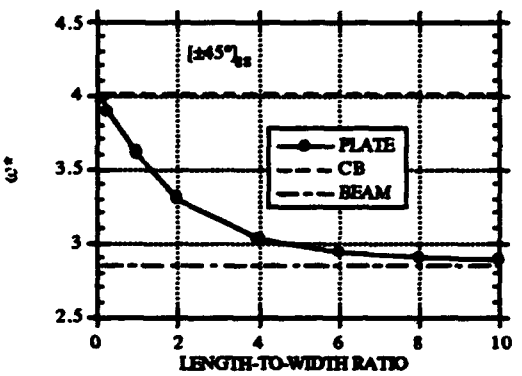

Figure 3. Normalized fundamental frequency.

We note that cylindrical bending (CB) results are obtained for length-to-width ratios (R) less than 0.1, while beam theory is approached for R > 8. Similar results are obtained for the $[\pm 45°/0°_2]_{3S}$ laminate.

In order to ascertain the effect of width-to-thickness ratio on beam response, the Kirchhoff theory is modified to include transverse shear deformation in the width direction. Fundamental frequencies are obtained as a function of width-to-thickness ratios for plates with large values of R. Length-to-thickness ratios are small so that shear deformation is not required in the length direction. Numerical results show that the fundamental frequencies are rather insensitive to width-to-thickness ratios. Thus, beam behavior is controlled by R.

References

A. G. H. Dietz, *Engineering Laminates*, John Wiley, 1949.

Keith T. Kedward, "On the Short Beam Test Method," *Fibre Science and Technology*, Vol. 5, 1972, pp. 85-95.

Valery V. Vasiliev, *Mechanics of Composite Structures*, English Edition Editor Robert M. Jones, Taylor and Francis, Washington, D. C., 1993.

J. R. Vinson and R. L. Sierakowski, *The Behavior of Structures Composed of Composite Materials*, Martinus Nijhoff Publishers, Boston, 1986.

J. M. Whitney, "One-Dimensional Analysis of Laminated Plates", Chapter 4, *Structural Analysis of Laminated Anisotropic Plates*, Technomic Publishing Co., Lancaster, PA, 1987.

CHARACTERIZATION AND MODELING OF VISCOELASTIC RESPONSE OF PEEK RESIN AND PEEK COMPOSITE

X.R.XIAO
Department of Mechanical Engineering,
Concordia University
1455 de Maisonneuve Blvd. W., Montreal,
Quebec, Canada H3G 1M8

Viscoelastic behaviour is much more significant in polymeric materials than in other types of materials. In polymer based composites, the viscoelastic response manifests strongly in matrix dominated properties. Service conditions, such as stresses, elevated temperature and moisture can accelerate the viscoelastic processes and thus further degrade the stiffness and strength of the composite. However, the viscoelastic properties are not always harmful. For instance, the damping properties of the materials can be utilized in controlling the vibration of the structures. Fiber reinforced polymer composites, incorporating the high stiffness with the high damping properties, are excellent candidates for structures subjected to dynamic loading.

The analysis and modeling of viscoelastic response of composite structures are based on the viscoelastic Correspondence Principle. The viscoelastic properties of the composite need to be determined experimentally and then modeled by a viscoelastic constitutive equation. The viscoelastic properties of the composite may also be predicted by micromechanics approaches from individual constituents. The latter allows a broad range selection of material combination in design.

The viscoelastic constitutive modeling as well as the extension of micromechanics models to the time domain are based on experimental characterization of real resin and composite systems. This paper presents experimental results on the viscoelastic properties of PEEK resin and PEEK composite APC-2. The viscoelastic response of the composite is compared with that of the pure resin. The constitutive modeling for the linear and nonlinear viscoelastic responses is discussed.

The viscoelastic properties of PEEK resin and APC-2 composite were characterized by creep and creep-recovery tests following an accelerated testing procedure based on the time-temperature and superposition principle (TTSP) and time-stress superposition principle (TSSP) [1]. Additional information was obtained by dynamic mechanical measurements.

As compared with the pure resin, APC-2 composite shows a higher damping over the β' relaxation region and a lower temperature for the glass transition. The discrepancy is likely caused by the interphase layer in the composite. Thus the two-phase micro-mechanical model may not be adequate to predict the viscoelastic properties.

The recoverable creep response, which is required for viscoelastic modeling, can be determined through proper mechanical models rather than mechanically conditioning the specimens. PEEK resin displays both instantaneous plastic deformation and time-dependent flow. A mechanical model is proposed to represent such a behaviour.

The Schapery's nonlinear viscoelastic equation is mostly used in viscoelastic constitutive modeling. For the case of uniaxial loading it is given by [2]:

$$\varepsilon(t) = g_0 S_0 \sigma + \int_0^t g_1 \Delta S(\psi-\psi') \frac{dg_2\sigma}{dt'} dt'$$

$$\psi = \psi(t) = \int_0^t \frac{d\tau}{a_\sigma} \qquad \psi' = \psi(t') = \int_0^{t'} \frac{d\tau}{a_\sigma} \tag{1}$$

where g_0, g_1, g_2 and a_σ are the nonlinear parameters with clear physical meaning [1], $\Delta S(\psi)$ is the kernel function representing the linear viscoelastic response, and t is time.

The kernel function may be described by a modified power law containing four parameters, the so called general power law. For the creep compliance S(t), it has the following form:

$$S(t) = S_0 + \frac{S_\infty - S_0}{(1+\frac{\tau_0}{t})^n} \qquad (2)$$

where τ_0 is the characteristic time parameter, S_0 and S_∞ are the initial compliance and the compliance at infinite time, respectively, and n is a material parameter. It has been shown that the general power law can describe the viscoelastic responses over a broad time domain, such as fitting the master curves. The effect of temperature can be readily considered by the time-temperature shift function a_T and b_T, which are known from the TTSP procedure.

For the case of uniaxial loading, under the step stress input $\sigma[H(t)-H(t-t_1)]$, the creep response predicted by the Schapery's equation with a kernel of general power law is:

$$\varepsilon(t) = g_0 S_0 \sigma + g_1 g_2 \sigma \frac{S_\infty - S_0}{(1+\frac{\tau_0 a_\sigma}{t})^n} \qquad t<t_1 \qquad (3)$$

As can be seen, it is impossible to determine g_1, g_2 and a_σ from creep tests only. Lou and Schapery have proposed a procedure to determine the above parameters from creep and creep-recovery tests [2]. However, the procedure given in [2] implies that the creep-recovery response follows the Boltzmann superposition principle. PEEK resin and the composite show severe nonlinearity in creep-recovery response and thus the Schapery's procedure cannot be used.

It has been shown that for a graphite/epoxy composite g_1 and g_2 vary with stress level in such a way that their product is nearly unity [1]. Some experimental evidences suggest that a_D, the nonlinear parameter for the dissipation element in Schapery's model, is stress independent and thus can be related to the time-temperature shift factor a_T. Consequently, the stress and temperature dependent nonlinearity of the dissipation element and modulus element can be decoupled such that the former is characterized by a_T while the latter is represented by parameters a_σ and $g_1 g_2$. If the temperature dependence of the nonlinearity between the generalized external force and internal force is much significant than the stress dependence of the modulus element, $g_1 g_2$ becomes the shift factor b_T. Thus Equation 3 becomes:

$$\varepsilon(t) = \frac{g_0 S_0 \sigma}{b_T} + \sigma \frac{(S_\infty - S_0)/b_T}{(1+\frac{\tau_0 a_T a_\sigma}{t})^n} \qquad (4)$$

thereby the nonlinear parameters g_0 and a_σ can be determined from creep data only.

The stress-dependent viscoelastic responses of APC-2 composite were measured by 90° and 15° off-axis creep tests for the transverse tensile mode and shear mode, respectively. The linear parameters in Eq.2 were determined by a graphical TTSP procedure. While the nonlinear parameters g_0 and a_σ were determined by a numerical TSSP procedure. The temperature-time shift factor a_T follows the Arrhenius relation. The stress-time shift factor a_σ appears to follow an exponential law, which can be traced back to the energy barrier theory for the nonlinearity of viscosity. With the equations and parameters presented, the linear and nonlinear viscoelastic behaviours of APC-2 composite laminate from ambient temperature up to the glass transition temperature can be described analytically.

References

1. Hiel, C.C., Cardon, A.H., Brinson, H.F., 1984, NASA Contractor Report 3772.
2. Lou, Y.C., Schapery, R.A., J., 1971, Composite Materials, 5: 208-234.
3. Xiao, X.R., Ph.D Dissertation, 1987, VUB, Brussels.

List of Attendees:

Anderson, Gary (Dr.)
ARO workshop monitor
US Army Research Office
Engineering Sciences Div
Chief Structural Mechanics Branch
PO Box 12211
Research Triangle Park
NC 27709-2211
Tel: (919)-549-4317
FAX: -4310
email: in%"anderson@aro-emh1.army.miL"

Averill, Ronald C. (Prof.)
Michigan State University
Dept of Materials Science and Mechanics
A304 Engineering Building
East Lansing, Mi 48824-1226
Tel: (517)-355-5141
FAX: 353-9842

Barrett, Ron (Dr.)
Barrett Aerospace Technologies
1500 West 9th Street, Suite 3
Lawrence, KS 66044
Tel and FAX: (913)-841-1293

Batra, Romesh C. (Prof.)
University of Missouri-Rolla
Dept of Mechanical and Aerospace
Engineering and Engrg Mechanics
125 Mechanical Engineering Annex
Rolla, MO 65401-0249
Tel: (314)-341-4589
FAX: -4607

Baz, Amr (Prof.)
The Catholic University of America
Dept of Mechanical Engineering
Washington, DC 20064
Tel: (202)-319-5170

Berdichevsky, Victor L. (Prof.)
Georgia Institute of Technology
School of Aerospace Engineering
Atlanta, GA 30332-0150
Tel: (404)-894-3000
FAX: -2760

Bogdanovich, Alexander E. (Prof.)
North Carolina State University
Dept of Textile Material Science
NCSU Box 8301
Raleigh, NC 27695-8301
Tel: (919)-515-6679
FAX: -6532
email: in%"abogdano@tx.ncsu.edu"

Burns, Bruce
Chief Mechanics and Structures Branch
Attn: AMSRL-WT-PD
Aberdeen Proving Ground
MD 21005-5066
Tel: (410)-278-6130/6132

Cantwell, Wesley (Dr.)
Polymers Laboratory
Ecole Polytechnique Federale
de Lausanne
Department des Materiaux
EPFL, Lausanne
Switzerland AIR MAIL
FAX: (021)-693-2935
email:
in%"wesLey_cantweLL@dmxqm.epfL.ch"

Carman, Greg (Prof.)
University of California
at Los Angeles (UCLA)
Dept of Mechanical, Aerospace
and Nuclear Engineering
38-137m Eng. IV
Los Angeles, CA 90024
Tel: (310)-825-6030
FAX: -206-2302
email: in%"carman@seas.ucLa.edu"

Chang, Fu-Kuo (Prof.)
Stanford University
Dept of Aeronautics and Astronautics
Durland Building, Room 385
Stanford, CA 94305-6060
Tel: (415)-723-3466
FAX: 725-3377
email:
in%"wiLLiam.b.webster@forsythe.stanford.edu"

Chattopadhyay, Aditi (Prof.)
Arizona State University
Dept of Mechanical and Aerospace Engineering
Tempe, AZ85287
Tel: (602)-965-3291
FAX: -1384
email:
in%"chattopa@enws148.eas.asu.edu"

Chaudhuri, Reaz A. (Prof.)
University of Utah
Dept of Civil Engineering
3220 Merrill Engineering Bldg
Salt Lake City, Utah 84112
Tel: (801)-581-6931
FAX: 585-5477

Coulter, John (Prof.)
Lehigh University
Dept of Mechanical Engineering and Mechanics
Bethlehem, PA 18015
Tel: (215)-758-4503
-4125 (Coulter)
FAX: -4041
email: in%"jc01@Lehigh.edu"

Czarnecki, Gregory J.
Wright Laboratory
WL/FIVS
Vehicle Sybsystems Div
Wright Patterson Air Force Base
Ohio 45433

Dong, Stanley B. (Prof.)
University of California at Los Angeles (UCLA)
Dept of Civil Engineering
3173 Engineering I
Los Angeles, CA 90024-1593
email: in%"dong@ea.ucLa.edu"

Dutta, Piyush (Dr.)
US Army Cold Regions Research and Engineering Laboratory
72 Lyme Road
Hanover, NH 03755
Tel: (603)-646-4212
FAX: -4640
email: in%"pkdutt@hanover-crrel.army.mil"

Fahrenthold, Eric (Prof.)
University of Texas at Austin
Dept of Mechanical Engineering
Austin, TX 78712

Gibson, Ronald F. (Prof.)
Wayne State University
Dept of Mechanical Engineering
Detroit, MI 48202
Tel: (313)-577-3702
FAX: -3881
email:
in%"ronald_gibson@eng.wayne.edu"

Gramoll, Kurt (Prof.)
Georgia Institute of Technology
School of Aerospace Engineering
Atlanta, GA 30332-0150
Tel: (404)-894-3065
FAX: -9313

Hakala, Bill
National Science Foundation
1800 G Street NW
Washington, DC 20550
Tel: (202)-357-9542
FAX: -0167

Hanagud, S. (Prof.)
Georgia Institute of Technology
School of Aerospace Engineering
Atlanta, GA 30332-0150
Tel: (404)-894-3040 (Hanagud)
-2000 (main)
email:
in%"ae203nb@prism.gatech.edu"

Herrington, Paul (Prof.)
University of New Orleans
Dept of Mechanical Engineering
New Orleans, LA 70148
Tel: (504)-286-6050
FAX: -5539
email: in%"pdhme@uno.edu"

Hoa, Suong V. (Prof.)
Concordia University
Dept of Mechanical Engineering
1455 de Maisonneuve Blvd. West
Montreal, Quebec H3G-1M8
CANADA
Tel: (514)-848-3131
FAX: -3175
email:
in%"cabfL59@vax2.concordia.ca"

Horgan, Cornelius O. (Prof.)
University of Virginia
Dept of Applied Mathematics
School of Engineering and
Applied Science
Charlottesville, VA 22903-2442
Tel: (804)-924-7230
FAX: -6270
email: in%"coh8p@virginia.bitnet"

Hui, David (Prof.)
ARO workshop chairman
University of New Orleans
Dept of Mechanical Engineering
New Orleans, LA 70148
Tel: (504)-286-6652
FAX: -5539
email: in%"dxhme@uno.edu"

Jaeger, Zeev
Israel Atomic Energy Commission
Soreq Nuclear Research Center
Dept. of Physics and Applied Math
Yavne, ISRAEL 70600
FAX: 972-8-437361

Joshi, S. P. (Prof.)
University of Texas at Arlington
Dept of Aerospace Engineering
PO Box 19018
Arlington, TX 76019
Tel: (817)-273-3746
FAX: -794-5010
email: in%"me@matrix.uta.edu"

Kapania, R.K. (Prof.)
Virginia Polytechnic Institute
Dept of Aerospace and Ocean
Engineering
Blacksburg, VA 24061

Kelly, James
Advanced Research Projects Agency
(ARPA)
Undersea Warfare Office
3701 North Fairfax Drive
Arlington, VA 22203-1714
Tel: (703)-696-2331
FAX: -2204
email: in%"jkeLLy@a.darpa.miL"

Khorrami, Farshad (Prof.)
Polytechnic University
Dept of Electrical Engineering
Five Metrotech Center
Brooklyn, NY 11201
Tel: (718)-260-3227
FAX: -3906
-3136
email: in%"khorrami@puee1.poLy.edu"

Lee, James (Prof.)
George Washington University
Dept of Mechanical Engineering
School of Engineering and Applied Sci
Washington, DC 20052
Tel: (202)-994-6749
FAX: -0238

Mayer, Arnold (Dr.)
Wright Laboratory
WL/FIV
Wright Patterson
Air Force Base, OH 45433
email: in%"mayerah.wLfiv@fivmailgw"

Measures, Ray (Prof.)
University of Toronto
Institute for Aerospace Studies
4925 Dufferin Street
Downsview, Ontario
Canada M3H-5T6

Nayfeh, Adnan H. (Prof.)
University of Cincinnati
Dept of Aerospace Engineering
and Engineering Mechanics
Cincinnati, OH 45221
Tel: (513)-556-3548
FAX: -5038

Pang, Su-Seng (Prof.)
Louisiana State University
Dept of Mechanical Engineering
Baton Rouge, LA
Tel: (504)-388-5792
FAX: -5990

Rajapakse, Yapa D.S. (Dr.)
Office of Naval Research
Mechanics Division
Code 1132-SM
800 North Quincy St.
Arlington, VA 22217-5000
Tel: (703)-696-4405
FAX: -0934
email:
in%"onrmech@ccf.nrL.navy.miL"

Rao, Vitta (Prof.)
University of Missouri-Rolla
Dept of Electrical Engineering
Intelligent Systems Center
Rolla, Mo 65401-0249
Tel: (314)-341-6371
FAX: -6512
email: in%"rao@isc.umr.edu"

Shahkinpoor, Mohsen
University of Mexico
Dept of Mechanical Engineering
Albuquerque, NM 87131-1361
Tel: (505)-277-3966
FAX -1571
email: in%"shah@unmb.unm.edu"

Sigur, Wanda
Martin Marietta Space System
Section Chief Composites Technology
PO Box 29304, mail stop 4345
13000 Old Gentilly Road
New Orleans, LA 70189
Tel: (504)-257-2133 (Sigur)
-3311 (main)
FAX: -4406

Simitses, George (Prof.)
University of Cincinnati
Dept of Aerospace Engineering
and Engineering Mechanics
797 Rhodes Hall (#70)
Cincinnati, OH 45221
Tel: (513)-556-3548
FAX: -5038

Spicola, Frank
Naval Undersea Warfare Center
Code 8215, Bldg 679
Structures Technology Branch
Newport Laboratory
Newport, RI 02841-5047
Tel: (401)-841-2553
FAX: -1144

Tessler, Alexander (Dr.)
NASA Langley Research Center
Computational Mechanics Branch
mail stop 240
Hampton, VA 23681-0001
Tel: (804)-864-3178
email:
in%"tessLer@bLackbird.Larc.nasa.gov"

Tzeng, Jerome T. (Dr.)
US Army Research Laboratory
Weapon Technologies Directorate
AMSRL-WT-PD
Aberdeen Proving Ground,
MD 21005-5066
Tel: (410)-278-6121
email: in%"jtzeng@brL.miL"

Vandiver, Terry
US Army Missile Command
Mail Code AMSMI-RD-ST-CN
Redstone Arsenal
AL 35898
Tel: (205)-876-1015
FAX: -842-9800

Voyiadjis, George Z. (Prof.)
Louisianaz State University
Dept of Civil Engineering
Baton Rouge, LA 70803
Tel: (504)-388-8668
FAX: -5990

Weiss, Marc S. (Dr.)
Chief Scientist
Naval Biodynamics Laboratory
13800 Old Gentilly Road
P.O. Box 29407
New Orleans, LA 70189-0407
Tel: (504)-257-3979
-3917 (main)
FAX: -5456
email:
in%"bdl0maw@bumed30.med.navy.mil"

Whitney, James (Prof.)
The University of Dayton
Graduate Materials Engineering
300 College Park
Dayton, OH 45469-0240
Tel: (513)-229-2679
FAX: -3433

Xiao, X.R. (Prof.)
Concordia University
Dept of Mechanical Engineering
Montreal, Quebec H3G-1M8
CANADA
Tel: (514)-848-3131
-3166 (Xiao)
FAX: -3175
email:
in%^"mecheng@vax2.concordia.ca"